VERTICES

Duke's Undergraduate Research Journal

Spring 2025
Volume 4, Issue 1

What You Don't Know Won't Hurt You: A Survey of Cryptic Insect Biodiversity on Duke University's Campus

Exploring Olfactory Circuits in Drosophila: Connectomic Insights into Neural Connectivity, Behavioral Outputs, and Neurotransmitter Pathways

Gender Inequality in Healthcare Delivery: Differences in System Satisfaction During the COVID-19 Pandemic in the United States

A Comparative Analysis of Attractive and Repulsive Olfactory Circuits in the Drosophila Connectome

Table of Contents

Letter from the Editor 5

Articles

What You Don't Know Won't Hurt You: A Survey of Cryptic Insect Biodiversity on Duke University's Campus 7
Alex Ozonoff, Riley Hamp, Lydia Cox, Jayla Eckhoff

Exploring Olfactory Circuits in Drosophila: Connectomic Insights into Neural Connectivity, Behavioral Outputs, and Neurotransmitter Pathways 21
Nicholas Sangvai, Jinchen Wen, Joanna Kang, Walter Kornfeld, Talia Penn

Gender Inequality in Healthcare Delivery: Differences in System Satisfaction During the COVID-19 Pandemic in the United States 35
Haizhu Song

A Comparative Analysis of Attractive and Repulsive Olfactory Circuits in the Drosophila Connectome 61
Kuzey Sozat, Trenton Jones, Natalia Bojorquez, Cia Varelas, Sanjana Kalagara

Meet Our Editing Team 79

Meet Our Design Team 89

Acknowledgements 93

Letter from the Editors

Dear Reader,

Welcome to the first issue of *Vertices* Volume IV, where four standout articles reflect the curiosity, creativity, and scientific acumen of Duke's undergraduate research community.

This issue spotlights the many scales at which science seeks understanding, from the microscopic to the societal. Two articles delve into the neural circuitry of olfactory behavior in *Drosophila melanogaster,* using connectomic data to unravel the structural and functional differences between pheromone- and odor-processing pathways. These works highlight the power of modern neuroscience to decode how anatomy translates to behavior. Another article surveys insect biodiversity hidden in plain sight across Duke's campus, revealing the astonishing abundance and ecological importance of soil-dwelling arthropods in urban green spaces. Finally, we feature a timely sociological analysis of gender disparities in U.S. healthcare satisfaction during the COVID-19 pandemic, challenging assumptions about how systemic inequities manifest in public attitudes.

Together, these articles exemplify our mission: to showcase undergraduate research that is not only methodologically rigorous but also deeply curious, critically engaged, and socially relevant. We are grateful to our peer review and artistic teams for their contributions to this issue, as well as our faculty, postdoctoral, and graduate student collaborators who helped review these articles. We hope you enjoy reading and engaging with these works as much as we did.

Sincerely,

Sasha Bacot, Co-Editor in Chief

Kaeden Hill, Co-Editor in Chief

What You Don’t Know Won’t Hurt You: A Survey of Cryptic Insect Biodiversity on Duke University’s Campus

Alex Ozonoff, Riley Hamp, Lydia Cox, Joy Buchi-Ahiabuike, Jayla Eckhoff, Gurnoor Majhail, Nirali Patel, Kit Shauf, Neha Shaw, Redeat Takele, Anna Tharakan, Emily Brady, H. Frederik Nijhout

Volume 4, Issue 1

Graphic by Monet Shum

Vertices: Duke's Undergraduate Research Journal Volume 4, Issue 1 | Spring 2025

What You Don't Know Won't Hurt You: A Survey of Cryptic Insect Biodiversity on Duke University's Campus

Alex Ozonoff, Riley Hamp, Lydia Cox, Joy Buchi-Ahiabuike, Jayla Eckhoff, Gurnoor Majhail, Nirali Patel, Kit Shauf, Neha Shaw, Redeat Takele, Anna Tharakan, Emily Brady, H. Frederik Nijhout Alex Ozonoff, Riley Hamp, Lydia Cox, Joy Buchi-Ahiabuike, Jayla Eckhoff, Gurnoor Majhail, Nirali Patel, Kit Shauf, Neha Shaw, Redeat Takele, Anna Tharakan, Emily Brady, H. Frederik Nijhout

Duke University
https://doi.org/10.55894/dv4.11

Abstract

We surveyed soil-dwelling insects and other arthropods across eight sites on Duke University's West Campus, collecting and identifying specimens to the taxonomic order. Results revealed Acari (mites and ticks) and Collembola (springtails) as the dominant groups, reflecting their adaptability to varied microhabitats and reliance on moist, organically rich soils. Site-specific diversity highlighted the influence of vegetation, microclimate, and habitat structure on insect and arthropod populations. Based on site-specific data, Duke's campus supports millions of arthropods, underscoring the ecological significance of urban green spaces. These findings emphasize the importance of biodiversity conservation in urban ecosystems and call for further research on the critical ecological roles of soil arthropods.

Keywords: insects | cryptic biodiversity

Introduction

Insects, class Insecta, are a principal group of phylum Arthropoda and comprise up to 80% of known animal species [1]. There are as many as 30 million estimated insect species, of which over three-quarters are yet undiscovered [1]. Despite this prolific biodiversity, insects face global declines [1]. On average, terrestrial insect abundance is declining at a rate of 9% each decade [2]. Climate change, habitat loss, pesticides, and pollution are principal factors causing these declines [1]. Additionally, urbanization has significant effects on insect populations [3]. Urbanization—associated with human-induced stressors such as habitat loss, deforestation, artificial lighting, and land use—results in, on average, approximately a 40% decrease in both insect abundance and richness compared to conserved areas [3].

Soil-dwelling arthropods, in particular, have experienced declines. Soil arthropods in temperate forests demonstrate declines in abundance, with increased precipitation as a key explanatory factor [4]. Climate change is predicted to increase extreme precipitation events [5], thus the effects of increased precipitation on the abundance of these organisms will likely increase over time. However, climate change is simultaneously predicted to increase drought and decrease soil moisture [6]. Dry conditions likewise threaten soil arthropods, with desiccation-prone species experiencing declines in

abundance with lower average rainfall [7]. Declines in soil arthropod species are ecologically important, as these organisms are crucial ecosystem engineers due to their contributions to soil fertility and nutrient cycling [8].

Informed by these threats facing insects, we sought to reveal, identify, and measure cryptic soil-dwelling urban insect biodiversity on Duke University's West Campus in Durham, North Carolina, U.S. We collected and assessed data as a semester-long class project for Entomology (Biology 349L), an upper-level undergraduate biology course. Our goals in conducting this study were to A) assess and quantify the cryptic insect biodiversity present on Duke's campus and B) provide information to raise awareness about the importance of insects and their declines.

2 | Methods

2.1 | *Sample Collection*

To establish a representative survey of Duke University's West campus, leaf litter and topsoil samples were collected from eight regions across campus (Figure 1). These eight regions were strategically selected to ensure an even distribution across the area Duke's campus occupies and to highlight variations in insect population density within campus hotspots. We collected ten samples from each area using haphazard sample site selection. The dimensions of the collection area were demarcated using a sheet of standard 8.5 by 11 inch letter paper, either full size or folded in half. Sampling was conducted during September and November of 2024 to ensure consistent environmental conditions between the regions, as well as to ensure that insects had not begun overwintering, thus drastically changing sample makeup. After clearing dry surface debris, we collected the moist leaf litter (~2 inches) and approximately the first inch of moist topsoil at each of the ten sample sites for each area. The samples were stored in labeled, airtight plastic bags to preserve moisture and prevent contamination during transportation to the laboratory.

Figure 1. Project sample sites on Duke University's West Campus.

Berlese funnels were used to extract insects from the soil samples. Our Berlese funnels were categorized into "small" or "big" sizes, either holding one or five samples, respectively. The "small" Berlese funnels were constructed using a 25.4 cm diameter plastic funnel to hold each sample and an approximately 38.7 cm2 metal mesh sheet (each hole of the small mesh measured 0.2286 cm2) placed at the base of the funnel to prevent the sample soil from passing through while allowing small insects and other arthropods to pass through. The "small" Berlese funnels were placed over mason jars containing a 1.2 cm depth of 70% ethanol to collect and preserve the insect specimens that fell through the mesh. The "big" Berlese funnel was constructed using a 12 in diameter plastic funnel and a 930 cm2 metal mesh sheet (each hole of the big mesh measured 0.635 cm2). In the same way as the "small" Berlese funnels, the "big" Berlese funnels were placed over 5-gallon buckets containing a 1.2 cm depth of 70% ethanol to collect and preserve the insect specimens from the sets of five samples. After 24-48 hours of extraction time in the funnels, the ethanol-preserved specimens were transferred to petri dishes for long-term storage and examination.

2.2 | *Identification & Estimation*

We used microscopes to identify and count insects and other arthropods—identified to taxonomic order—in each petri dish. Using these counts, we summed the number of insects in each order for all samples of each sampled region to get a total count of insects per order for each survey region. Based on these survey area totals, we found the mean

count for each insect order for each sample collected by dividing these totals by the number of samples collected in each region. To estimate the total number of insects per order for each sample region—beyond the limited sample sites within the area that we surveyed—we multiplied the mean insect order count per sample by the area (meters2) of the sample region. We then extrapolated these estimates to Duke University's West Campus and Durham. For these calculations, we multiplied the total count estimate for each order across all site areas by the area of Duke's campus divided by the total site area, and by the area of Durham [9] divided by the total site area, respectively:

Total insects (by order) in a set of regional samples =

$$N_{order,\,sample\ set} = \sum_{i=1}^{10} n_{sample,\,i}$$

Mean insects (by order) per regional sample =

$$X_{sample,\,region} = \frac{N_{order,\,sample\ set}}{10\ samples}$$

Insect (by order) per unit area in a region =

$$\rho_{region} = \frac{X_{sample,region}}{A_{region}}$$

Total insects in a region =

$$N_{order,region} = \rho_{region} * A_{region}$$

3 | Results

The following tables present a detailed breakdown of the insect counts observed in each sample region on Duke University's West Campus. These tables summarize raw counts by taxonomic order, mean counts across samples, and extrapolated estimates to represent total insect populations within each region and across larger areas (West Campus and Durham). For each table, insect orders and other arthropod orders are listed in black and gray font, respectively.

3.1 | *Site 1*

Sample 1 is located in the forested area behind Duke University's chapel, specifically on the side closest to the chapel. The total area of this site measures 8,154.84 m², with a sampling area of 0.604 m² (10 samples of approximately 8.5 × 11 inches). Samples were collected across multiple dates between September and November 2024 to capture a representative survey of the insect and arthropod population under consistent environmental conditions. The distance of the site from a central reference point is 460.88 m.

Total Count	n =	Mean per Sample	n =	Total Estimate for Area	n =
Blattodea	1	Blattodea	0.1	Blattodea	1350.14
Coleoptera	13	Coleoptera	1.3	Coleoptera	17551.81
Collembola	73	Collembola	7.3	Collembola	98560.15
Dermaptera	1	Dermaptera	0.1	Dermaptera	1350.14
Diplura	1	Diplura	0.1	Diplura	1350.14
Hymenoptera	18	Hymenoptera	1.8	Hymenoptera	24302.50
Protura	1	Protura	0.1	Protura	1350.14
Psocoptera	14	Psocoptera	1.4	Psocoptera	18901.95
Thysanura	22	Thysanura	2.2	Thysanura	29703.06
Acari	820	Acari	82	Acari	1107114.04
Araneae	32	Araneae	3.2	Araneae	43204.45
Isopoda	12	Isopoda	1.2	Isopoda	16201.67
Myriapoda	11	Myriapoda	1.1	Myriapoda	14851.53

Table 1.

Acari (mites and ticks) emerged as the most abundant group, comprising over 82% of the total arthropod count. Other frequently observed orders included Coleoptera (beetles) and Collembola (springtails), which varied significantly across individual samples. Less abundant orders, such as Diplura, Protura, and Dermaptera, were represented by only a single individual each. Additionally, the data revealed that Hymenoptera (ants, bees, wasps) exhibited notable activity during mid-October. Extrapolated estimates indicated that the site supports approximately 1,107,114 individuals of Acari and 29,703 individuals of Thysanura (silverfish).

3.2 | *Site 2*

Sample 2 was collected from the lawn behind the Biological Sciences Building on Duke University's

campus. This site encompasses an area of 439.9 m^2, with sampling conducted across 0.604 m^2 (approximately 8.5 × 11 inches for each of the 10 samples). The samples were taken on various dates, primarily during November 2024, to ensure representative data under consistent environmental conditions.

Total Count	n =	Mean per Sample	n =	Total Estimate for Area	n =
Blatteria	3	Blatteria	0.3	Blatteria	55.569
Coleoptera	28	Coleoptera	2.8	Coleoptera	518.644
Collembola	9	Collembola	0.9	Collembola	166.707
Diplura	3	Diplura	0.3	Diplura	55.569
Diptera	7	Diptera	0.7	Diptera	129.661
Hemiptera	1	Hemiptera	0.1	Hemiptera	18.523
Homoptera	1	Homoptera	0.1	Homoptera	18.523
Hymenoptera	3	Hymenoptera	0.3	Hymenoptera	55.569
Acari	79	Acari	7.9	Acari	1463.317
Araneae	6	Araneae	0.6	Araneae	111.138
Myriapoda	4	Myriapoda	0.4	Myriapoda	74.092

Table 2.

Acari (mites and ticks) emerged as the most abundant, accounting for approximately 53.5% of the total arthropod count. Other prominent orders included Coleoptera (beetles) and Collembola (springtails), which reflected the presence of organic debris in the grassy terrain. Some orders, such as Hemiptera (true bugs) and Homoptera (leafhoppers), were observed in very low numbers, with only one individual each recorded across all samples. Moderate representation was noted for Diplura (two-pronged bristletails) and Blattodea (cockroaches), though they were not dominant. Extrapolated data suggests a total population of approximately 1,463 individuals of Acari and 519 individuals of Coleoptera within the entire sampling area.

3.3 | *Site 3*

Sample 3 was collected from the area adjacent to the Campus Pharmacy on Duke University's campus. The total site area measures 5,673.01 m^2, with a perimeter of 322.93 m. Samples were collected on various dates between late September and early November 2024, ensuring representative data under consistent environmental conditions. The sampling area consisted of a combination of compacted soil and limited vegetation, characteristic of a semi-urbanized campus location. Each sample measured approximately 8.5 × 11 inches, with the total sampled area amounting to 0.604 m^2.

Total Count	n =	Mean per Sample	n =	Total Estimate for Area	n =
Acari	103	Acari	10.3	Acari	96741.72682
Collembola	7	Collembola	0.7	Collembola	6574.680464
Hymenoptera	4	Hymenoptera	0.4	Hymenoptera	3756.960265
Thysanoptera	23	Thysanoptera	2.3	Thysanoptera	21602.52152
Blattodea	1	Blattodea	0.1	Blattodea	939.2400662
Diptera	4	Diptera	0.4	Diptera	3756.960265
Coleoptera	3	Coleoptera	0.3	Coleoptera	2817.720199
Araneae	4	Araneae	0.4	Araneae	3756.960265
Isopoda	3	Isopoda	0.3	Isopoda	2817.720199
Total	152				

Table 3.

Sample 3, collected near the Campus Pharmacy, exhibited diverse arthropod populations, with Acari (mites and ticks) being the most abundant order. Acari accounted for a total of 103 individuals across all samples, representing a mean count of 10.3 per sample. Extrapolated estimates suggest that this site supports approximately 96,742 individual Acari, indicating a high density of microarthropods in this area. Thysanoptera (thrips) was the second most abundant order, with a total of 23 individuals and an extrapolated estimate of 21,603 individuals.

Less abundant orders included Collembola (springtails), Hymenoptera (ants, bees, wasps), and Diptera (flies), each with fewer than 10 individuals observed. Notably, rarer arthropods, such as Blattodea (cockroaches) and Coleoptera (beetles), were represented by a single individual each, while Isopoda (roly-polies) and Araneae (spiders) were observed in moderate numbers but were not dominant.

3.4 | *Site 4*

Sample 4 was collected from the Card Lot area on Duke University's campus, an expansive open site covering 10,862.16 m^2 with a perimeter of 399.78 m. Sampling focused on a total area of 0.302 m^2, with samples measuring approximately 8.5 × 11 inches each. The samples were collected on multiple dates, ensuring data reliability under consistent environmental conditions. This area, characterized by a mix of hard surfaces and nearby vegetation, was

characteristic of a semi-urban habitat.

Total Count	n =	Mean per Sample	n =	Total Estimate for Area	n =
Acari	153	Acari	15.3	Acari	183433.83
Araneae	51	Araneae	5.1	Araneae	61144.61
Coleoptera	24	Coleoptera	2.4	Coleoptera	86321.80
Collembola	106	Collembola	10.6	Collembola	381254.62
Diplura	4	Diplura	0.4	Diplura	14386.97
Diptera	2	Diptera	0.2	Diptera	7193.48
Ephemeroptera	3	Ephemeroptera	0.3	Ephemeroptera	10790.23
Hymenoptera	29	Hymenoptera	2.9	Hymenoptera	104305.51
Isopoda	4	Isopoda	0.4	Isopoda	14386.97
Lepidoptera	6	Lepidoptera	0.6	Lepidoptera	21580.45
Myriapoda	6	Myriapoda	0.6	Myriapoda	21580.45
Protura	7	Protura	0.7	Protura	25177.19
Psocoptera	2	Psocoptera	0.2	Psocoptera	7193.48
Scorpiones	4	Scorpiones	0.4	Scorpiones	14386.97
Thysanoptera	28	Thysanoptera	2.8	Thysanoptera	100708.77

Table 4.

Sample 4 revealed a rich diversity of arthropods, with Acari (mites and ticks) being the most abundant order, comprising a total of 153 individuals across all samples. The mean count of Acari was 15.3 per sample, and extrapolated estimates suggest a total population of approximately 183,434 Acari in the entire site. Collembola (springtails) were the second most prevalent, with a total of 106 individuals observed and an estimated population of 381,255 individuals.

The site also featured notable numbers of Araneae (spiders) and Coleoptera (beetles), with total counts of 51 and 24, respectively. Rarer orders, such as Diplura, Scorpiones (scorpions), and Psocoptera (booklice), were represented by only a few individuals each. Additionally, Hymenoptera (ants, bees, wasps) were moderately abundant, with 29 individuals recorded and an estimated total of 104,306 individuals.

Other arthropods, including Isopoda (roly-polies), Myriapoda (millipedes and centipedes), and Lepidoptera (moth and butterfly larvae), were observed, albeit at a lower rate. Extrapolated population estimates for these orders ranged from 14,387 to 21,580 individuals, reflecting their presence in the site's mixed terrain. Protura (tiny soil arthropods), typically rare in other sites, were observed at a count of 7 individuals, with an estimated population of 25,177 individuals.

3.5 | *Site 5*

Sample 5 was collected from the Edens "backyard" area on Duke University's campus. The total site area spans 1,250.72 m^2, with a perimeter of 108.72 m. Sampling focused on a total area of 0.302 m^2, with individual samples measuring approximately 8.5 × 11 inches each. The samples were collected on multiple dates from late September to late November 2024, ensuring comprehensive coverage of seasonal arthropod activity. The site features a mix of natural and landscaped environments, providing an opportunity to observe arthropod diversity in semi-controlled conditions.

Total Count	n =	Mean per Sample	n =	Total Estimate for Area	n =
Acari	74	Acari	7.4	Acari	30646.78
Araneae	36	Araneae	3.6	Araneae	14909.25
Coleoptera	5	Coleoptera	0.5	Coleoptera	2070.73
Collembola	70	Collembola	7	Collembola	28990.20
Diplura	4	Diplura	0.4	Diplura	1656.58
Diptera	2	Diptera	0.2	Diptera	828.29
Hymenoptera	2	Hymenoptera	0.2	Hymenoptera	828.29
Thysanoptera	9	Thysanoptera	0.9	Thysanoptera	3727.31

Table 5.

Sample 5 revealed substantial arthropod diversity, with Acari (mites and ticks) being the dominant order, representing a total of 74 individuals across all samples. The mean count of Acari was 7.4 per sample, with extrapolated estimates indicating a population of approximately 30,647 Acari within the site. Collembola (springtails) were the second most abundant order, with a total of 70 individuals observed and an estimated population of 28,990 individuals, reflecting their prevalence in the moist and shaded microhabitats within the area.

Moderate counts of Araneae (spiders) were observed, totaling 36 individuals and an extrapolated population of 14,909 individuals. Other arthropods, including Coleoptera (beetles), Diplura (two-pronged bristletails), and Thysanoptera (thrips), were present in smaller numbers but remained ecologically significant. Orders such as Diptera (flies) and Hymenoptera (ants, bees, wasps) were rare, with only two individuals recorded for each, resulting in extrapolated populations of approximately 828 individuals for each order.

3.6 | ***Site 6***

Sample 6 was collected from the forested area behind Duke University's chapel, specifically on the side closest to the Biological Sciences Building. The total site area spans 5,669.36 m², with a perimeter of 339.85 m. Sampling was conducted across a total area of 0.604 m², with individual samples measuring 0.0603 m² each. Collections occurred on three different dates: September 23, October 10, and October 25, 2024 to capture seasonal variations in arthropod activity. This site is characterized by dense tree coverage and moist leaf litter, creating an environment conducive to diverse arthropod populations.

Total Count	n =	Mean per Sample	n =	Total Estimate for Area	n =
Collembola	50	Collembola	5	Collembola	46931.79
Coleoptera	9	Coleoptera	0.9	Coleoptera	8447.72
Diplura	1	Diplura	0.1	Diplura	938.64
Diptera	3	Diptera	0.3	Diptera	2815.91
Hymenoptera	8	Hymenoptera	0.8	Hymenoptera	7509.09
Protura	9	Protura	0.9	Protura	8447.72
Thysanoptera	22	Thysanoptera	2.2	Thysanoptera	20649.99
Acari	405	Acari	40.5	Acari	380147.48
Araneae	26	Araneae	2.6	Araneae	24404.53
Myriapoda	4	Myriapoda	0.4	Myriapoda	3754.54

Table 6.

Sample 6 demonstrated high arthropod diversity, with Acari (mites and ticks) being the most abundant order. A total of 405 Acari individuals were observed, with a mean of 40.5 per sample and an extrapolated population of approximately 380,147 individuals across the entire site. Collembola (springtails) were the second most prevalent, with a total count of 50 individuals, a mean of 5 per sample, and an estimated population of 46,932 individuals, reflecting the suitability of this site's moist microhabitats for these organisms.

Other frequently observed orders included Araneae (spiders), with 26 individuals and an estimated population of 24,405 individuals, and Thysanoptera (thrips), which accounted for 22 individuals and an extrapolated population of 20,650 individuals. Moderate populations of Coleoptera (beetles), Hymenoptera (ants, bees, wasps), and Protura (tiny soil arthropods) were also noted, with estimated populations ranges of 7,509 to 8,448 individuals.

Rarer orders, such as Diplura (two-pronged bristletails), Myriapoda (millipedes and centipedes), and Diptera (flies), were represented by fewer individuals. Notably, Protura populations were slightly elevated compared to other sample sites.

3.7 | ***Site 7***

Sample 7 was collected from the Hollows residential and Towerview road area on Duke University's campus. This site spans a total area of 11,348.89 m², with sampling conducted over 0.603 m², divided into multiple smaller samples (each approximately 0.060 m²). The samples were collected on two dates, September 29 and October 6, 2024, ensuring that the data represents a range of early autumn arthropod activity. This site features a mix of landscaped grounds and surrounding natural vegetation.

Total Count	n =	Mean per Sample	n =	Total Estimate for Area	n =
Collembola	28	Collembola	2.8	Collembola	52610.75
Coleoptera	23	Coleoptera	2.3	Coleoptera	43215.97
Hymenoptera	8	Hymenoptera	0.8	Hymenoptera	15031.64
Blattodea	7	Blattodea	0.7	Blattodea	13152.69
Araneae	4	Araneae	0.4	Araneae	7515.82
Diptera	2	Diptera	0.2	Diptera	3757.91

Table 7.

The Hollows and Towerview site demonstrated moderate arthropod diversity, with Collembola (springtails) being the most dominant order, totaling 28 individuals across all samples. The mean count of Collembola per sample was 2.8, and the extrapolated population for the entire site was estimated to be 52,611 individuals, highlighting the prevalence of springtails in this area.

Coleoptera (beetles) was the second most abundant order, with 23 individuals observed. The mean count was 2.3 per sample, leading to an extrapolated population estimate of 43,216 individuals. Other notable but less abundant orders included Hymenoptera (ants, bees, wasps), Blattodea (cockroaches), and Araneae (spiders), which had estimated site populations of 15,032, 13,153, and 7,516 individuals, respectively. These arthropods were present in varying quantities across the different sampling periods, with higher concentrations observed during the October 6 collections.

Diptera (flies) were the least abundant, with only two individuals observed, resulting in a site-wide extrapolated population of 3,758 individuals.

3.8 | ***Site 8***

Sample 8 was collected from the area in front of the Sarah P. Gardens on Duke University campus. The total site area covers 3,995.64 m², with sampling conducted over 0.603 m² in total, divided into 10 smaller samples of 0.0603 m² each. All samples were collected on October 10, 2024, ensuring consistency in environmental conditions during the collection period. The area is characterized by landscaped grounds, open spaces, and nearby shaded regions.

Total Count	n =	Mean per Sample	n =	Total Estimate for Area	n =
Acari	422	Acari	42.2	Acari	279165.58
Collembola	119	Collembola	11.9	Collembola	78722.05
Hymenoptera	16	Hymenoptera	1.6	Hymenoptera	10584.48
Araneae	22	Araneae	2.2	Araneae	14553.66
Coleoptera	6	Coleoptera	0.6	Coleoptera	3969.18
Thysanoptera	4	Thysanoptera	0.4	Thysanoptera	2646.12
Diptera	6	Diptera	0.6	Diptera	3969.18
Blattodea	5	Blattodea	0.5	Blattodea	3307.65
Protura	2	Protura	0.2	Protura	1323.06
Isopoda	1	Isopoda	0.1	Isopoda	661.53
Myriapoda	4	Myriapoda	0.4	Myriapoda	2646.12

Table 8.

The most abundant arthropod order observed was Acari (mites and ticks), with a total count of 422 individuals across all samples, resulting in a mean count of 42.2 per sample. The extrapolated population for Acari across the entire site is estimated at 279,166 individuals, reflecting the site's suitability for mite populations, likely due to its combination of soil and vegetation.

Collembola (springtails) were the second most abundant, with a total count of 119 individuals, a mean of 11.9 per sample, and an extrapolated population estimate of 78,722 individuals.

Other notable arthropod orders include Hymenoptera (ants, bees, wasps), with 16 individuals and an estimated site population of 10,584 individuals, and Araneae (spiders), with 22 individuals and an extrapolated population of 14,554 individuals. Orders such as Coleoptera (beetles), Blattodea (cockroaches), and Diptera (flies) were observed in smaller numbers, each with an estimated site population ranging from 3,969 to 3,307 individuals.

Rarer orders, including Thysanoptera (thrips), Protura, Isopoda (roly-polies), and Myriapoda (millipedes and centipedes), contributed to the overall biodiversity but were represented by fewer than 5 individuals each.

3.9 | ***Site 9***

Sample 9 was collected from the Duke Pond area on Duke University's campus, a large and diverse habitat covering 37,808.38 m² with a perimeter of 865.09 m. Sampling was conducted over a total area of 0.302 m², with each individual sample measuring approximately 8.5 × 5.5 inches. All samples were collected on October 10, 2024, under consistent environmental conditions to capture a snapshot of arthropod diversity in this aquatic and semi-aquatic ecosystem. This site includes areas of water, riparian zones, and surrounding vegetation.

Total Count	n =	Mean per Sample	n =	Total Estimate for Area	n =
Coleoptera	1	Coleoptera	0.1	Coleoptera	2700.28
Collembola	11	Collembola	1.1	Collembola	29703.06
Diptera	5	Diptera	0.5	Diptera	13501.39
Hymenoptera	3	Hymenoptera	0.3	Hymenoptera	8100.83
Thysanoptera	3	Thysanoptera	0.3	Thysanoptera	8100.83
Acari	67	Acari	6.7	Acari	180918.64

Table 9.

The Duke Pond site displayed moderate arthropod diversity, with Acari (mites and ticks) being the dominant order. A total of 67 Acari individuals were observed across all samples, resulting in a mean count of 6.7 per sample. The extrapolated population estimate for Acari at this site is approximately 180,919 individuals, reflecting their high prevalence in this environment. Collembola (springtails) were the second most abundant order, with 11 individuals recorded, a mean count of 1.1 per sample, and an extrapolated population estimate of 29,703 individuals. Diptera (fly larvae) were also prominent, with 5 individuals observed, translating to a mean of 0.5 per sample and an estimated population of 13,501 individuals.

Other notable orders include Hymenoptera (ants, bees, wasps) and Thysanoptera (thrips), each represented by 3 individuals, with a mean count of 0.3 per sample and an extrapolated population of 8,101 individuals per order. Coleoptera (beetles) was the least abundant order, with just one individual recorded across all samples, resulting in an estimated site population of 2,700 individuals.The data also revealed localized variability in arthropod counts, particularly for Acari, which ranged from 7 to 18 individuals across different samples.

4 | Discussion

Overall, these nine samples provide a comprehensive picture of the diversity of insects across a broad variety of habitats, including forested and lawn plots as well as paved areas with more foot traffic. This data emphasizes the influence of habitat structure, microclimate, local vegetation, and unique environmental differences on the abundance and composition of different insect orders within Duke's campus.

4.1 | *High Acari Density Across Multiple Sites*

Across multiple sites, the Arachnid order Parasitiformes composed of ticks and mites, vastly outnumbered other orders and classes of insects. The Acari order predominated in forested and moist collection sites, such as Site 1 and Site 6 (both in the forested area behind Duke Chapel) as well as landscaped, more urban sites, such as Site 3 (near Campus Pharmacy) and Site 4 (Card Lot). Their abundance ranged from ~53.5% of the total arthropod (insects and other species in the Arthropoda phylum) population for Site 2 to over 80% of the total arthropod population for forested plots such as Site 1.

A testament to the adaptability and resistance of ticks and mites, particularly on Duke's campus, this dominance may be due to a number of factors, each stemming from their environment selection and physiological adaptations to harsher conditions. Species within the Acari order typically live in moist leaf litter and soil with high organic content (Walter & Proctor, 2013), allowing them to occupy a wide range of microhabitats at especially high rates. Furthermore, the relatively short life cycles and high reproductive rates of species in the Acari order allow them to propagate rapidly within the substrate. Additionally, the roles mites and ticks occupy within their ecosystems vary significantly–for example, mites may either function as predators or detritivores, aiding in decomposition–an indication that they harbor efficient nutrient cycling processes and stable, detritus-based food webs [10].

4.2 | *High Collembola Density in Forested, Moist Areas*

Collembola (springtail) population density was particularly high within sites containing large quantities of dense, moist soil–these sites could either be forested or landscaped and semi-urban, where mulch and irrigation processes can simulate typical habitat conditions in natural forests for springtails. Collembola are known soil quality indicators, given their reliance on moist environments and organic debris [11]. The extrapolated population sizes of Collembola in both forested sites, such as Sites 1 and 6 (~98,560 individuals in Site 1 and ~46,932 individuals in Site 6, respectively), and in semi-urban, landscaped sites, such as Site 4 (~381,255 individuals), points to the heterogeneity and high soil quality of habitats across campus. Furthermore, the Collembola population density in areas with lower quality, more compacted soil and less vegetation coverage, such as in Site 3 (~6575 individuals), was much lower, emphasizing their dependence on the nutrient-rich, moist soil found in other areas on Duke's campus.

4.3 | *Site-Specific Variation*

While some insect and arthropod orders, such as Acari and Collembola, were more consistently dense across multiple sites, other orders varied more significantly by site. For example, members of the Hymenoptera order, including bees, ants, and wasps, were moderately abundant in Sites 1 and 8 (~24,303 individuals in Sample 1 and ~10,584 individuals in Sample 8, respectively), but fluctuated seasonally, with samples collected in mid-October bearing higher density measurements. October 2024 was a particularly warm month, ranking as the second-highest October since the National Oceanic and

Atmospheric Administration began weather record-keeping in 1850 [12], which may have contributed to more favorable weather conditions for vegetation such as flowers and other plants. This warm weather and flowering vegetation may have been more suitable for bees and wasps, for example, that rely heavily on flowers and pollination for nutrients. Furthermore, the particularly high numbers of Hymenoptera in Sites 4 and 8 (~104,306 individuals in Site 4, ~10,585 individuals in Site 8) indicate a preference for exposed soil and flowering vegetation.

Other orders also fluctuated by site. For example, species in the Thysanoptera (thrips) order were more abundant in sites with floral surfaces and vegetation, such as Sites 3, 4, and 6 (~21,603 individuals in Site 3, ~100,709 individuals in Site 4, ~20,650 individuals in Site 6). This abundance reflects their pollen-feeding and plant-feeding habits, similar to Hymenoptera above. Furthermore, the thrips population exceeded 100,000 individuals in Site 4, indicating their potential to surge in numbers when environmental conditions allow it [13]. These findings underscore the variety of conditions, microhabitats, and climates of sites on Duke's campus, each able to harbor different species at different abundances.

4.4 | *Rare Orders*

A striking finding was the abundance of rare insect orders such as Diplurans and Proturans in certain sites. Although typically rare and only represented by a few insects per sample, there was a moderately high abundance in forested sites such as Sites 1 and 6 of both Diplura (~1,351 individuals in Site 1, ~939 individuals in Site 6) and Protura (~1,351 individuals in Site 1, ~8,448 individuals in Site 6). These sites, which are less disturbed than other, more urban sites due to less foot traffic, may be more conducive to greater Diplura and Protura propagation and better survival conditions.

4.5 | *Ecological Implications, Limitations, and Future Directions*

Based on our extrapolated population estimates, the amount of insects on Duke's campus is extensive. For example, using the campus area of approximately 3,500,000 m2, we estimate a total population of roughly 2.5 billion Acari across all sampled habitats. Assuming proportional arthropod distribution, a single Duke dorm room, with an average area of approximately 17 m2 [14], could contain over 10,000 Acari!

Such extrapolations provide a perspective on the density and ecological impact of soil-dwelling arthropods. These organisms play critical roles in nutrient cycling, soil aeration, and organic matter decomposition, highlighting their ecological value even in highly urbanized environments like Duke's campus. However, it is important to note the limitations of our study. These population estimates are based on localized sampling and assume uniform distribution across habitats. This approach may not fully account for the considerable ecological diversity present in urban landscapes, such as variations in soil composition, vegetation density, and microclimatic conditions. Additionally, seasonal fluctuations in insect populations, driven by factors like temperature and rainfall, could influence the accuracy and reliability of our findings. These limitations further the need for more comprehensive sampling strategies to better capture the complexity of urban biodiversity.

Future research should expand sampling efforts to include additional habitats, such as aquatic ecosystems and underrepresented urban niches, to provide a more comprehensive picture of campus-wide biodiversity. Investigating the function roles of dominant taxa, such as Acari and Collembola, could also illuminate their contributions to ecosystem processes. Furthermore, studies on the resilience of these populations to urbanization and climate stressors would provide insights into their adaptive mechanisms, such as behavioral and physiological changes, that enable survival in challenging conditions. This information could directly inform conservation strategies aimed at preserving biodiversity by identifying habitat features that support resilient populations. For instance, understanding how soil moisture, organic matter, and temperature variations influence population dynamics can guide urban planning efforts to create more hospitable environments for arthropods. Additionally, these studies could aid in predicting how future environmental changes, such as increased urban

sprawl or shifting climate patterns, might impact the diversity and functionality of soil arthropod communities in urban landscapes.

Acknowledgements

Data collected by Alex Ozonoff, Anna Tharakan, Gurnoor Majhail, Jayla Eckhoff, Joy Buchi-Ahiabuike, Kit Shauf, Lydia Cox, Neha Shaw, Nirali Patel, Redeat Takele, and Riley Hamp. Special thanks to Dr. H. Frederick Nijhout and Emily Brady for their guidance!

References

1. Gebremariam, H.G. (2024). A systematic review of insect decline and discovery: Trends, drivers, and conservation strategies over the past two decades. *Psyche: A Journal of Entomology*, 5998962. doi.org/10.1155/2024/5998962
2. van Klink, R., Bowler, D.E., Gongalsky, K.B., Swengel, A.B., Gentile, A., Chase, J.M. (2020). Meta-analysis reveals declines in terrestrial but increases in freshwater insect abundances. *Science, 368*: 417-420.doi.org/10.1126/science.aax9931
3. Vaz, S., Manes, S., Khattar, G., Mendes, M., Silveira, L., Mendes, E., de Morais Rodrigues, E., Gama-Maia, D., Lucia Lorini, M., Macedo, M., Cesar Paiva, P. (2023). Global meta-analysis of urbanization stressors on insect abundance, richness, and traits. *Science of the Total Environment, 903*: 165967. doi.org/10.1016/j.scitotenv.2023.165967
4. Kwon, T., Kim, Y.S., Lee, S.W., Park. Y. (2016). Changes of soil arthropod communities in temperate forests over 10 years (1998-2007). Journal of Asia-Pacific *Entomology, 19*(1): 181-189. doi.org/10.1016/j.aspen.2016.01.003.
5. Tabari, H. (2022). Climate change impact on flood and extreme precipitation increases with water availability. *Scientific Reports, 10*: 13768. doi.org/10.1038/s41598-020-70816-2
6. Trenberth, K.E., Dai, A., van der Schrier, G., Jones, P.D., Barichivich, J., Briffa, K.R, & Sheffield, J. (2014). Global warming and changes in drought. *Nature Climate Change, 4*, 17-22. doi.org/10.1038/nclimate2067
7. Wise, D.H., Lensing, J.R. (2019). Impacts of rainfall extremes predicted by climate-change models on major trophic groups in the leaf litter arthropod community. *Journal of Animal Ecology, 88*: 1486-1497. doi.org/10.1111/1365-2656.13046
8. Bagyaraj, D.J., Nethravathi, C.J., Nitin, K.S. (2016). Soil biodiversity and arthropods: Role in soil fertility. In: Chakravarthy, A., Sridhara, S. (eds) Economic and Ecological Significance of Arthropods in Diversified Ecosystems. Springer, Singapore. doi.org/10.1007/978-981-10-1524-3_2
9. U.S. Census Bureau. *Durham County, North Carolina*. Retrieved December 6, 2024, from https://data.census.gov/profile/Durham_County,_North_Carolina?g=050XX00US37063
10. Walter, D. E., & Proctor, H. C. (2013). Mites: Ecology, Evolution & Behaviour: Life at a Microscale. Springer.
11. Hopkin, S. P. (1997). Biology of the Springtails (Insecta: Collembola). Oxford University Press.
12. National Oceanic and Atmospheric Administration [NOAA]. (2024, November 13). Planet saw its 2nd warmest October in 175-year record. [Press release]. https://www.noaa.gov/news/planet-saw-its-2nd-warmest-october-in-175-year-record
13. Mound, L. A. (2005). Thysanoptera: Diversity and interactions. Annual Review of Entomology, 50(1), 247–269.
14. Duke University Housing and Residence Life, Duke Student Affairs. *Upper Class Housing*. https://students.duke.edu/living/housing/upperclass-housing/

Vertices: Duke's Undergraduate Research Journal Volume 4, Issue 1 | Spring 2025

Exploring Olfactory Circuits in Drosophila: Connectomic Insights into Neural Connectivity, Behavioral Outputs, and Neurotransmitter Pathways

Nicholas Sangvai, Jinchen Wen, Joanna Kang, Walter Kornfeld, Talia Penn

Volume 4, Issue 1

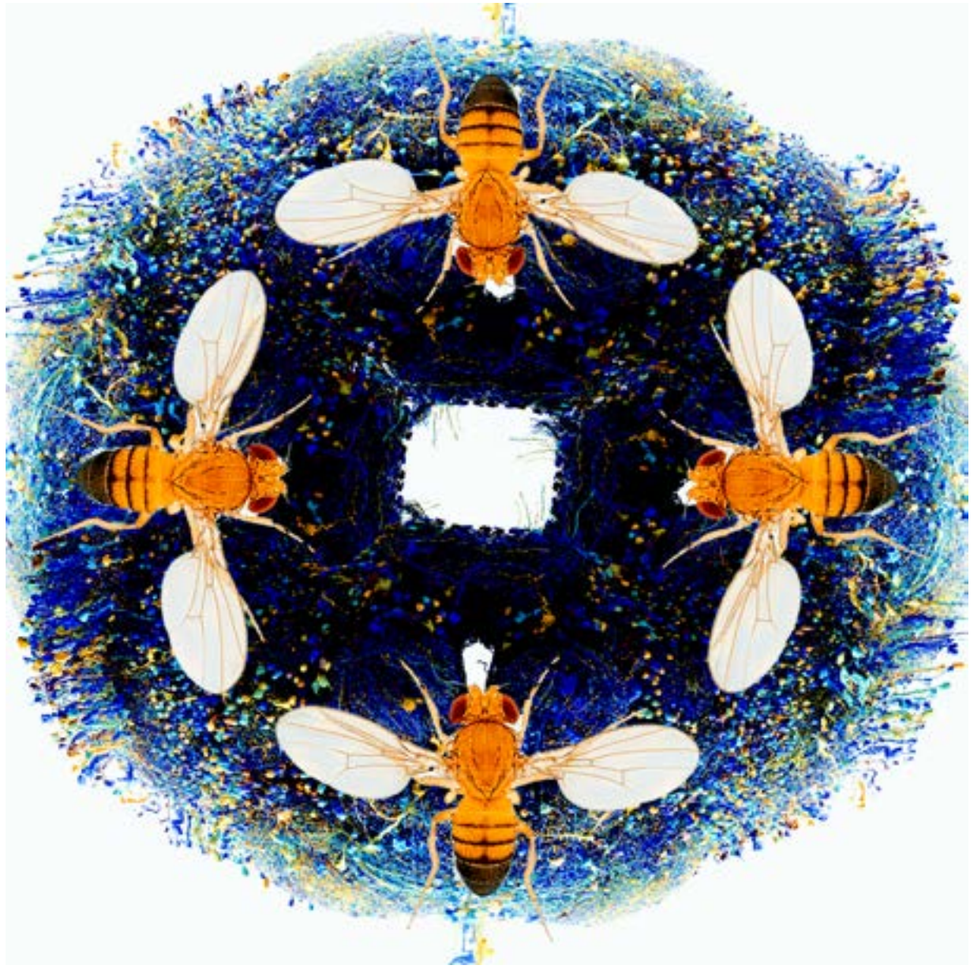

Graphic by Monet Shum

Vertices: Duke's Undergraduate Research Journal Volume 4, Issue 1 | Spring 2025

Exploring Olfactory Circuits in Drosophila: Connectomic Insights into Neural Connectivity, Behavioral Outputs, and Neurotransmitter Pathways

Nicholas Sangvai, Jinchen Wen, Joanna Kang, Walter Kornfeld, Talia Penn

Duke University
https://doi.org/10.55894/dv4.12

Abstract

Using the FlyWire connectome, we conducted a comparative analysis of olfactory pathways in the female Drosophila melanogaster brain to investigate the relationship between neuronal structure, connectivity, and behavioral function. Our findings confirmed functional segregation at early neuronal levels and revealed conserved higher-order connectivity across attractive pheromonal and aversive food-odorant pathways, with distinct differences for the Ir64a receptor, potentially linked to its role as an acid-sensing ionotropic receptor. Connectivity to serotonergic, dopaminergic, insulin-producing, and circadian circuits highlighted potential roles in mediating innate and social behaviors, such as mating and aggression. While the static nature of the Drosophila connectome limits insights into developmental and sex-specific variations, this study provides a foundation for future research into connectomics and the structural and connective bases of behavior.

Introduction

Before the advent of the fly connectome, the understanding of olfactory connections and odor responses relied on single-cell labeling and manual tractography analysis of individual flies through complicated experimentation (Jefferis et al., 2004). With the release of the electron microscopy dataset of a full adult fly brain, researchers relied on manual skeletonization to reconstruct neural circuits from existing data (Cardona et al., 2012). FlyWire, in contrast, enables true three-dimensional interactive proofreading and serves as a searchable data bank of all neuronal connections in a Drosophila melanogaster hemibrain using Electron Microscopy and deep learning. The connectome, a comprehensive collection of neuronal connections of the hemibrain, is of increasing interest because it serves as a foundational framework to study individual circuits and their relevance to behavioral outputs at an unprecedented level of detail (Scheffer et al., 2020). The focus of the fly connectome specifically is of significance due to its role of D. melanogaster as a model organism in circuit neuroscience. Understanding neuronal connectivities in Drosophila may prove crucial to advancing our knowledge and understanding of universal principles of brain function, neuroplasticity, learning and memory, and disease that can be subsequently applied to various organisms including the human brain.

To evaluate these circuits, we performed a connectomic analysis of the female Drosophila brain using FlyWire. Five unique olfactory receptors were chosen for their unique glomerular targets and involvement in opposing behavioral processes. For each receptor, comprehensive profiles of the downstream neuronal partners were constructed in a class-based manner, from the peripheral receptor neuron to third-order connections. From these profiles, representative neurons were selected to build olfactory circuit motifs and pathways that both localize to the antenna lobe and span the entire hemibrain. Individually constructing representative circuit pathways that extend beyond the projection neuron enabled a comparative visual analysis of these pathways across the five receptors. This revealed architectural differences that, along with the structure and function of the circuit-terminating neuron, may provide the basis for differences in the behaviors mediated by these receptors.

Background

Exploratory research was conducted using FlyWire.AI, an AI-segmented whole-brain connectome of a 5-day-old female of wild-type Canton S strain *Drosophila melanogaster*. The connectome itself was constructed through a joint effort of researchers and engineers to reconstruct neurons and chemical synapses using Focused Ion Beam Scanning Electron Microscopy, machine-learning algorithms, and 50-person years of proofreading effort to create neuron skeletons, synapse locations, and connectivity graphs (Scheffer et al., 2020). To conduct the investigation, five well-known olfactory receptors (Ors) that engage different social processes were explored along with their respective neural circuits.

FlyWire was used to determine the connectivity between individual neurons and neuronal classes to trace paths from peripheral sensory neurons to higher olfactory centers. For each receptor, the numbers of olfactory receptor neurons (ORNs), projection neurons (PNs), and local neurons (LNs) were found using FlyWire's Search and Explore (Cell Type) toolbar. This analysis was only performed on the left side of the fly brain. From this, preliminary neuronal circuit motifs that localize to the antennal lobe (AL) neuropil of the *Drosophila* brain were identified. Next, available PNs were analyzed and representative PNs were then selected for each PN type—on the basis of neurotransmitter type, morphology, and connectivity—to further explore pathways reaching third-order neurons. FlyWire's 3D and Connectivity (Pathways) tools were used to map from the representative PN's glomerulus to the mushroom body cortex (MB), lateral horn (LH), and third-order brain regions, noting patterns of innervation and synaptic density, as well as the strength of synapses and the number of hops from the PN to the third-order neuron.

Pathways to terminal neurons expressing different neurotransmitter types (dopamine, serotonin, insulin) in addition to CRY-expressing clock neurons, used to develop and stabilize the circadian rhythm, were also explored using FlyWire's Connectivity (Pathways) tool. Individual pathways were superimposed on a 3D-represented modular fly brain to visually represent complete neural circuits for each receptor. These pathways were then layered to compare differences in region, connectivity, and morphology between each circuit. Together these approaches enabled a more complete representation and understanding of the neural pathways in *D. melanogaster*.

Connectomic analysis was performed using FlyWire's pathway connectivity tool under *Connectivity/Pathway*. The minimum synapse count was set to 10 to represent a robust synapse and reduce noise. A representative starting PN was then picked for each glomerulus and the target cells were those expressing the specific neurotransmitter of interest. This generated a table (Table 1.) of connection counts between different neuron types and the number of hops necessary for connection.

Results

By understanding the differences between olfactory circuit structures across different behavioral contexts, we can begin to elucidate the relationships between neuronal connectivity and behavioral function. Ultimately, deciphering these pathways may lead to a greater overall understanding of systems neuroscience and lead to advancements in more complex organisms.

General Findings

ORNs gather information from the periphery and

Table 1: Distance table between a representative neuron and downstream partners

LEFT SIDE ONLY	Or47b (VA1v) Attractive ->>> Pheromone ->>	Or88a (VA1d)	Or67d (DA1) - cVA	Or56a (DA2) Repulsive ->>> Food ->>	Ir64a (DC4)
ORNs	**48** *NT breakdown:* 28 ACH 5 SER 15 unclassified	**48** *NT breakdown:* 29 ACH 3 SER 14 unclassified	**60** *NT breakdown:* 49 ACH 4 SER 7 unclassified	**17** *NT breakdown:* 16 ACH 1 unclassified	**11** *NT breakdown:* 11 ACH
PNs	**6** adPN: 4 (ACH) vPN: 2 (GABA)	**3** adPN: 2 (ACH) vPN: 1 (GABA)	**9** lPN: 8 (ACH) vPN: 1 (GABA)	**5** lPN: 5 (ACH)	**3** adPN: 1 (ACH) vPN: 2 (GABA)
LNs	*From 1 adPN:* *(AL.LH.61)* 18 upstream 28 downstream *From 1 vPN:* *(AL.LH.100)* 20 upstream 0 downstream	*From 1 adPN:* *(AL.MB_CA.43)* 35 upstream 36 downstream *From 1 vPN:* *(AL.LH.118)* 5 upstream 0 downstream	*From 1 lPN:* *(AL.MB_CA.129)* 16 upstream 18 downstream *From 1 vPN:* *(AL.LH.97)* 12 upstream 0 downstream	*From 1 lPN:* *(AL.LH.112)* 6 upstream 2 downstream	*From 1 adPN:* *(AL.LH.23)* 61 upstream 53 downstream *From 1 vPN:* *(AL.LH.271)* 0 upstream 0 downstream
MB Paths	*From 1 adPN:* *(AL.LH.61)* 39 Kenyon Cells 1 MBIN *From 1 vPN:* *(AL.LH.100)* 0 Kenyon Cells	*From 1 adPN:* *(AL.MB_CA.43)* 87 Kenyon Cells 1 MBIN *From 1 vPN:* *(AL.LH.118)* 0 Kenyon Cells	*From 1 lPN:* *(AL.MB_CA.129)* 38 Kenyon Cells *From 1 vPN:* *(AL.LH.97)* 1 Kenyon cell 1 MBIN	*From 1 lPN:* *(AL.LH.112)* 21 Kenyon Cells	*From 1 adPN:* *(AL.LH.23)* 74 Kenyon Cells 1 MBIN *From 1 vPN:* *(AL.LH.271)* 0 Kenyon Cells
LH Paths	*From 1 adPN:* *(AL.LH.61)* 27 LHLNs 1 LHCENT 54 No Class *From 1 vPN:* *(AL.LH.100)* 13 LHLNs 53 No Class	*From 1 adPN:* *(AL.MB_CA.43)* 22 LHLNs 1 LHCENT 70 No Class *From 1 vPN:* *(AL.LH.118)* 12 LHLNs 43 No Class	*From 1 lPN:* *(AL.MB_CA.129)* 2 LHLNs 49 No Class *From 1 vPN:* *(AL.LH.97)* 3 LHLNs 2 LHCENT 62 No Class	*From 1 lPN* *(AL.LH.112)* 7 LHLNs 36 No Class	*From 1 adPN:* *(AL.LH.23)* 31 LHLNs 2 LHCENT 106 No Class *From 1 vPN:* *(AL.LH.271)* 4 LHLNs 1 LHCENT 4 No Class

Table 2: Profiles of five olfactory receptors (Or) with their corresponding ORNs, projection neurons (PNs), local interneurons (LNs), Mushroom Body neurons, and Lateral Horn neurons. LNs, MB path, and LH path neuron counts are totaled from a representative projection neuron of the respective receptor. Only neurons on the left side of the hemibrain are counted.

convert the chemical reception into electrical signals transmitting a centralized signal to their respective (Couto et al., 2005). For all five receptor neuron classes, acetylcholine is the primary neurotransmitter utilized in synaptic transmission. The three receptors involved in pheromonal sensing, Or47b, Or88a, and Or67d, which also are all attractive, also utilize serotonin, however to a lesser extent. In addition to a more diversified neurotransmitter profile, the three pheromone-sensing ORN classes have a greater average neuron count (n = 52) compared to the two non-pheromonal receptor neurons, which are all aversive, (n = 14) (Table 2).

PNs are the acting relay centers between higher orders of the brain and sensory neurons—such as those in the antennae—that act in both bottom-up and top-down processing and determine responses to external stimuli (Marin et al., 2002). There are three classes of PNs that are defined by both the neuropil(s) to which they project and their respective neurotransmitter profiles. Anterodorsal PNs (adPNs) are cholinergic. They project to lateral horn (LH) neurons (n=28 on average) and mushroom body (MB) neurons via the inner antennocerebral tract (iACT), as well as to AL local neurons. Ventral PNs (vPNs) are gabaergic and their axons project through the medial antennocerebral tract (mACT). They typically have fewer connections to LH neurons (n = 8); they do not project to MB neurons or AL local neurons. Lastly, lateral PNs (lPNs) are cholinergic and their axons project through the iACT onto LH neurons and MB neurons, and back onto AL local neurons. However, they project to fewer LH neurons (n=4.5) than either adPNs or vPNs (Table 2).

Extracellular serotonin concentration at the steady state was graphed on the x-axes, and the number of individuals in a given population of 1000 for a given range of *eht* values was graphed on each y-axis. While there were some visible differences between the three populations, the distribution of extracellular serotonin at the steady state was roughly the same, with an approximately bell-curved shape with maximum frequencies near 60 nM. It should be noted well that the numerical values of extracellular serotonin concentration are not as important, since again, the steady state values and enzyme expression levels are known to differ across different projection regions **[6]**. While we focused on the CA2 region of the hippocampus in these simulations, the steady state values of extracellular serotonin could very well be distributed around 40 nM or 80 nM in other regions of the brain.

Local neurons (LNs) in the AL mediate the responsiveness of ORNs and PNs to olfactory stimuli (Chou et al., 2010). Among the three PN classes, adPNs have the highest average number of LNs both upstream (n = 38) and downstream (n = 39). Compared to adPNs, lPNs have fewer numbers of upstream (n = 11) and downstream LNs (n = 10), on average. The vPNs have a comparable average number of upstream LNs (n = 9.25) to lPNs, but no downstream LN partners (n = 0) (Table 2).

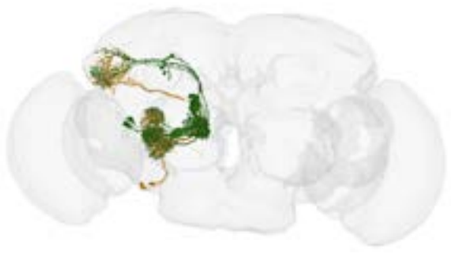

Figure 1: Nine representative projection neurons from the five olfactory receptors and respective glomeruli. Colored by neurotransmitter type: GABA neurons are orange, and acetylcholine neurons are green. All four vPNs (AL.LH.100, AL.LH.118, AL.LH.97, AL. LH.271) take the mACT tract, bypass the Mushroom Body, innervate the Lateral Horn, and use GABA. The three adPNs (AL.LH.61, AL.MB_CA.43, AL.LH.23) and two lPNs (AL.MB_CA.129, AL.LH.112) share a spatial and neurotransmitter profile; they take the iACT tract, innervating the Mushroom Body and the Lateral Horn in a bifurcated branch pattern, and use acetylcholine.

Attraction

ORNs expressing Or47b localize to the VA1v glomerulus to mediate sociosexual interactions via pheromone sensing (Dweck et al., 2015). Forty-eight ORNs synapse onto the left VA1v glomerulus and adPNs and vPNs project from this glomerulus. The representative adPN, AL.LH.61, projects to 4 types of higher-order classified cells in the MB and LH, including an MB interneuron (MBIN), Kenyon

cells, and LH centrifugal neurons (LHCENT; Table 2). ORNs expressing Or88a localize to the VA1d glomerulus and are responsible for mediating attraction in male and female flies (Dweck et al., 2015). Forty-eight ORNs synapse onto the left VA1d glomerulus, and adPNs and vPNs also project from this glomerulus. ORNs expressing Or67d localize to the DA1 glomerulus and mediate responses to the male sex pheromone cis vaccenyl-acetate (cVA) (Kurtovic et al., 2007). Sixty ORNs synapse onto the left DA1 glomerulus and lPNs and vPNs project from this glomerulus. These three glomeruli—VA1v, VA1d, DA1—are clustered in the Antenna Lobe (Figure 2).

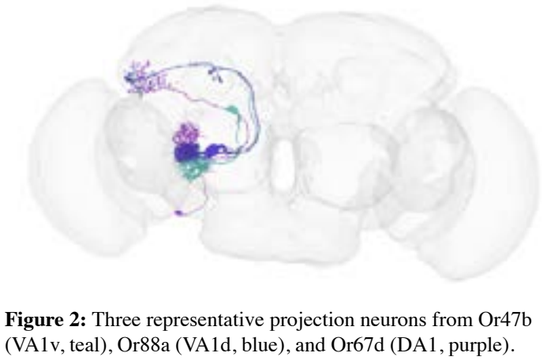

Figure 2: Three representative projection neurons from Or47b (VA1v, teal), Or88a (VA1d, blue), and Or67d (DA1, purple). These three olfactory receptors receive attractive pheromonal cues. The three respective glomeruli cluster on the lateral edge of the antenna lobe.

Aversion

ORNs expressing Or56a localize to the DA2 glomerulus and mediate avoidance behaviors to substances produced by potentially harmful microbes; one example is geosmin, a substance produced by fungi that is not itself toxic but co-occurs with other harmful substances (Stensmyr et al., 2012). Seventeen ORNs synapse onto the left DA2 glomerulus; lPNs project from this glomerulus. Receptor neurons that express Ir64a localize to the DC4 glomerulus and similarly to Or56a mediate avoidance behaviors to acidic pH that is harmful to the fly (Ai et al., 2010). Eleven ORNs synapse into the DC4 glomerulus, all of which are cholinergic; adPNs and vPNs project from this glomerulus. These two glomeruli—DA2 and DC4—are clustered in the Antenna Lobe (Figure 3).

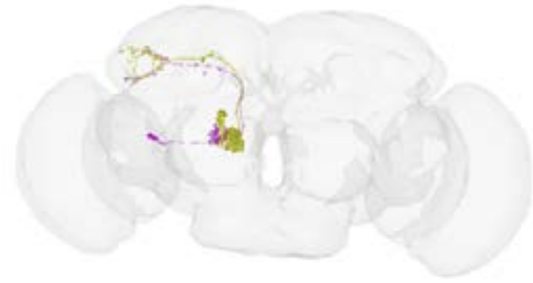

Figure 3: Two representative projection neurons from Or56a (DA2, pink) and Ir64a (DC4, yellow). These two olfactory receptors receive repulsive food-odor cues. The two respective glomeruli cluster in the antenna lobe.

Neurotransmitter Specific Pathways

Dopamine

Dopamine is involved in locomotion, learning & memory, sleep, and arousal cycles, as well as sexual behavior in courtship (Yamamoto et al., 2014). In the VA1v glomerulus the Or47b ORN, whose primary function is to detect methyl laurate (ML), a pheromone for copulation behavior, we see very few, if any, higher-order neurons that utilize Dopamine as its neurotransmitter (Dweck et al., 2015). This is evidenced by a search query of a representative adPN (AL.LH.61) as well as a representative vPN (AL.LH.100) in Flywire of the number of hops required to reach a dopamine-producing third-order neuron with a minimum synapse count of 10. For the representative Or47b adPN, the modal hop count is 4 interconnects. For the representative Or47b vPN, the modal hop count is also 4 interconnects.

Similarly, Or88a, which coexists with Or47b in the same sensory neuron (at4) and responds to methyl laureate (ML), methyl myristate (MM), and methyl palmitate (MP), also utilizes dopamine minimally in third-order neurons (Dweck et al., 2015). For the representative Or88a adPN (AL.MB_CA.43), the modal hop count is 3 interconnects before reaching a dopamine-expressing neuron. For representative Or88a vPN (AL.LH.118), the modal hop count is 4 interconnects

In the DA1 glomerulus, Or67d utilizes dopamine to mediate the detection of male pheromone cVA

Figure 4a: Dopamine neuron, SCL.WED.1, of neuron class Dnp32. This neuron produces neuropeptide dromyosuppressin (DMS).
Figure 4b: Projection neuron AL.LH.97 from olfactory receptor Or67d synapses directly onto SCL.WED.1 (one hop, 6 synapses).

Figure 5a: Serotonin neuron, SLP.GNG.3, of neuron class Dnp62. This neuron produces neuropeptide drosulfakinin (DSK). **Figure 5b**: Projection neuron AL.LH.97 from olfactory receptor Or67d synapses onto lateral horn neuron, LH.SLP.802, which synapses onto SLP.GNG.3 (two hops).

and subsequently instigate a response in drosophila (Kurtovic et al., 2007). In females, cVA acts as an attractive pathway encouraging mating whereas cVA is a repulsive pathway in male drosophila (Kurtovic et al., 2007). Again, we see minimal Dopamine expressing higher-order neurons. For both of the representative Or67d lPN (AL.MB_CA.129) and Or67d vPN (AL.LH.97), the modal hop count is 4 interconnects.

From the Or67d glomerulus, a unique class of dopamine neurons was identified—Dnp32—that synapses directly onto the representative projection neuron AL.LH.97. This neuron, SCL.WED.1, has arborizations that span half the hemibrain and produces the neuropeptide dromyosuppressin (DMS).

Serotonin

Serotonin is involved in behavioral states including aggression & stress response, learning & memory, and mediating the circadian rhythm & sleep cycles (Casture et al., 2018). We utilized the same exploratory search used to define the modal hop count for dopaminergic neurons from representative PNs originating in the VA1v glomerulus and synapsing with Or47b ORNs. From the representative Or47b adPN, (AL.LH.61), we found the modal hop count is 4 interconnects before reaching a serotonin-expressing neuron. For representative Or47b vPN (AL.LH.100), the modal hop count is 3 interconnects.

In the VA1d glomerulus, for the representative Or88a adPN (AL.MB_CA.43), the modal hop count is 4 interconnects before reaching a serotonin-expressing neuron. For representative Or88a vPN (AL.LH.118), the modal hop count is 5 interconnects.

In the DA1 glomerulus, for the representative Or67d lPN (AL.MB_CA.129), the modal hop count is 4 interconnects before reaching a serotonin-expressing neuron. For the representative Or67d vPN

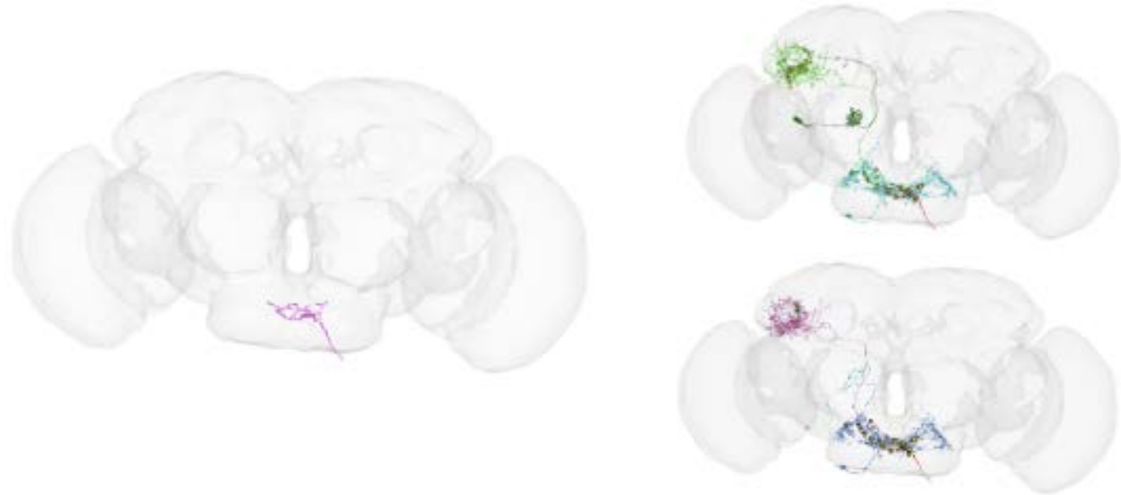

Figure 6a. Serotonin neuron, GNG.1894. This neuron is localized to the Gnathal Ganglia neuropil and has a projection that enters/exits the brain. **Figure 6b.** Pathway from DA2 representative projection neuron AL.LH.112 from olfactory receptor Or56a. **Figure 6c.** Pathway from DC4 representative projection neuron AL.LH.271 from ionotropic receptor Ir64a. Both the DA2 and DC4 pathways terminate in three-neuron pathway LH.SLP.20, GNG.13, GNG.1894 (15+ hops).

(AL.LH.97), the modal hop count is 5 interconnects before reaching a serotonin-expressing neuron. From the Or67d glomerulus, a unique class of serotonin neurons was identified—Dnp62—that is two hops away from the representative projection neuron AL.LH.97. This neuron, SLP.GNG.3 has arborizations that span the hemibrain and produces the neuropeptide drosulfakinin (DSK).

These scatterplots provide further evidence that In the DA2 glomerulus the Or56a ORN, for the representative Or56a lPN (AL.LH.112), the modal hop count is 4 interconnects before reaching a serotonin-expressing neuron. Similarly, in the DC4 glomerulus the Ir64a receptor neuron, for the representative Ir64a adPN (AL.LH.23), and the modal hop count is 4 interconnects before reaching a serotonin-expressing neuron. Interestingly, for Ir64a vPN (AL.LH.271), the modal hop count is 6 interconnects.

From the DA2 and DC4 glomeruli, a conserved three-neuron pathway, terminating in a serotonin neuron was identified, starting two hops away from the respective projection neurons AL.LH.112 (DA2) and AL.LH.271 (DC4). This terminating serotonin neuron, GNG.1894, has a projection that exits (or enters) the Gnathal Ganglia (GNG) neuropil and may be involved in gustatory reception.

Insulin

Insulin is primarily involved in metabolism & growth, feeding behavior, development, and stress resistance (Viola et al., 2023). Across different glomeruli, the connectivity patterns reveal varying degrees of interaction with insulin-expressing neurons.

In the VA1v glomerulus (Or47b ORN), the representative adPN (AL.LH.61) requires 5 interconnects to reach an insulin-expressing neuron, while the vPN (AL.LH.100) requires 4 interconnects. Similarly, in the VA1d glomerulus (Or88a ORN), both the adPN (AL.MB_CA.43) and vPN (AL.LH.118) exhibit a modal hop count of 5 interconnects to insulin-expressing neurons.

For the DA1 glomerulus (Or67d ORN), both the representative lPN (AL.MB_CA.129) and vPN (AL.LH.97) show a modal hop count of 5 interconnects.

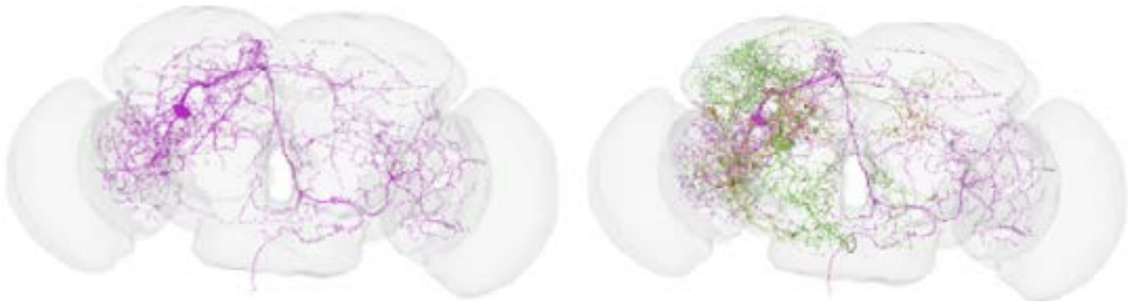

Figure 7a: Clock neuron, PLP.79. This neuron spans the entire hemibrain and has a projection that enters/exits the brain. **Figure 7b:** Pathway from DMS-expressing SCL.WED.1 (green) to allatostatin-C-expressing PLP.79 (purple), through ICL.3 (orange) (2 hops).

The same is observed in the DA2 glomerulus (Or56a ORN), where the representative IPN (AL.LH.112) also requires 5 interconnects to reach an insulin-expressing neuron.

In the DC4 glomerulus (Ir64a receptor neuron), the representative adPN (AL.LH.23) exhibits a modal hop count of 4 interconnects, whereas the vPN (AL.LH.271) requires 6 interconnects, the highest among the analyzed pathways. This variability underscores the distinct connectivity dynamics of the Ir64a pathway relative to other glomeruli.

Clock Neurons

Clock neurons are involved in regulating the natural sleep and wake cycles of the fly (Yao et al., 2016). In the VA1v glomerulus (Or47b), for the representative adPN (AL.LH.61), the modal hop count is 5 interconnects before reaching a clock neuron. For representative Or47b vPN (AL.LH.100), the modal hop count is 4 interconnects. In the VA1d glomerulus for the representative Or88a adPN (AL.MB_CA.43), the modal hop count is 5 interconnects before reaching a clock neuron. For representative Or88a vPN (AL.LH.118), the modal hop count is 4 interconnects.

In the DA1 glomerulus, the representative Or67d IPN (AL.MB_CA.129), the modal hop count is 5 interconnects before reaching a clock neuron. For representative Or67d vPN (AL.LH.97), the modal hop count is 5 interconnects.

A unique class of trissin-expressing clock neurons was identified, DNp27, that also expresses allatostatin-C, which suppresses gonadotropin production. This clock neuron, PLP.79 is two hops away from the DMS-expressing SCL.WED.1 dopamine neuron, which synapses onto an Or67d PN.

In the DA2 glomerulus, the representative Or56a IPN (AL.LH.112), the modal hop count is 4 interconnects before reaching a clock neuron. Similarly, in the DC4 glomerulus the clock representative Ir64a adPN (AL.LH.23), the modal hop count is 4 interconnects before reaching a clock neuron. For representative Ir64a vPN (AL.LH.271), the modal hop count is 6 interconnects.

Discussion

This paper aimed to explore the relationship between neuronal structure, connectivity, and their impacts on function in the female fly brain. Using connectomic data analysis, our research described various odorant pathways and potential contributions of different factors such as neurotransmitter type, connectivity partners, and density of connections on aversion/attraction and pathway specificity.

Consistent with research conducted to build the connectome, we confirmed that functional segregation exists at the first and second-order neuron levels. This supports the established understanding of the organization of the olfactory system in *Drosophila*. In addition to this, it was noted that there existed no significant difference in the neuronal connectivity

of the five ORNs (with the exception of Ir64a) with serotonergic, dopaminergic, insulin-producing, and circadian circuits. This suggests a common underlying architecture connecting most odorant pathways to higher-order neurons while highlighting the potential for specialized connectivity in specific cases.

Quantitatively, we found no significant difference in the number of modal hops required to reach a neuron producing a specific neurotransmitter for all vPNs except for the Ir64a receptor neuron. The modal hop count for the Ir64a vPN is notably higher than all other representative PNs, averaging six modal hops, before reaching the nearest serotonergic dopaminergic, insulin-producing, or clock neuron. This could be due to Ir64a's identity as an ionotropic, acid-sensing receptor, which may explain differences in connectivity to higher-order neurons compared to pathways from olfactory receptors.

Our findings are consistent with previous research on the *Drosophila* olfactory system. The identification of distinct structural differences and pathways for different odorants, as well as the role of specific neurotransmitters in mediating attraction and aversion behaviors, confirms previous observations. However, the use of the FlyWire connectome allowed for a more comprehensive and detailed analysis of these pathways, revealing new insights into their organization and complexity.

While some behaviors, such as geosmin detection and avoidance, may be strictly innate, others—such as the sociosexual behaviors mediated by Or67d and Or47d—appear to have the capacity for learning and adaptation. For example, wild-type flies raised in isolation exhibit increased aggression, mating, and feeding behaviors, but these behaviors normalize upon reintroduction to social populations, highlighting a dynamic interplay between innate predispositions and environmental influences (Deanhardt et al., 2023). Similarly, the special case of the SCL.WED.1 neuron (Figure 7b), which expresses the neuropeptide DMS to mediate muscle contraction, offers further insights into the intersection of innate and learned behaviors (Nassal 2018). Its direct synaptic connection to an Or67d projection neuron suggests a potential role in egg-laying or mating-related muscle mechanisms, bridging the gap between sensory input and motor output. This connection challenges the traditional dichotomy of innate versus learned behaviors, particularly in flies with mutations or natural variations in fruitless behavioral phenotypes. This example shows how the connectome can be leveraged to formulate hypotheses about structure- and connectivity-driven behaviors or social processes. For example, silencing Or67d in a fly mutant and subsequently counting the number of eggs laid may provide insights into the function of this neuron, beyond its spatial arrangement and synaptic partners.

The serotonergic neuron SLP.GNG.3 (Figure 5a) may be another neuron of interest in understanding mating-related and other social behaviors; it is downstream of Or67d and expresses drosulfakinin—a neuropeptide involved in aggression and sexual arousal regulation. This cell could drive further hypotheses surrounding mating behavior and aggression.

When examining food odorant pathways, the serotonergic neuron, GNG.1894 (Figure 6), contains processes that enter the hemibrain from below. It is well known that *Drosophila* have gustatory neurons in the extremities of its body, allowing it to "taste" their surroundings more effectively. This, in addition to the role of Or56a and Ir64a in processing food-odor information, may help to explain the interconnectedness of olfactory and gustatory information processing, especially relating to aversive food odorants in the immediate environment.

Lastly, the clock example may explain the role that circadian cycles can affect social processes. Clock neuron PLP.79 (Figure 7a) expresses allatostatin-C, which is involved in the suppression of gonadotropin production, and as previously mentioned, SCL.WED.1 expresses DMS which may have a role in egg-laying. Because these two neurons are only two hops away, this is a point of interest that could lead to further investigation into the role of pheromones in mating-related social behaviors.

Together, the neurons of interest identified from our comparative connectomic analyses may enable further research involving downstream genetic

experiments to better understand the roles of olfaction and odor processing in facilitating social and behavioral processes.

The research and subsequent analysis were limited by the connectome itself. While the research done to build the connectome was groundbreaking, because it only represents one time point (5 days old), it does not offer an accurate depiction of neuronal growth and death in the fly brain over time. Former research has implied that certain neuronal pathways form and are more active during adolescence but later are unused in adulthood; the lack of versatility throughout age ranges causes the connectome to fall short in exhibiting the changes in plasticity (Sugie et al., 2018). Future revisions of the connectome should focus on capturing *Drosophila* neuronal connectivity across different time points, under different conditions, such as social isolation, and analysis of the male brain. A new and comprehensive connectome for *Drosophila* is currently under development, aiming to address these limitations by mapping neuronal connectivity across various life stages and incorporating dynamic changes in synaptic plasticity.

Similarly, comparing neuronal differences of male drosophila was not possible due to the research done to build the connectome only being done on a female fly. As such, the connectome offers minimal insight into pathways that show sexual dimorphism, particularly fruitless & gender-specific aversive and attractive pathways (Kurtovic et al., 2007). While we were able to observe the attractive pathways for cVA in female *Drosophila*, these pathways could not be observed in a connectome for male *Drosophila* in the context of attractive pathways, which are expected to differ in males given that cVA acts as a repellent to wild-type male drosophila (Kurtovic et al., 2007).

Further observations are needed to determine whether or not this neuronal network is conserved in *Drosophila* species and mammals, as the current connectome lacks the opportunity to cross-compare species. Notably, even though the mammalian olfactory bulb shows similar functional organization as the antennal lobe, these structures evolved independently (Farris, 2015). Given the lack of common origin, the application of insect olfactory logic to mammal olfactory logic may be limited. However, understanding of the fly neuronal system may unlock higher-order insights into the mammalian nervous system. The *Drosophila* hemibrain connectome could serve as a leap forward in the connectomic field, bringing us one step closer to a human connectome and ultimately providing us a greater understanding of the impact of neuronal circuitry on innate behaviors and beliefs in comparison to learned behaviors and values. Combined with further advancements in other disciplines, connectomics serves as a biological basis of human action.

References

1. Ai, M., Min, S., Grosjean, Y., Leblanc, C., Bell, R., Benton, R., & Suh, G. S. (2010). Acid sensing by the Drosophila olfactory system. *Nature, 468*(7324), 691–695. https://doi.org/10.1038/nature09537

2. Blakely, T., Bogovic, J., Dolafi, T., … Plaza, S. M. (2020). A connectome and analysis of the adult drosophila central brain. *eLife*. https://elifesciences.org/articles/57443

3. Cardona, A., Saalfeld, S., Schindelin, J., Arganda-Carreras, I., Preibisch, S., Longair, M., Tomancak, P., Hartenstein, V., & Douglas, R. J. (2012). TrakEM2 software for neural circuit reconstruction. *PloS one*, 7(6), e38011. https://doi.org/10.1371/journal.pone.0038011

4. Chou, Y. H., Spletter, M. L., Yaksi, E., Leong, J. C., Wilson, R. I., & Luo, L. (2010). Diversity and wiring varIability of olfactory local interneurons in the Drosophila antennal lobe. *Nature Neuroscience, 13*(4), 439–449. https://doi.org/10.1038/nn.2489

5. Couto, A., Alenius, M., & Dickson, B. J. (2005).Molecular, anatomical, and functional organization of the Drosophila olfactory system. *Current biology: CB, 15*(17), 1535–1547. https://doi.org/10.1016/j.cub.2005.07.034

6. Deanhardt, B., Duan, Q., Du, C., Soeder, C., Morlote, A., Garg, D., Saha, A., Jones, C. D., & Volkan, P. C. (2023). Social experience and pheromone receptor activity reprogram gene expression in sensory neurons. *G3 (Bethesda, Md.), 13*(6), jkad072. https://doi.org/10.1093/g3journal/jkad072

7. Dweck, H. K., Ebrahim, S. A., Thoma, M., Mohamed, A. A., Keesey, I. W., Trona, F., Lavista-Llanos, S., Svatoš, A., Sachse, S., Knaden, M., & Hansson, B. S. (2015). Pheromones mediating copulation and attraction in Drosophila. *Proceedings of the National Academy of Sciences of the United States of America, 112*(21), E2829–E2835. https://doi.org/10.1073/pnas.1504527112

8. Farris, S. M. (2015). Evolution of brain elaboration. Philosophical Transactions of the Royal Society *B: Biological Sciences, 370*(1684), 20150054. https://doi.org/10.1098/rstb.2015.0054

9. Jefferis, G. S., Vyas, R. M., Berdnik, D., Ramaekers, A., Stocker, R. F., Tanaka, N. K., Ito, K., & Luo, L. (2004). Developmental origin of wiring specificity in the olfactory system of Drosophila. *Development (Cambridge, England), 131*(1), 117–130. https://doi.org/10.1242/dev.00896

10. Kasture, A. S., Hummel, T., Sucic, S., & Freissmuth, M. (2018). Big Lessons from Tiny Flies: *Drosophila melanogaster* as a Model to Explore Dysfunction of Dopaminergic and Serotonergic Neurotransmitter Systems. *International journal of molecular sciences, 19*(6), 1788. https://doi.org/10.3390/ijms19061788

11. Kurtovic, A., Widmer, A., & Dickson, B. J. (2007). A single class of olfactory neurons mediates behavioural responses to a Drosophila sex pheromone. *Nature, 446*(7135), 542–546. https://doi.org/10.1038/nature05672

12. Marin, E. C., Jefferis, G. S., Komiyama, T., Zhu, H., & Luo, L. (2002). Representation of the glomerular olfactory map in the Drosophila brain. *Cell, 109*(2), 243–255. https://doi.org/10.1016/s0092-8674(02)00700-6

13. Scheffer, L. K., Xu, C. S., Januszewski, M., Lu, Z., Takemura, S., Hayworth, K. J., Huang, G. B., Shinomiya, K., Maitlin-Shepard, J., Berg, S., Clements, J., Hubbard, P. M., Katz, W. T., Umayam, L., Zhao, T., Ackerman, D., Stensmyr, M. C., Dweck, H. K., Farhan, A., Ibba, I., Strutz, A., Mukunda, L., Linz, J., Grabe, V., Steck, K., Lavista-Llanos, S., Wicher, D., Sachse, S., Knaden, M., Becher, P. G., Seki, Y., & Hansson, B. S. (2012). A conserved dedicated olfactory circuit for detecting harmful microbes in Drosophila. *Cell, 151*(6), 1345–1357. https://doi.org/10.1016/j.cell.2012.09.046

14. Sugie, A., Marchetti, G. & Tavosanis, G. Structural aspects of plasticity in the nervous system of *Drosophila*. *Neural Dev* 13, 14 (2018). https://doi.org/10.1186/s13064-018-0111-z

15. Viola, C.M., Frittmann, O., Jenkins, H.T. et al. Structural conservation of insulin/IGF signalling axis at the insulin receptors level in *Drosophila* and humans. *Nat Commun 14*, 6271 (2023). https://doi.org/10.1038/s41467-023-41862-x

16. Yamamoto, S., & Seto, E. S. (2014). Dopamine dynamics and signaling in Drosophila: an overview of genes, drugs and behavioral paradigms. *Experimental animals, 63*(2), 107–119. https://doi.org/10.1538/expanim.63.107

17. Yao, Z., Bennett, A. J., Clem, J. L., & Shafer, O. T. (2016). The Drosophila Clock Neuron Network Features Diverse Coupling Modes and Requires Network-wide Coherence for Robust Circadian Rhythms. *Cell Reports, 17*(11), 2873–2881. https://doi.org/10.1016/j.celrep.2016.11.053

Gender Inequality in Healthcare Delivery: Differences in System Satisfaction During the COVID-19 Pandemic in the United States

Haizhu Song

Volume 4, Issue 1

Article Synopsis

This study examines gender differences in public evaluations of the U.S. healthcare system during the COVID-19 pandemic, using nationally representative data from the 2021–2022 General Social Survey (GSS). While prior research has documented significant gender-based disparities in healthcare access and outcomes, this analysis finds no statistically significant relationship between gender and reported dissatisfaction with the healthcare system, even after controlling for self-reported health status. These findings suggest that broad indicators of system satisfaction may not adequately reflect the gendered nature of healthcare experiences. However, supplementary analysis of perceived access to healthcare,reveals meaningful gender differences, pointing to potential limitations in using general satisfaction measures as proxies for structural inequities. The study underscores the importance of incorporating more specific and experience-based metrics in future research, as well as the need to examine intersecting factors such as income, race, and insurance status to better understand the complexity of gender disparities in healthcare delivery during public health emergencies.

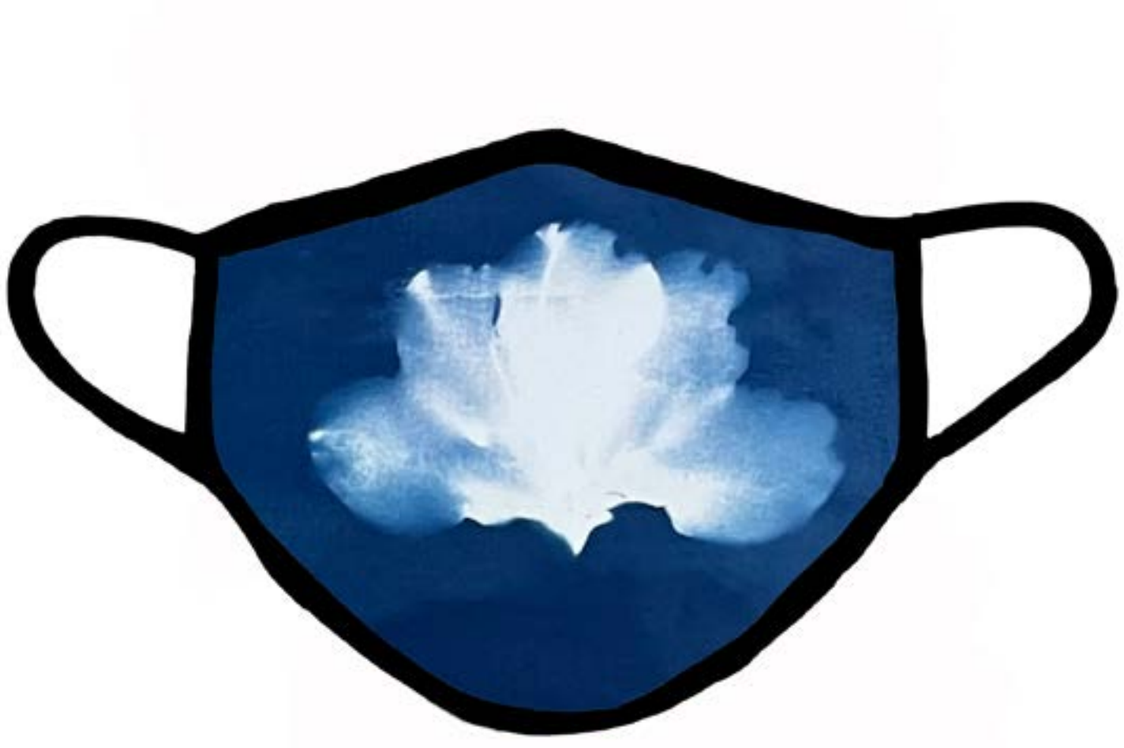

Graphic by Ava Kocher

Gender Inequality in Healthcare Delivery: Differences in System Satisfaction During the COVID-19 Pandemic in the United States

Haizhu Song
Trinity College of Arts and Sciences, Duke University
https://doi.org/10.55894/dv4.13

Abstract

This study examines gender differences in healthcare satisfaction during the COVID-19 pandemic in the United States using data from the 2021-2022 General Social Survey (GSS). Although existing literature generally points to the disadvantages women face in terms of healthcare access and health outcomes, this study assesses gender differences in satisfaction with the U.S. healthcare system, controlling for health conditions. This study is the first to systematically assess gender differences in healthcare satisfaction during an epidemic from a quantitative perspective using large-scale representative data, filling a gap in the existing literature on this critical issue. Bivariate and multivariate analyses of the article showed no statistically significant relationship between gender and healthcare satisfaction, challenging the hypothesis that women are less satisfied. However, the findings also suggest that it is difficult to capture small gender differences by relying solely on broad satisfaction metrics. Future research could consider introducing more specific variables and exploring the interaction between gender and socioeconomic factors. The results of the study not only provide data-based insights for policymakers, but also provide a quantitative foundation for achieving gender equity in the U.S. health system.

Introduction

Gender disparities in healthcare delivery have existed in the United States and globally. Although women have poorer health outcomes than men (Macintyre, Hunt, and Sweeting 1982), they often face greater challenges in accessing primary healthcare services (Sialubanje 2015), reflecting underlying gender inequalities in healthcare delivery.

Taking diabetes as an example, it is more difficult for women to access specialized care, which negatively impacts their quality of life and disease outcomes (Suresh and Thankappan 2019). Also, in the U.S., 10% fewer female coronary heart disease patients receive professional medical care than male patients (Arber et al. 2006), reflecting the disadvantage of women's access to healthcare delivery. Also, in other countries, such as Ghana, women have more difficulty accessing health care due to economic constraints and low health insurance coverage (Seidu et al. 2020). The COVID-19 pandemic has disrupted healthcare systems globally (Bisht, Saharia, and Sarma 2020), increasing the likelihood of expanding these pre-existing inequalities. In this crisis, women have taken on more caregiving responsibilities (Guerrina et al. 2021) and are more susceptible to virus infection (Penfold and Magee 2020).

Thus, to examine the possible gender inequalities in healthcare delivery in the U.S. during the pandemic, this paper aims to examine gender differences in Americans' evaluations of the healthcare system during the COVID-19 pandemic, using data from the General Social Survey (GSS). This is a direct way to study gender differences in healthcare system evaluation. Additionally, a deeper understanding of these disparities can help recognize the existing healthcare system problem and establish a strong foundation for future improvements.

This paper begins with a review of the relevant literature on gender differences and healthcare accessibility, followed by the statement of hypothesis. The methodology section presents data sources, sample selection, and measures. The results of the correlation and impact of gender on evaluating the healthcare system during the pandemic are presented. The key contributions of the study are the possible policy improvements based on these findings discussed.

Literature Review

Research on gender disparities in healthcare delivery, particularly during the COVID-19 pandemic in the U.S., has highlighted inequalities that affect women's health outcomes and life quality. Thus, reviewing the existing literature is essential to understand the broader context and identify gaps that require further research. This literature review is therefore organized into three key subtopics: existing gender disparities in healthcare delivery, the pandemic's impact on these disparities, and gender differences in satisfaction with healthcare delivery.

Gender Differences in Health Care Delivery

Gender has played an essential role in influencing individuals' receiving healthcare services. Generally, research has shown that women are more likely than men to need healthcare services to manage chronic conditions and reproductive healthcare and more likely to seek healthcare services (Case and Paxson 2005; Long et al. 2011). However, women tend to face more barriers to accessing necessary healthcare services than men and have less favorable healthcare experiences than men (Ng 2010; Elliott et al. 2012). Also, in the U.S., the health gap between men and women is well documented over time (Rapp et al. 2021). First, women are more likely than men to delay or forgo medical care for financial reasons or insurance gaps because women generally have higher prices for treatment and insurance costs than men (Lavelle and Smock 2012). Moreover, general gender discrimination within the U.S. influences health service utilization, with many states with high levels of gender discrimination exacerbating gender disparities in health care (Rapp et al. 2021), which is more detrimental to women's receiving health care services. Thus, this existing research shows that women face more challenging conditions than men in receiving healthcare delivery in the U.S. and globally.

Impact of the COVID-19 Pandemic on Healthcare Delivery

Even worse, the COVID-19 pandemic has dramatically changed the landscape of healthcare delivery, which increases the likelihood of enlarging this gender disparity. During the pandemic, demand for healthcare services outstripped supply, resource constraints, and overwhelmed systems, severely impacting vulnerable populations (Rivenbark and Ichou 2020; Siegel and Mallow 2020). Based on this unique context, women, as a vulnerable group, face unique challenges during the pandemic. Firstly, since the majority of frontline healthcare workers are female, they are more susceptible to the virus (Penfold and Magee 2020). Also, due to the increased family responsibilities associated with the pandemic, women suffered severe negative physical and mental effects (Maposa 2024). Therefore, the pandemic increases the possibility that women need professional and comprehensive healthcare services and is likely to exacerbate gender-based challenges in healthcare (Heise et al. 2019). Thus, gender-specific challenges during this period widen the potential for exacerbating pre-existing gaps in health care delivery.

Gender Difference in Satisfaction with the Healthcare System

Considering the persistent gender inequality in the medical field and the unprecedented impact of the pandemic, satisfaction with the healthcare system becomes a crucial indicator for directly assessing these influences. First, gender differences in health care satisfaction have long existed. Women are more likely than men to report difficulties in accessing health care services and are less satisfied with the services they receive than men, particularly regarding drug costs and medical diagnoses (Daher 2021). Additionally, this lower satisfaction among women stems from various factors, including the complexity of the healthcare system and inadequate access to medical care in areas such as reproductive health

and chronic disease management (Bryant, Leaver, and Dunn 2009). These perceptions highlight gender differences in the receipt of health care services and reflect the disadvantaged position of women.

Existing Literature Gaps

While existing research provides insights into gender differences in healthcare satisfaction, few studies have used large-scale U.S. datasets such as the GSS to conduct systematic quantitative analyses. Most studies, such as that of Bryant, Leaver, and Dunn (2009), lack a specific focus on the pandemic period, thus leaving a gap in understanding how gender affects healthcare delivery satisfaction during this critical period. Therefore, this study fills this gap by utilizing GSS data to analyze gender differences in healthcare satisfaction during the most recent pandemic.

Hypothesis

Based on the context of gender disparity in the healthcare field, this paper presents one key hypothesis: gender is relevant to satisfaction with the healthcare system, and women are expected to report lower satisfaction during the pandemic compared to men. This hypothesis is grounded in existing research, which indicates that women generally face more barriers to receiving healthcare than men. Also, this gender gap may be exacerbated by the challenges of a pandemic because research has shown women faced more difficulties than men during this critical time period.

Methods

Data

This paper utilizes data from the General Social Survey (GSS), which targets the adult (age 18 and older) household population of the U.S., is a comprehensive, nationally representative survey that captures public opinions, attitudes, and demographic information across the US (Marsden and Smith 2016; NORC at the University of Chicago 2021). The analysis focuses on healthcare system satisfaction as the dependent variable, with gender as the independent variable and health status as a control. Also, the study specifically examines data from the COVID-19 pandemic period (2021-2022) to assess relevant social trends.

Sample Selection

The sample for this study consists of respondents from the 2021-2022 General Social Survey (GSS) who provided complete responses on gender, health status, and healthcare system satisfaction in the United States. By focusing on this subset of respondents, the study aims to analyze gender disparities in healthcare satisfaction during the pandemic.

Measures

Dependent Variable. The dependent variable in this study is the respondents' dissatisfaction with the U.S. healthcare system during 2021-2022, which can directly reflect public attitudes and perceptions of healthcare delivery. Thus, the dissatisfaction level helps to understand the complexity of accessing and receiving healthcare services and gender disparities. In the planned cross-tabulation analysis, the original GSS variable representing healthcare system inefficiency ('HLTHINF') was recoded to collapse attributes into three categories: 1 for "Agree," 2 for "Neither agree nor disagree," and 3 for "Disagree" rather than original five categories. This recording combines responses into distinct categories, clearly reflecting the dissatisfaction level. To be more specific, Table 1 below presents the recoded variable with its attributes, codes, and percentages, and the GSS question prompting this variable will be included verbatim in Appendix A.

Independent Variable. Due to the long history of gender health disparity in the U.S. and worldwide, the chosen independent variable is the respondents' gender. Thus, gender is significant in exploring existing and potential inequalities through analyzing healthcare satisfaction. The original variable 'SEX' was recoded to a binary format that 0 represents "Male" and 1 represents "Female." Also, Table 1 includes the gender variable, showing its attributes, metrics, and distribution percentages, and specific

GSS questionnaire items for gender will be provided in Appendix A.

Control Variable. This study's control variable is the respondents' self-reported health condition. It was chosen to avoid any possible influence on the satisfaction of the healthcare system from an individual's health status. The original variable 'HEALTH' was recoded to classify responses into three categories: 1 for "Excellent," 2 for "Good," and 3 for "Not good," which combines the original "Fair" and "Poor" attributions. This recording was crucial to simplifying interpretation and making the analysis clear and distinct by combining the less-than-good attributions. As previously mentioned, Table 1 presents the health status variable, its attributes, codes, and percentages. The corresponding GSS question will also be included verbatim in Appendix A.

Analytic Plan

To explore the relationships among the variables, this study will use SDA software to perform both bivariate and multivariate cross-tabulation, supported by a Rao-Scott chi-square test statistic at a 95% confidence level.

The bivariate analyses will include (1) a cross-tabulation of the dependent variable (healthcare system dissatisfaction) by the independent variable (gender) to examine the relationship between gender and healthcare dissatisfaction, reflecting the general changes and differences; (2) a cross-tabulation of the dependent variable by the control variable (health condition) to assess how health status relevant to healthcare; and (3) a cross-tabulation of the control variable by the independent variable to analyze relationship between gender and self-reported health status.

Furthermore, the multivariate analysis will involve a cross-tabulation of the dependent variable by the independent variable, with the control variable included. This analysis will help recognize whether the relationship between gender and healthcare satisfaction persists, weakens, or strengthens when considering health status.

Also, each table generated from these analyses will be assessed using the Rao-Scott chi-square statistic, which considers the complexity of the p-values to check the statistical significance. Finally, the elaboration model will be applied to recognize and evaluate the relationship among these three variables, which can show the types of their relevance and impact clearly.

Results

Generally, as Table 2 shows, there are minor differences between genders in healthcare satisfaction. First, 58.4% of males and 60.0% of females consider the U.S. health system inefficient, which does not indicate a large difference between the genders. Similarly, The proportion of respondents who neither agree nor disagree is 22.3% for males and 22.0% for females, while those who disagree are 19.3% for males and 18.0% for females. This phenomenon can also be supported by the chi-square test result ($\chi^2 = 0.37$, $p = 0.93$), which indicates no statistically significant relationship between gender and attitude towards the healthcare system ($p > 0.05$).

Table 1. Variable Descriptions, Metrics, and Descriptive Statistics for Key Variables

Variable Name	Description	Metric	Percentages (%)
Dependent Variable			
HLTHINF	Respondent's perception of the U.S. healthcare system's inefficiency	1=Agree 2=Neither 3=Disagree	60.0 22.0 18.0
Independent Variable			
SEX	Respondents' sex	0=Male 1=Female	45.1 54.9
Control Variable			
HEALTH	Self-reported health status	1=Excellent 2=Good 3=Not good	20.2 54.1 25.7

Vertices: Duke's Undergraduate Research Journal Volume 4, Issue 1 | Spring 2025

Table 2: Bivariate Cross Tabulation Analysis for Dissatisfaction with the U.S. Healthcare System by Gender (Unweighted N= 1,118)

	Gender	
Healthcare Dissatisfaction	Male	Female
Agree (Dissatisfied)	58.4	60.0
Neither agree nor disagree	22.3	22.0
Disagree (Satisfied)	19.3	18.0
Column Total	100%	100%
Unweighted Column Total	(501)	(617)
Chi-Square = 0.37	p = 0.93	

Table 3: Bivariate Cross Tabulation Analysis for Dissatisfaction with the U.S. Healthcare System by Health Condition (Unweighted N= 1,119)

	Health Condition		
Healthcare Dissatisfaction	Excellent	Good	Not Good
Agree (Dissatisfied)	49.5	61.3	61.2
Neither agree nor disagree	24.7	23.2	18.1
Disagree (Satisfied)	25.8	15.5	20.7
Column Total	100%	100%	100%
Unweighted Column Total	(226)	(591)	(302)
Chi-Square = 17.20	p = 0.19		

Table 3 shows the percentage difference between healthcare satisfaction and self-reported health condition. First, the respondents in "Excellent" health are less likely to agree that the U.S. healthcare system is inefficient (49.5%) compared to those in "Good" (61.3%) and "Not Good" (61.2%) health. Also, the percentage of respondents who disagree is higher among those in "Excellent" health (25.8%) compared to those in "Good" (15.5%) and "Not Good" (20.7%) health status. This phenomenon shows that the respondents with excellent health status are more satisfied than those with less good health status. Moreover, the respondents who have "Not Good" health status are less likely to choose the neutral option (18.1%) compared to others (24.7% for excellent and 23.2% for good). These percentage differences seem to suggest there may be an association, as those with excellent health report being less dissatisfied.

Table 4: Bivariate Cross Tabulation Analysis for the Health Condition by Gender (Unweighted N= 7,458)

	Gender	
Health Condition	Male	Female
Excellent	20.8	18.4
Good	53.0	55.8
Not Good	26.2	25.7
Column Total	100%	100%
Unweighted Column Total	(3,360)	(4,098)
Chi-Square = 8.13	p = 0.08	

However, the chi-square statistic ($\chi^2 = 17.20$, $p = 0.19$) indicates that the relationship between health conditions and healthcare satisfaction is not statistically significant ($p > 0.05$). Thus, the percentage differences are insignificant enough to confirm a strong relevance between health conditions and attitudes toward the U.S. healthcare system.

According to Table 4, there appear to be slight differences between gender and health conditions. First, the data shows that a higher percentage of males (20.8%) report being in "Excellent" health compared to females (18.4%). A more significant percentage of females (55.8%) report being in "Good" health compared to males (53.0%). Also, the "Not Good" health status percentage is similar for both genders (26.2% for males and 25.7% for females). Moreover, the chi-square test shows these slight differences do not bear out a relationship between the two variables, which is not statistically significant ($\chi^2 = 8.13$, $p = 0.08$, $p > 0.05$).

The trivariate analysis provides comprehensive and detailed data on the relationship between gender and satisfaction with the U.S. healthcare system, controlled for health conditions, and the chi-square test shows the significance of each relationship.

Partial Table 5a, controlling for people with excellent health, shows a difference in satisfaction levels between genders of the healthcare system. Males are more likely to agree (63.0%) than females (39.3%), and females have a higher percentage of disagreement (29.6%) compared to males (19.4%). Also, female respondents are more likely to choose the neutral option than males (31.1% for women and 17.6% for men). In addition, although the chi-square test result ($\chi^2 = 12.63$, $p = 0.06$) is close, it did not reach conventional significance ($p < 0.05$), reflecting that the likelihood of an existing relationship between the dependent and independent variables is not supported.

For respondents who have a good health status, the percentages for dissatisfaction with the healthcare system ("Agree" (the system is inefficient)) are relatively similar, with males at 58.9% and females at 63.2%. Similarly, the proportion of respondents who neither agree nor disagree is also close (23.5% for males and 23.0% for females). Regarding the dissatisfaction choice ("Disagree" (the system is efficient)), the rates are higher for males (17.6%) than for females (13.7%). The chi-square test ($\chi^2 = 1.85$, $p = 0.70$) indicates no significant relationship between gender and satisfaction in this health group.

Finally, there is a significant difference in the "Agree" choice for the unhealthy respondents, with 68.3% of females agreeing compared to 54.2% of males. Also, the percentage of respondents who neither agree nor disagree is higher among males (23.2%) than females (12.8%). Similarly, for the "Disagree" option, the males (22.5%) are also higher than females (18.9%). Despite those apparent differences, the chi-square statistic ($\chi^2 =$

Table 5a: Trivariate Cross Tabulation Analysis for Dissatisfaction with the U.S. Healthcare System by Gender, Controlling for Health Condition = Excellent (Unweighted N= 225)

	Gender	
Healthcare Dissatisfaction	Male	Female
Agree (Dissatisfied)	63.0	39.3
Neither agree nor disagree	17.6	31.1
Disagree (Satisfied)	19.4	29.6
Column Total	100%	100%
Unweighted Column Total	(100)	(125)
Chi-Square = 12.63	p = 0.06	

Table 5b: Trivariate Cross Tabulation Analysis for Dissatisfaction with the U.S. Healthcare System by Gender, Controlling for Health Condition = Good (Unweighted N= 590)

	Gender	
Healthcare Dissatisfaction	Male	Female
Agree (Dissatisfied)	58.9	63.2
Neither agree nor disagree	23.5	23.0
Disagree (Satisfied)	17.6	13.7
Column Total	100%	100%
Unweighted Column Total	(264)	(326)
Chi-Square = 1.85	p = 0.70	

Table 5c: Trivariate Cross Tabulation Analysis for Dissatisfaction with the U.S. Healthcare System by Gender, Controlling for Health Condition = Not Good (Unweighted N= 302)

	Gender	
Healthcare Dissatisfaction	Male	Female
Agree (Dissatisfied)	54.2	68.3
Neither agree nor disagree	23.2	12.8
Disagree (Satisfied)	22.5	18.9
Column Total	100%	100%
Unweighted Column Total	(137)	(165)
Chi-Square = 7.45	p = 0.12	

7.45, p = 0.12) suggests that these differences are not statistically significant.

To conclude, although there are some observable proportion differences in satisfaction levels between genders based on various health statuses, these differences do not reach statistical significance in all health situations. This result shows that when considering health status, gender alone cannot significantly influence the satisfaction of the healthcare system.

Finally, based on the results from Tables 2 to 5, this study's most fitting elaboration model appears to be replication. The initial relationship between gender and satisfaction with the U.S. healthcare system remains consistent across different levels of the control variable (health condition) without huge changes. Thus, while the satisfaction level may change due to different genders and health conditions, these do not result in a statistically significant change when the health condition is controlled. Therefore, the original relationship between gender and satisfaction, which was not statistically significantly different, is not significantly impacted by the control variable since each partial table shows no statistical significance.

Discussion

The results section of this study indicates no statistically significant relationship between gender (IV), the U.S. healthcare system dissatisfaction (DV), and health conditions (CV) based on the cross-tabulation analyses. This conclusion is supported by p-values greater than 0.05 for all chi-square tests. However, Table 4 (cross-tabulation of health conditions by gender) demonstrates a p-value of 0.08, which suggests a potential relationship between gender and health status at the 90% confidence level. This result, while not reaching the traditional threshold of significance, suggests a potential relationship between health conditions and gender that warrants further investigation.

Additionally, the findings align with the replication elaboration model. According to this model, the initial relationship between gender and healthcare system dissatisfaction remains consistent even after controlling for health conditions. Thus, in this study, the relationship between dissatisfaction and gender was not statistically significant, and the health conditions neither significantly strengthened nor significantly weakened the observed relationship. In addition, this result reflects that other unexamined factors, such as respondents' age, may contribute to differences in satisfaction (Xesfingi and Vozikis 2016).

Thus, the results refute the hypothesis that women would report lower satisfaction with the healthcare system than men during the pandemic, as no significant relationship was found between the two variables. Also, while prior literature suggests that women face more significant challenges in accessing healthcare and are often less satisfied with healthcare systems (Daher et al. 2021; Bryant, Leaver, and Dunn 2009), this study did not find statistically significant gender disparities. One possible explanation is that healthcare system satisfaction may be too broad to measure and capture the subtle experiences of gender disparities. In addition, the widespread stress caused by a pandemic may produce consistent feelings of health system dissatisfaction across genders, thus masking the specific differences. Therefore, although the results refute the hypothesis and do not align with existing literature, the gender disparities in healthcare need more diverse and specific measures to explore.

Moreover, this study's limitations could have influenced the findings. First, some demographic factors, such as respondents' age, were not included in the analysis, and these factors may intersect with gender in influencing healthcare experiences. Thus, excluding these variables may have masked essential or subtle changes during analysis. In addition, the dependent variable - dissatisfaction with the healthcare system - may not be sufficient to measure differences in healthcare access. For example, other measures, such as HLTHACC3 in GSS data (Appendix A), which focuses on gender perspectives on ease of access to healthcare services, show significant gender differences during the pandemic (Appendix B). This result suggests the likelihood of exploring other more appropriate and specific measurements of gender differences in access to

healthcare delivery in the U.S.

Based on the findings and limitations of the study, this paper suggests that future research use more targeted measurement to address these issues, such as accessibility, affordability, and timeliness of healthcare services, rather than relying solely on the broad satisfaction variable. Also, including cross-cutting variables such as socio-economic status provides a more complete description of healthcare disparities. Specifically, future research could analyze gender interaction with age or income to better capture subtle differences. In addition, qualitative methods such as qualitative interviews can complement quantitative analysis by capturing the lived experiences and perceptions behind the statistics. By closing these gaps, future research can better explore the structural and contextual factors contributing to gender disparities in healthcare delivery, ultimately contributing to a more equitable U.S. healthcare system.

Conclusion

This study explored gender disparities in satisfaction with the U.S. healthcare system during the COVID-19 pandemic and aimed to find and improve this potential unequal social issue. While no statistically significant differences were found, the results suggest that potential and subtle gender disparities need more precise measurements to capture in healthcare experiences.

This research is essential because it focuses on how healthcare inequalities persist or evolve during a pandemic, providing insights into the challenges women face in accessing equitable healthcare delivery. Also, by addressing gender disparities, we can build a health system that better meets the needs of all people and promotes greater trust and accessibility. By identifying gaps in current measurements and emphasizing the role of external factors, this study provides a foundation for future research to develop targeted solutions that promote healthcare gender equity and improve outcomes for all populations.

References

Arber, Sara, John McKinlay, Ann Adams, Lisa Marceau, Carol Link, and Amy O'Donnell. 2006. "Patient Characteristics and Inequalities in Doctors' Diagnostic and Management Strategies Relating to CHD: A Video-Simulation Experiment." Social Science and Medicine 62(1):103–15. doi: 10.1016/j.socscimed.2005.05.028.

Bisht, Ramila, Rajashree Saharia, and Jyotishmita Sarma. 2021. "COVID-19 and the Burden of Ill-Health: A Double Crisis of Disruptions and Inequalities." Journal of Social and Economic Development 23:342–56. doi: 10.1007/s40847-020-00117-x.

Bryant, Toba, Chad Leaver, and James Dunn. 2009. "Unmet Healthcare Need, Gender, and Health Inequalities in Canada." Health Policy 91(1):24–32. doi: 10.1016/j.healthpol.2008.11.002.

Case, Anne, and Christina Paxson. 2005. "Sex Differences in Morbidity and Mortality." Demography 42(2):189–214. doi: 10.1353/dem.2005.0011.

Daher, Marilyne, Mahmoud Al Rifai, Riyad Y. Kherallah, Fatima Rodriguez, Dhruv Mahtta, Erin D. Michos, Safi U. Khan, Laura A. Petersen, and Salim S. Virani. 2021. "Gender Disparities in Difficulty Accessing Healthcare and Cost-Related Medication Non-Adherence: The CDC Behavioral Risk Factor Surveillance System (BRFSS) Survey." Preventive Medicine. doi: 10.1016/j.ypmed.2021.106779.

Elliott, Marc N., William G. Lehrman, Megan K. Beckett, Elizabeth Goldstein, Katrin Hambarsoomian, and Laura A. Giordano. 2012. "Gender Differences in Patients' Perceptions of Inpatient Care." Health Services Research 47(4):1482–1501. doi: 10.1111/j.1475-6773.2012.01389.x.

Guerrina, Roberta, Bettina Borisch, Leigh F. Callahan, Jeremy Howick, Jean-Yves Reginster, and Ali Mobasheri. 2021. "Health and Gender Inequalities of the COVID-19 Pandemic: Adverse

Impacts on Women's Health, Wealth and Social Welfare." Frontiers in Global Women's Health. doi: 10.3389/fgwh.2021.670310.

Heise, Lori, Margaret E. Greene, Neisha Opper, Maria Stavropoulou, Caroline Harper, Marcos Nascimento, and Debrework Zewdie. 2019. "Gender Inequality and Restrictive Gender Norms: Framing the Challenges to Health." Lancet 393:2440-2454. doi: 10.1016/S0140-6736(19)30652-X

Lavelle, Bridget, and Pamela J. Smock. 2012. "Divorce and Women's Risk of Health Insurance Loss." Journal of Health and Social Behavior 53(4):413–31. doi: 10.1177/0022146512465758.

Long, Sharon K., Karen Stockley, and Shanna Shulman. 2011. "Have Gender Gaps in Insurance Coverage and Access to Care Narrowed under Health Reform? Findings from Massachusetts." American Economic Review 101(3):640–44. doi: 10.1257/aer.101.3.640.

Macintyre, Sally, Kate Hunt, and Helen Sweeting. 1996. "Gender Differences in Health: Are Things Really as Simple as They Seem?" Social Science and Medicine 42(4):617–24. doi: 10.1016/0277-9536(95)00335-5.

Maposa, Abraham. 2024. "Addressing Gender Disparities in Healthcare Delivery: Strategies and Innovations for a Post-COVID-19 Era." Zimbabwe Journal of Health Sciences 4(1):17–35.

Ng, Judy H., Shakeh J. Kaftarian, Wilma M. Tilson, Paul Gorrell, Xiuhua Chen, Francis D. Chesley Jr, and Sarah Hudson Scholle. 2010. "Self-Reported Delays in Receipt of Health Care among Women with Diabetes and Cardiovascular Conditions." Women's Health Issues: Official Publication of the Jacobs Institute of Women's Health 20(5):316–22. doi: 10.1016/j.whi.2010.06.002.

NORC at the University of Chicago. 2023. "50 Years of the General Social Survey." https://gss.norc.org/us/en/gss/gss50.html.

Penfold, Rose, and Lucia Magee. 2020. "Gender Balance in an Unprecedented Time." Future Healthcare Journal 7(3):212–13. doi: 10.7861/fhj.2020-0029.

Rapp, Kristen Schorpp, Vanessa V. Volpe, Tabitha L. Hale, and Dominique F. Quartararo. 2022. "State–Level Sexism and Gender Disparities in Health Care Access and Quality in the United States." Journal of Health and Social Behavior 63(1):2–18. doi: 10.1177/00221465211058153.

Rivenbark, Joshua G., and Mathieu Ichou. 2020. "Discrimination in Healthcare as a Barrier to Care: Experiences of Socially Disadvantaged Populations in France from a Nationally Representative Survey." BMC Public Health 20(1):31-31. https://doi.org/10.1186/s12889-019-8124-z.

Seidu, Abdul-Aziz, Eugene Kofuor Maafo Darteh, Ebenezer Agbaglo, Louis Kobina Dadzie, Bright Opoku Ahinkorah, Edward Kwabena Ameyaw, Justice Kanor Tetteh, Linus Baatiema, and Sanni Yaya. 2020. "Barriers to Accessing Healthcare among Women in Ghana: A Multilevel Modelling." BMC Public Health 20(1). doi: 10.1186/s12889-020-10017-8.

Sialubanje, Cephas, Karlijn Massar, Marit S. G. van der Pijl, Elisa Maria Kirch, Davidson H. Hamer, and Robert A. C. Ruiter. 2015. "Improving Access to Skilled Facility-Based Delivery Services: Women's Beliefs on Facilitators and Barriers to the Utilisation of Maternity Waiting Homes in Rural Zambia." Reproductive Health 12(1). doi: 10.1186/s12978-015-0051-6.

Siegel, Robert M., and Peter J. Mallow. 2021. "The Impact of COVID-19 on Vulnerable Populations and Implications for Children and Health Care Policy." Clinical Pediatrics 60(2):93–98. doi: 10.1177/0009922820973018.

Suresh, Neethu, and Kavumpurathu Raman Thankappan. 2019. "Gender Differences and Barriers Women Face in Relation to Accessing Type 2 Diabetes Care: A Systematic Review." Indian Journal of Public Health 63(1):65–72. doi: 10.4103/ijph.IJPH_26_18.

Xesfingi, Sofia, and Athanassios Vozikis. 2016. "Patient Satisfaction with the Healthcare System: Assessing the Impact of Socio-Economic and Healthcare Provision Factors." BMC Health Services Research 16:94. https://doi.org/10.1186/s12913-016-1327-4.

Marsden, Peter V., and Tom W. Smith. 2016. "Overview: The General Social Survey Project." GSS Project Report No. 31. Chicago, IL: NORC, University of Chicago. https://gss.norc.org/content/dam/gss/get-documentation/pdf/reports/project-reports/PR31%20-%20GSS%20Overview.pdf.

Vertices: Duke's Undergraduate Research Journal Volume 4, Issue 1 | Spring 2025

APPENDIX A: Original GSS Question Wording

Variable Name	Original Codebook Question Wording
Dependent Variable (HLTHINF)	(How much do you agree or disagree with the following statements?) In general, the healthcare system in the United States is inefficient.
Independent Variable (SEX)	CODE RESPONDENT'S SEX
Control Variable (HEALTH)	Would you say your own health, in general, is excellent, good, fair, or poor?
Other Variable Mentioned Above (HLTHACC3)	In the United States, do you think it is easier or harder to get access to health care... for women than for men?

APPENDIX B:

Bivariate Cross-tabulation Analysis for HLTHACC3 (men vs. women access to healthcare) and Gender (Unweighted N = 1,058)

	Gender	
HLTHACC3	Male	Female
Much easier	5.7	3.4
Somewhat easier	8.5	7.8
About the same	72.6	64.6
Somewhat harder	10.0	18.2
Much harder	3.2	6.0
Column Total	100%	100%
Unweighted Column Total	(471)	(587)
Chi-Square=22.29	p=0.00	

APPENDIX C: SDA Output

Univariates Output

1.

SDA 4.1.5: Tables

GSS 1972-2022 Cumulative Datafile - Release 2

Dec 10, 2024 (Tue 07:14 AM PST)

Variables

Role	Name	Label	Range	MD	Dataset
Row	**hlthinf**	health care system in us inefficient	1-5	.d,.i,.j,.m,.n,.p,.q,.r,.s,.u,.x,.y,.z	1
Filter	**year(2021-2022)**	gss year for this respondent	1972-2022	.d,.i,.j,.m,.n,.p,.q,.r,.s,.u,.x,.y,.z	1

Frequency Distribution

Cells contain:
-Column percent
-N of cases

	Distribution
hlthinf 1: strongly agree	**22.9** 257
2: agree	**37.1** 415
3: neither agree nor disagree	**22.0** 246
4: disagree	**14.8** 166
5: strongly disagree	**3.2** 36
COL TOTAL	*100.0* *1,120*

Summary Statistics

Mean =	2.38	Std Dev =	1.09	Coef var =	.46
Median =	2.00	Variance =	1.19	Min =	1.00
Mode =	2.00	Skewness =	.49	Max =	5.00
Sum =	2,669.00	Kurtosis =	-.58	Range =	4.00

Inference about the mean:
Std Err = .03 CV(mean) = .01

Statistics exclude missing-data and out-of-range values.

2.

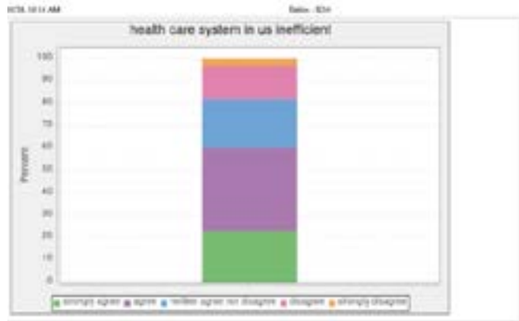

Allocation of cases

Valid cases	1,120
Cases excluded by filter	64,814
Cases with invalid codes on row variable	6,456
Total cases	72,390

Datasets

1 /sda/cesa/gss22/rw2
2 /data/gss22/sd2/NEWVARS

CSM, UC Berkeley

SDA 4.1.5: Tables

GSS 1972-2022 Cumulative Datafile - Release 2

Dec 10, 2024 (Tue 07:14 AM PST)

Variables

Role	Name	Label	Range	MD	Dataset
Row	**sex**	respondents sex	1-2	.d,.i,.j,.m,.n,.p,.q,.r,.s,.u,.x,.y,.z	1
Filter	**year(2021-2022)**	gss year for this respondent	1972-2022	.d,.i,.j,.m,.n,.p,.q,.r,.s,.u,.x,.y,.z	1

Univariates Output, cont.

3.

		-N of cases
sex	1: male	45.1 3,363
	2: female	54.9 4,101
	COL TOTAL	*100.0* *7,464*

Summary Statistics

Mean =	1.55	Std Dev =	.50	Coef var =	.32
Median =	2.00	Variance =	.25	Min =	1.00
Mode =	2.00	Skewness =	-.20	Max =	2.00
Sum =	11,565.00	Kurtosis =	-1.96	Range =	1.00

Inference about the mean:
Std Err = .01 CV(mean) = .00

Statistics exclude missing-data and out-of-range values.

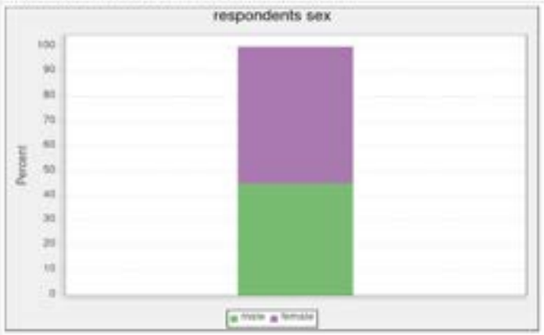

Allocation of cases	
Valid cases	7,464
Cases excluded by filter	64,814
Cases with invalid codes on row variable	112
Total cases	*72,390*

Datasets	
1	/sda/data/gss22rel2

4.

2 /data/gss22rel2/NEWVARS

CSM, UC Berkeley

SDA 4.1.5: Tables

GSS 1972-2022 Cumulative Datafile - Release 2

Dec 10, 2024 (Tue 07:14 AM PST)

Variables

Role	Name	Label	Range	MD	Dataset
Row	**health**	condition of health	1-4	.d, i, j, m, n, p, q, r, s, u, x, y, z	1
Filter	**year(2021-2022)**	gss year for this respondent	1972-2022	.d, i, j, m, n, p, q, r, s, u, x, y, z	1

Frequency Distribution

Cells contain:
-Column percent
-N of cases

		Distribution
health	1: excellent	**29.2** 1,526
	2: good	**54.1** 4,092
	3: fair	**21.3** 1,614
	4: poor	**4.4** 332
	COL TOTAL	*100.0* *7,564*

Summary Statistics

Mean =	2.10	Std Dev =	.76	Coef var =	.36
Median =	2.00	Variance =	.58	Min =	1.00
Mode =	2.00	Skewness =	.43	Max =	4.00
Sum =	15,880.00	Kurtosis =	-.01	Range =	3.00

Inference about the mean:
Std Err = .01 CV(mean) = .00

Statistics exclude missing-data and out-of-range values.

Univariates Output, cont.

5.

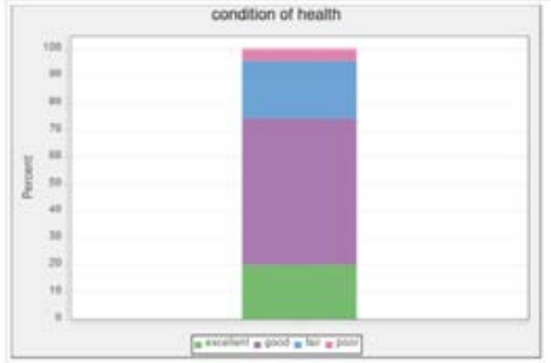

Allocation of cases	
Valid cases	7,564
Cases excluded by filter	64,814
Cases with invalid codes on row variable	12
Total cases	*72,390*

Datasets	
1	/sda/data/gss22rel2
2	/data/gss22rel2/NEWVARS

CSM, UC Berkeley

Recoding Output

1.

Recoding Output

SDA 4.1.5: Tables

GSS 1972-2022 Cumulative Datafile - Release 2

Dec 10, 2024 (Tue 07:18 AM PST)

Variables

Role	Name	Label	Range	MD	Dataset
Row	**hlthinf(Recoded)**	health care system in us inefficient	1-3		1
Filter	**year(2021-2022)**	gss year for this respondent	1972-2022	.d, i, j, m, n, p, q, r, s, u, x, y, z	1

Frequency Distribution

Cells contain:
-Column percent
-N of cases

		Distribution
hlthinf	1: Agree	**60.0** 672
	2: Neither agree or disagree	**22.0** 246
	3: Disagree	**18.0** 202
	COL TOTAL	*100.0* *1,120*

Summary Statistics

Mean =	1.58	Std Dev =	.78	Coef var =	.49
Median =	1.00	Variance =	.60	Min =	1.00
Mode =	1.00	Skewness =	.88	Max =	3.00
Sum =	1,770.00	Kurtosis =	-.79	Range =	2.00

Inference about the mean:
Std Err = .02 CV(mean) = .01

Statistics exclude missing-data and out-of-range values.

Recoding Output, cont.

2.

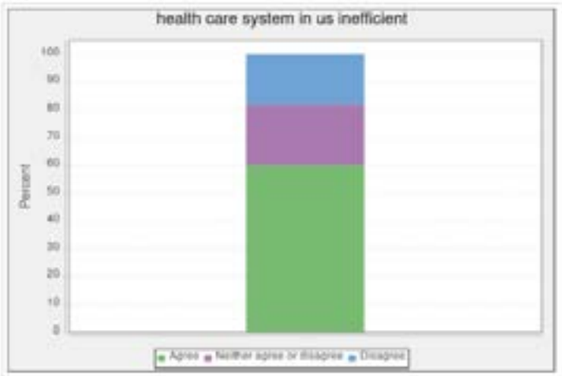

Recode for 'hlthinf'
1 = 1-2 "Agree"; 2 = 3 "Neither agree or disagree"; 3 = 4-5 "Disagree"

Allocation of cases	
Valid cases	1,120
Cases excluded by filter	64,814
Cases with invalid codes on row variable	6,456
Total cases	*72,390*

Datasets	
1	/sda/data/gss22rel2
2	/data/gss22rel2/NEWVARS

CSM, UC Berkeley

Recoding Output

SDA 4.1.5: Tables

GSS 1972-2022 Cumulative Datafile - Release 2

Dec 10, 2024 (Tue 07:18 AM PST)

3.

Variables

Role	Name	Label	Range	MD	Dataset
Row	**sex(Recoded)**	respondents sex	0-1		1
Filter	**year(2021-2022)**	gss year for this respondent	1972-2022	d, i, j, m, n, p, q, r, s, u, x, y, z	1

Frequency Distribution

Cells contain: -Column percent -N of cases		Distribution
sex	0: male	**45.1** 3,363
	1: female	**54.9** 4,101
	COL TOTAL	***100.0*** *7,464*

Summary Statistics

Mean =	.55	Std Dev =	.50	Coef var =	.91
Median =	1.00	Variance =	.25	Min =	.00
Mode =	1.00	Skewness =	-.20	Max =	1.00
Sum =	4,101.00	Kurtosis =	-1.96	Range =	1.00

Inference about the mean:
Std Err = .01 CV(mean) = .01

Statistics exclude missing-data and out-of-range values.

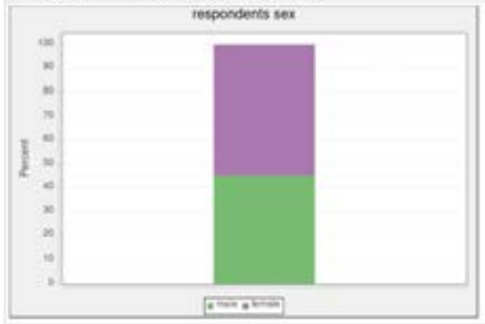

Recoding Output, cont.

4.

Recode for 'sex'
0 = 1 "male"; 1 = 2 "female"

Allocation of cases	
Valid cases	7,464
Cases excluded by filter	64,814
Cases with invalid codes on row variable	112
Total cases	*72,390*

Datasets	
1	/sda/data/gss22rel2
2	/data/gss22rel2/NEWVARS

CSM, UC Berkeley

Recoding Output

SDA 4.1.5: Tables

GSS 1972-2022 Cumulative Datafile - Release 2

Dec 10, 2024 (Tue 07:18 AM PST)

Variables

Role	Name	Label	Range	MD	Dataset
Row	**health(Recoded)**	condition of health	1-3		1
Filter	**year(2021-2022)**	gss year for this respondent	1972-2022	d, i, j, m, n, p, q, r, s, u, x, y, z	1

Frequency Distribution

Cells contain: -Column percent -N of cases		Distribution
health	1: excellent	**20.2** 1,526
	2: good	**54.1** 4,092
	3: not good	**25.7** 1,946
	COL TOTAL	***100.0*** *7,564*

Summary Statistics

Mean =	2.06	Std Dev =	.68	Coef var =	.33
Median =	2.00	Variance =	.46	Min =	1.00
Mode =	2.00	Skewness =	-.07	Max =	3.00

5.

Sum = 15,548.00 Kurtosis = -.81 Range = 2.00
Inference about the mean:
Std Err = .01 CV(mean) = .00

Statistics exclude missing-data and out-of-range values.

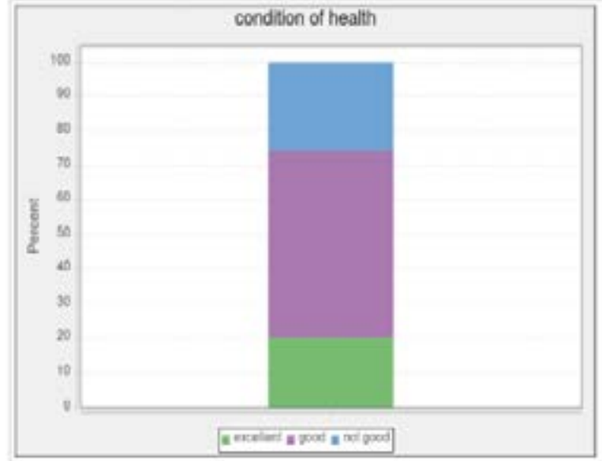

Recode for 'health'
1 = 1 "excellent"; 2 = 2 "good"; 3 = 3-4 "not good"

Allocation of cases	
Valid cases	7,564
Cases excluded by filter	64,814
Cases with invalid codes on row variable	12
Total cases	*72,390*

Datasets	
1	/sda/data/gss22rel2
2	/data/gss22rel2/NEWVARS

CSM, UC Berkeley

Bivariate Output

1.

Bivariate Output

SDA 4.1.5: Tables

GSS 1972-2022 Cumulative Datafile - Release 2

Dec 10, 2024 (Tue 07:31 AM PST)

Variables

Role	Name	Label	Range	MD	Dataset
Row	**hithinf(Recoded)**	health care system in us inefficient	1-3		1
Column	**sex(Recoded)**	respondents sex	0-1		1
Weight	**compwt**	Composite Weight	.0761-17.0027		1
Filter	**year(2021-2022)**	gss year for this respondent	1972-2022	.d,.i,.j,.m,.n,.p,.q,.r,.s,.u,.x,.y,.z	1

Frequency Distribution

Cells contain: -**Column percent** -N of cases -Weighted N		**sex** 0 male	1 female	*ROW TOTAL*
hithinf	1: Agree	**58.4** 308 305.2	**60.0** 363 352.2	**59.3** *671* *657.4*
	2: Neither agree or disagree	**22.3** 104 116.6	**22.0** 142 128.9	**22.1** *246* *245.5*
	3: Disagree	**19.3** 89 100.6	**18.0** 112 105.6	**18.6** *201* *206.2*
	COL TOTAL	***100.0*** *501* *522.4*	***100.0*** *617* *586.6*	***100.0*** *1,118* *1,109.1*
Means		1.61	1.58	1.59
Std Devs		.79	.78	.78
Unweighted N		501	617	1,118

Color coding:	<-2.0	<-1.0	<0.0	>0.0	>1.0	>2.0	Z
N in each cell:	Smaller than expected			Larger than expected			

Summary Statistics

Eta* = .02 Gamma = -.03 Rao-Scott-P: F(2,68) = .07 (p= 0.93)
R = -.02 Tau-b = -.02 Rao-Scott-LR: F(2,68) = .07 (p= 0.93)

2.

Somers' d* = -.02 Tau-c = -.02 Chisq-P(2) = .37
Chisq-LR(2) = .37

*Row variable treated as the dependent variable.

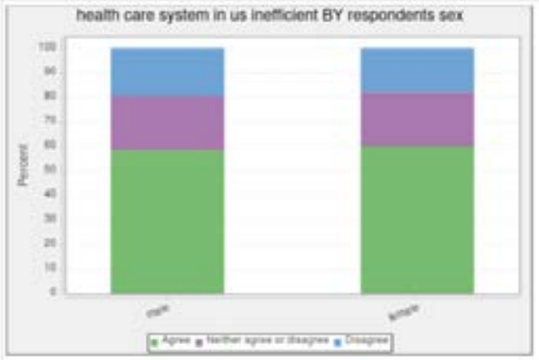

Recode for 'hithinf'
1 = 1-2 "Agree"; 2 = 3 "Neither agree or disagree"; 3 = 4-5 "Disagree"

Recode for 'sex'
0 = 1 "male"; 1 = 2 "female"

Standard error calculations

Sample design: stratified cluster sample

Stratum variable = sdastrata
Cluster variable = sdaclusters

Method: Taylor series approximation

Allocation of cases (unweighted)

Valid cases	1,118
Cases excluded by filter or weight	64,814
Cases with invalid codes on row or column variable	6,458
Total cases	72,390

Datasets

1	/sda/data/gss22rel2
2	/data/gss22rel2/NEWVARS

Bivariate Output, cont.

3.

Bivariate Output

SDA 4.1.5: Tables

GSS 1972-2022 Cumulative Datafile - Release 2

Dec 10, 2024 (Tue 07:34 AM PST)

Variables

Role	Name	Label	Range	MD	Dataset
Row	**hithinf(Recoded)**	health care system in us inefficient	1-3		1
Column	**health(Recoded)**	condition of health	1-3		1
Weight	**compwt**	Composite Weight	.0761-17.0027		1
Filter	**year(2021-2022)**	gss year for this respondent	1972-2022	.d,.i,.j,.m,.n,.p,.q,.r,.s,.u,.x,.y,.z	1

Frequency Distribution

Cells contain: -**Column percent** -N of cases -Weighted N		**health** 1 excellent	2 good	3 not good	*ROW TOTAL*
hithinf	1: Agree	**49.5** 126 109.4	**61.3** 362 371.0	**61.2** 153 170.0	**58.9** *677* *650.4*
	2: Neither agree or disagree	**24.7** 63 54.5	**23.2** 126 140.8	**18.1** 61 50.2	**22.2** *246* *245.5*
	3: Disagree	**25.8** 41 57.1	**15.5** 103 93.5	**20.7** 58 57.7	**18.9** *202* *208.7*
	COL TOTAL	***100.0*** *226* *221.0*	***100.0*** *591* *605.6*	***100.0*** *302* *277.9*	***100.0*** *1,119* *1,104.5*
Means		1.76	1.54	1.60	1.60
Std Devs		.84	.75	.81	.79
Unweighted N		226	591	302	1,119

Color coding:	<-2.0	<-1.0	<0.0	>0.0	>1.0	>2.0	Z
N in each cell:	Smaller than expected			Larger than expected			

Summary Statistics

Eta* = .11 Gamma = -.10 Rao-Scott-P: F(4,136) = 1.54 (p= 0.19)

4.

R = -.06 Tau-b = -.06 Rao-Scott-LR: F(4,136) = 1.54 (p= 0.19)
Somers' d* = -.06 Tau-c = -.05 Chisq-P(4) = 17.20
Chisq-LR(4) = 17.14

*Row variable treated as the dependent variable.

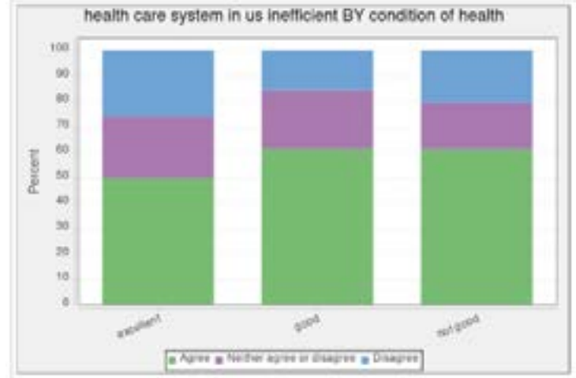

Recode for 'hithinf'
1 = 1-2 "Agree"; 2 = 3 "Neither agree or disagree"; 3 = 4-5 "Disagree"

Recode for 'health'
1 = 1 "excellent"; 2 = 2 "good"; 3 = 3-4 "not good"

Standard error calculations

Sample design: stratified cluster sample

Stratum variable = sdastrata
Cluster variable = sdaclusters

Method: Taylor series approximation

Allocation of cases (unweighted)

Valid cases	1,119
Cases excluded by filter or weight	64,814
Cases with invalid codes on row or column variable	6,457
Total cases	72,390

Datasets

1	/sda/data/gss22rel2

Bivariate Output, cont.

5.

Bivariate Output

SDA 4.1.5: Tables

GSS 1972-2022 Cumulative Datafile - Release 2

Dec 10, 2024 (Tue 07:36 AM PST)

Variables

Role	Name	Label	Range	MD	Dataset
Row	**health(Recoded)**	condition of health	1-3		1
Column	**sex(Recoded)**	respondents sex	0-1		1
Weight	**compwt**	Composite Weight	.0761-17.0027		1
Filter	**year(2021-2022)**	gss year for this respondent	1972-2022	.d,.i,.j,.m,.n,.p,.q,.r,.s,.u,.x,.y,.z	1

Frequency Distribution

Cells contain: -Column percent -N of cases -Weighted N		sex 0 male	1 female	*ROW TOTAL*
health	1: excellent	**20.8** 711 752.8	**18.4** 797 699.3	**19.6** *1,508* *1,452.0*
	2: good	**53.0** 1,787 1,920.2	**55.8** 2,251 2,118.3	**54.5** *4,038* *4,038.4*
	3: not good	**26.2** 862 948.8	**25.7** 1,050 976.7	**26.0** *1,912* *1,925.5*
	COL TOTAL	***100.0*** *3,360* *3,621.7*	***100.0*** *4,098* *3,794.2*	***100.0*** *7,458* *7,415.9*
Means		2.05	2.07	2.06
Std Devs		.68	.66	.67
Unweighted N		3,360	4,098	7,458

Color coding:	<-2.0	<-1.0	<0.0	>0.0	>1.0	>2.0	Z
N in each cell:	Smaller than expected			Larger than expected			

Summary Statistics

Eta* = .01 Gamma = .02 Rao-Scott-P: F(2,146) = 2.59 (p= 0.08)
R = .01 Tau-b = .01 Rao-Scott-LR: F(2,146) = 2.59 (p= 0.08)

6.

Somers' d* = .01 Tau-c = .01 Chisq-P(2) = 8.13
Chisq-LR(2) = 8.13

*Row variable treated as the dependent variable.

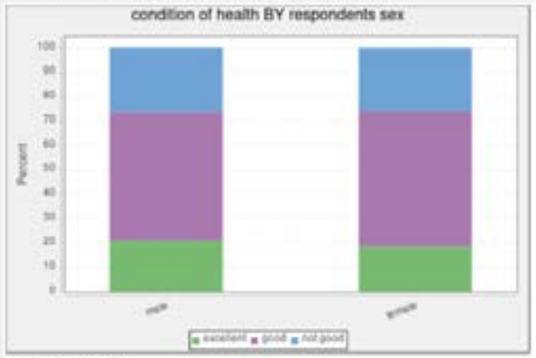

Recode for 'health'
1 = 1 "excellent"; 2 = 2 "good"; 3 = 3-4 "not good"

Recode for 'sex'
0 = 1 "male"; 1 = 2 "female"

Standard error calculations

Sample design: stratified cluster sample

Stratum variable = sdastrata
Cluster variable = sdaclusters

Method: Taylor series approximation

Allocation of cases (unweighted)

Valid cases	7,458
Cases excluded by filter or weight	64,814
Cases with invalid codes on row or column variable	118
Total cases	72,390

Datasets	
1	/sda/data/gss22rel2
2	/data/gss22rel2/NEWVARS

Trivariate Output

1.

Trivariate Output

SDA 4.1.5: Tables

GSS 1972-2022 Cumulative Datafile - Release 2

Dec 10, 2024 (Tue 07:39 AM PST)

Variables

Role	Name	Label	Range	MD	Dataset
Row	**hlthinf(Recoded)**	health care system in us inefficient	1-3		1
Column	**sex(Recoded)**	respondents sex	0-1		1
Control	**health(Recoded)**	condition of health	1-3		1
Weight	**compwt**	Composite Weight	.0761-17.0027		1
Filter	**year(2021-2022)**	gss year for this respondent	1972-2022	.d,.i,.j,.m,.n,.p,.q,.r,.s,.u,.x,.y,.z	1

Statistics for health = 1(excellent)

Cells contain: -Column percent -N of cases -Weighted N		sex 0 male	1 female	*ROW TOTAL*
hlthinf	1: Agree	**63.0** 64 62.6	**39.3** 62 46.8	**50.1** 126 109.4
	2: Neither agree or disagree	**17.6** 22 17.5	**31.1** 37 37.0	**24.9** 59 54.5
	3: Disagree	**19.4** 14 19.3	**29.6** 26 35.3	**25.0** 40 54.6
	COL TOTAL	***100.0*** *100* *99.4*	***100.0*** *125* *119.2*	***100.0*** *225* *218.6*
Means		1.56	1.90	1.75
Std Devs		.80	.83	.83
Unweighted N		100	125	225

Color coding:	<-2.0	<-1.0	<0.0	>0.0	>1.0	>2.0	Z
N in each cell:	Smaller than expected			Larger than expected			

2.

Summary Statistics for health = 1(excellent)

Eta* = .20 Gamma = .36 Rao-Scott-P: F(2,68) = 2.97 (p= 0.06)
R = .20 Tau-b = .20 Rao-Scott-LR: F(2,68) = 3.00 (p= 0.06)
Somers' d* = .23 Tau-c = .23 Chisq-P(2) = 12.63
Chisq-LR(2) = 12.76

*Row variable treated as the dependent variable.

Chart for health = 1(excellent)

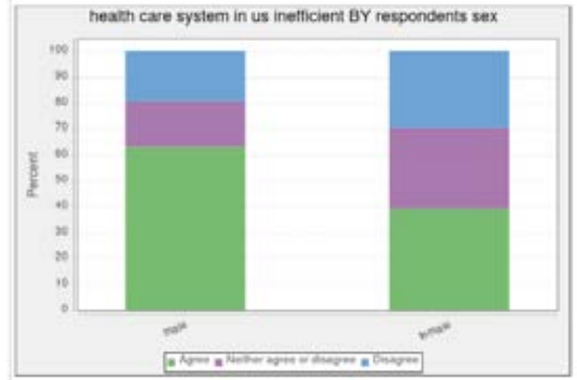

Statistics for health = 2(good)

Cells contain: -Column percent -N of cases -Weighted N		sex 0 male	1 female	*ROW TOTAL*
hlthinf	1: Agree	**58.9** 166 166.2	**63.2** 195 204.1	**61.2** *361* *370.4*
	2: Neither agree or disagree	**23.5** 53 66.4	**23.0** 73 74.3	**23.3** *126* *140.8*
	3: Disagree	**17.6** 45 49.6	**13.7** 58 44.3	**15.5** *103* *93.9*
	COL TOTAL	***100.0*** *264* *282.2*	***100.0*** *326* *322.8*	***100.0*** *590* *605.0*
Means		1.59	1.51	1.54

Trivariate Output, cont.

3.

	Std Devs	.77	.73	.75
	Unweighted N	264	326	590

Color coding: <-2.0 | <-1.0 | <0.0 | >0.0 | >1.0 | >2.0 | Z
N in each cell: Smaller than expected | Larger than expected

Summary Statistics for health = 2(good)

Eta² =	.05	Gamma =	-.09	Rao-Scott-P: F(2,68) =	.35 (p= 0.70)
R =	-.05	Tau-b =	-.05	Rao-Scott-LR: F(2,68) =	.35 (p= 0.70)
Somers' d² =	-.05	Tau-c =	-.05	Chisq-P(2) =	1.85
				Chisq-LR(2) =	1.84

*Row variable treated as the dependent variable.

Chart for health = 2(good)

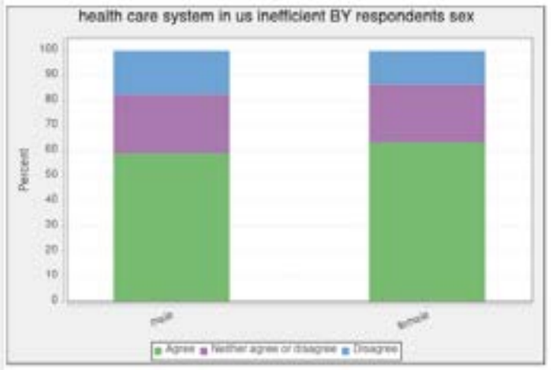

Statistics for health = 3(not good)

Cells contain: -Column percent -N of cases -Weighted N		sex: 0 male	1 female	ROW TOTAL
hlthinf	1: Agree	**54.2** 78 76.4	**68.3** 105 93.6	**61.2** *183* *170.0*
	2: Neither agree or disagree	**23.2** 29 32.7	**12.8** 32 17.5	**18.1** *61* *50.2*
	3: Disagree	**22.5** 30	**18.9** 28	**20.7** *58*

4.

		31.7	25.9	57.7
	COL TOTAL	***100.0*** *137* *140.8*	***100.0*** *165* *137.0*	***100.0*** *302* *277.9*
	Means	1.68	1.51	1.60
	Std Devs	.82	.80	.81
	Unweighted N	137	165	302

Color coding: <-2.0 | <-1.0 | <0.0 | >0.0 | >1.0 | >2.0 | Z
N in each cell: Smaller than expected | Larger than expected

Summary Statistics for health = 3(not good)

Eta² =	.11	Gamma =	-.23	Rao-Scott-P: F(2,68) =	2.18 (p= 0.12)
R =	-.11	Tau-b =	-.12	Rao-Scott-LR: F(2,68) =	2.20 (p= 0.12)
Somers' d² =	-.13	Tau-c =	-.13	Chisq-P(2) =	7.45
				Chisq-LR(2) =	7.53

*Row variable treated as the dependent variable.

Chart for health = 3(not good)

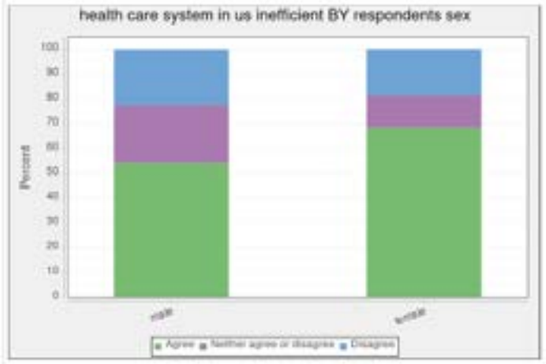

Statistics for all valid cases

Cells contain: -Column percent -N of cases -Weighted N	sex: 0 male	1 female	ROW TOTAL

Trivariate Output, cont.

5.

hlthinf	1: Agree	**58.4** 308 305.2	**59.5** 362 344.5	**59.0** *670* *649.8*
	2: Neither agree or disagree	**22.3** 104 116.6	**22.3** 142 128.9	**22.3** *246* *245.5*
	3: Disagree	**19.3** 89 100.6	**18.2** 112 105.6	**18.7** *201* *206.2*
	COL TOTAL	***100.0*** *501* *522.4*	***100.0*** *616* *579.0*	***100.0*** *1,117* *1,101.5*
	Means	1.61	1.59	1.60
	Std Devs	.79	.78	.78
	Unweighted N	501	616	1,117

Color coding: <-2.0 | <-1.0 | <0.0 | >0.0 | >1.0 | >2.0 | Z
N in each cell: Smaller than expected | Larger than expected

Summary Statistics for all valid cases

Eta² =	.01	Gamma =	-.02	Rao-Scott-P: F(2,68) =	.04 (p= 0.96)
R =	-.01	Tau-b =	-.01	Rao-Scott-LR: F(2,68) =	.04 (p= 0.96)
Somers' d² =	-.01	Tau-c =	-.01	Chisq-P(2) =	.21
				Chisq-LR(2) =	.21

*Row variable treated as the dependent variable.

Chart for all valid cases

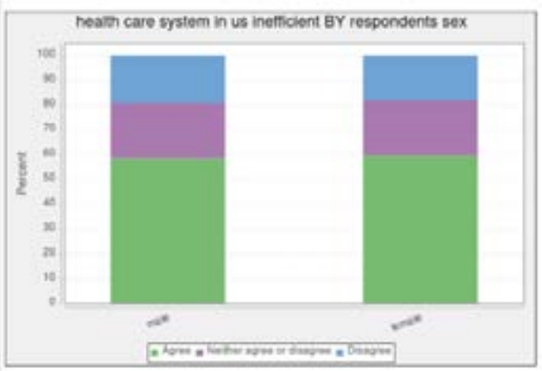

A Comparative Analysis of Attractive and Repulsive Olfactory Circuits in the Drosophila Connectome

Kuzey Sozat, Trenton Jones, Natalia Bojorquez, Cia Varelas, Sanjana Kalagara

Volume 4, Issue 1

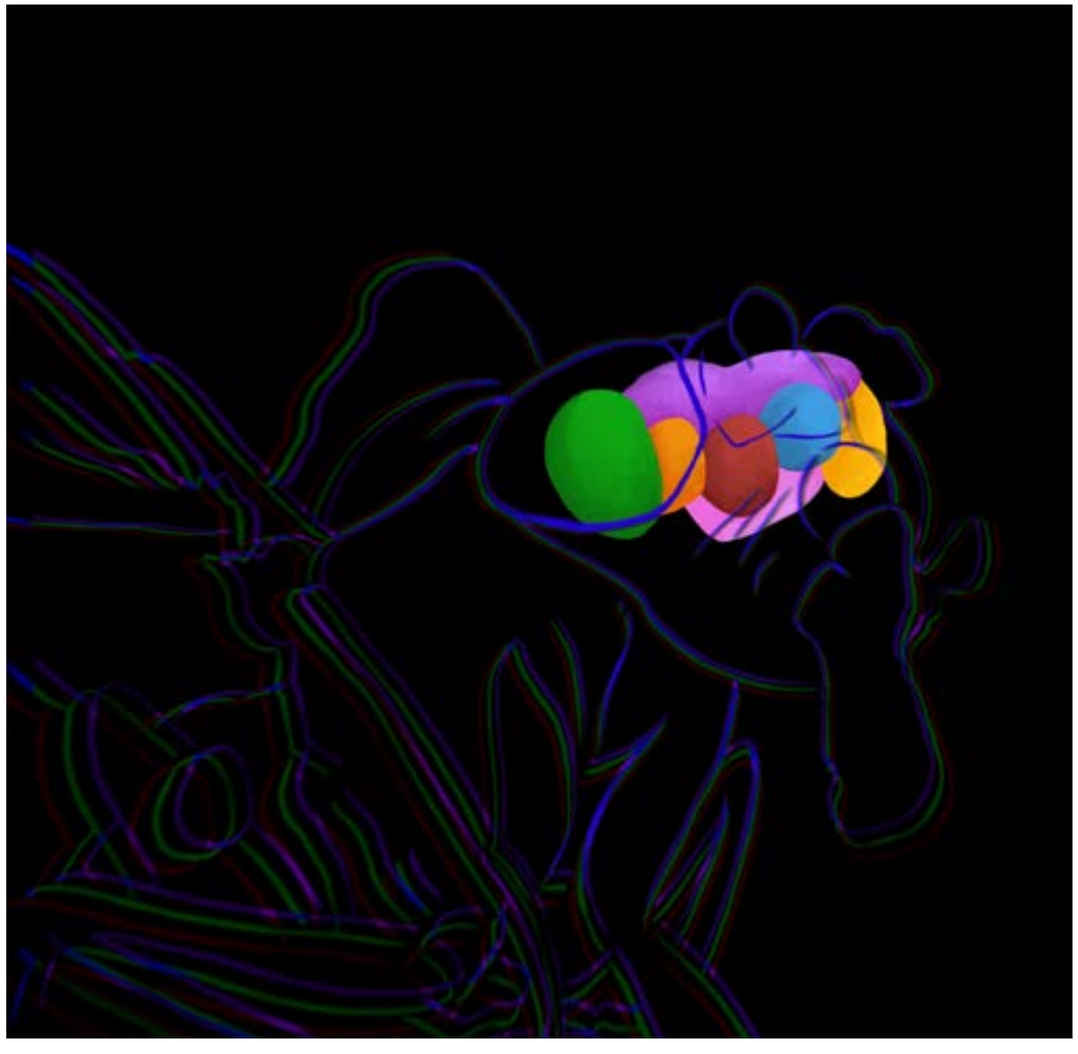

Graphic by Chelsea Gan

Vertices: Duke's Undergraduate Research Journal Volume 4, Issue 1 | Spring 2025

A Comparative Analysis of Attractive and Repulsive Olfactory Circuits in the Drosophila Connectome

Kuzey Sozat, Trenton Jones, Natalia Bojorquez, Cia Varelas, Sanjana Kalagara

Duke University
https://doi.org/10.55894/dv4.14

Abstract

The brain consists of complex sets of neural networks that support sensory integration, computation, and behavior. Olfactory circuits in the *D. melanogaster* brain serve as a model for understanding how the distinct structure and connectivity of these neural circuits mediate diverse behaviors. Currently, the network-level differences between pheromone-detecting olfactory circuits (DA1, VA1v, VA1d) for attraction and odor-detecting circuits (DA2, DC4) for repulsion remain unclear. Conducting a comparative analysis on neural data from the FlyWire connectome of a female adult *D. melanogaster* brain, we found that pheromone-detecting glomeruli are laterally located, while repulsive odor-detecting glomeruli are positioned medially in the antennal lobe (AL) and lateral horn (LH). The DA1 olfactory circuit, characterized by high specificity to its ligand cVA, exhibits few local interneurons (LNs) and minimal lateral inhibition, supporting selective attraction behaviors. In contrast, DC4, associated with acidic compound detection, shows extensive LN connectivity, facilitating broad sensory integration. In higher-order pathways to neuromodulatory neurons, pheromone circuits (DA1, VA1v, VA1d) more directly connect to dopaminergic neurons (DSK, PAM), supporting sexual behavior and associative learning. Furthermore, inputs from olfactory circuits to insulin-producing cells connect through dopaminergic DSK neurons, suggesting a metabolic influence on sexual attraction behaviors. Finally, clock neurons regulating circadian rhythm receive attractive and repulsive olfactory inputs primarily through the lateral horn, which may align innate olfactory-driven behaviors with circadian activity patterns. These findings provide new insights into the structural and functional organization of *D. melanogaster* olfactory circuits, revealing how sensory information is spatially segregated and modulates neural networks for survival, learning, and attraction.

Introduction

Background –

Modern neuroscience seeks to elucidate how neural circuits orchestrate behavior, attempting to answer questions like: "How do brains produce behavior?", with implications for understanding neurodegenerative diseases, psychiatric disorders, and pain. According to contributors to the *Drosophila melanogaster* connectome, "Without a detailed understanding of how neurons connect to one another, we won't have a basic understanding of what goes right in a healthy brain or what goes wrong in disease" (Fuller-Wright, 2024).

Early efforts at neural circuit mapping, which used light microscopy (1957), electron microscopy (1959), electrophysiology (1997), and targeted lesions (2003), failed to afford scientists this "basic understanding" (Swanson et al., 2022). Indeed, these previous efforts only allowed single-cell and single-region resolution. More recent efforts at neural circuit mapping often used genetic labeling methods to visualize and count specific neuron types and identify upstream and downstream partners of these neurons. However, genetic labeling methods are time-consuming. These methods may also label neurons inconsistently due to varying expression levels, yielding false positives and negatives. Furthermore, recent in vivo studies of neural circuits frequently used brain samples from multiple specimens, which may have introduced confounding variables, therefore making comparisons between neural circuits less feasible (Scheffer et al., 2020).

The FlyWire Brain Dataset FAFB v783 ("FlyWire") is the connectome of a female adult *D. melanogaster* brain. FlyWire represents a groundbreaking advancement in connectomics, enabling unprecedented access to the complete neural circuit of the *D. melanogaster* brain. Flywire maps individual neurons, neurotransmitters, neural circuits, and neuropils within a 3D brain volume (Dorkenwald et al., 2024; Schlegel et al., 2024). This publicly available database consists of 140,000 neurons and over 50 million synapses between them (Dorkenwald et al., 2024). Consequently, in contrast to previous efforts at neural circuit mapping, the *D. melanogaster* connectome enables rapid visual and statistical comparisons across the entire fly brain. These comparisons may enable the use of computational and machine-learning methods to accelerate research on how neural circuits mediate behaviors in flies and other complex organisms.

FlyWire was created in four main steps. First, an adult female *D. melanogaster* brain was fixed and cut into thin sagittal slices. Next, each slice was imaged using focused ion beam scanning electron microscopy (FIB-SEM). Distinct neurons were then identified using automated 3D volume reconstruction and segmentation with flood-filling networks. Finally, synapses and neuropils were identified using automated image analysis and human proofreading.

Despite these advancements, the comparative structure and function of olfactory circuits mediating attraction to pheromones versus repulsion from odors remain poorly understood. Our study focuses on three olfactory circuits (DA1, VA1v, and VA1d) that detect pheromones and mediate mating attraction and two odor-detecting circuits (DA2, DC4) that detect repulsive odors to mediate avoidance. For all five olfactory circuits, ORNs expressing a distinct olfactory receptor detect a specific set of compounds and project to distinct glomeruli in the antennal lobe. From there, projection neurons (PNs) project from that glomerulus to the lateral horn (LH) and mushroom body (MB), from which LH and MB output neurons project to higher-order brain centers. For the DA1 circuit, ORNs expressing the Or67d olfactory receptor detect the cis-vaccenyl acetate (cVA) pheromone produced by male Drosophila flies and project via the DA1 glomerulus to mediate increased copulatory receptivity in females (Kurtovic et al., 2007). For the VA1v circuit, Or47b-expressing ORNs detect methyl laurate (ML) and project via the VA1v glomerulus to mediate copulatory behavior. Similarly, for the VA1d circuit, Or88a-expressing ORNs detect ML, methyl myristate (MM), and methyl palmitate (MP) and project via the VA1d glomerulus to mediate short-range attraction (Dweck et al., 2015). Thus, all three pheromone-detecting olfactory circuits mediate attraction in the female brain. For the DA2 glomerulus, Or56a-expressing ORNs detect geosmin (a bacterial or fungal odorant) and project via the DA2 glomerulus to mediate avoidance (Stensmyr et al., 2012). For the DC4 glomerulus, IR64a-expressing ORNs detect acidic compounds and project via the DC4 glomerulus to mediate avoidance. Thus, both odor-detecting olfactory circuits mediate repulsion (Ai et al., 2010). However, the organization of these neural circuits beyond the lateral horn and mushroom body remains less understood.

Unknown/Question –

Despite extensive research on the DC4, DA2, VA1d, VA1v, and DA1 glomeruli, it remains unclear how their respective circuits compare in terms of morphology, connectivity, and elicited behaviors. More specifically, the circuit-level differences between pheromone-detecting circuits (DA1, VA1v, VA1d) for attraction and odor-detecting circuits (DA2, DC4) for repulsion remain unclear. Structural differences between attractive and repulsive circuits may inform hypotheses that explain functional differences between these olfactory circuits. Consequently, our analysis revolves around the following research questions: How does the number of each neuron type differ between the DC4, DA2, VA1d, VA1v, and DA1 circuits? How do the morphologies of and connections between the neuron types vary amongst the five circuits? What does neuron count, structure, and connectivity of each circuit reveal about the divergent behaviors elicited by the five circuits?

Experimental approach –

Using FlyWire's Codex Connectome Data Explorer, we determined the numbers of olfactory receptor neurons (ORNs), projection neurons (PNs), local interneurons (LNs), lateral horn neurons (LHNs), and mushroom body neurons (MBONs) that connect to each of the 5 glomeruli of interest. We also identified pathways between PNs and target cells and visualized these pathways on 3D reconstructions of the *D. melanogaster* hemibrain.

Materials and Methods

Within FlyWire, the Codex Connectome Data Explorer was used to explore the five glomeruli of interest and their associated neural circuits. Individual neurons were identified within the "Search" tab, summary statistics were identified within the "Stats" tab, 3D views of neural circuits in the fruit fly brain were visualized within the "3D Viewer" tab, and neural circuit pathways were identified within the "Connectivity" tab to "Pathways" sub-tab.

Stats –

The "Stats" tab of FlyWire was primarily used to find the number of ORNs, PNs, LHNs, MBONs, and LNs and their NT type. For each type of olfactory neuron within a glomerulus, the upstream/downstream partners, numbers of synapses, types of connected cells, and input and output regions were also identified this way. The following search terms were used:

ORNs: "[Glomerulus] && type == ORN_[Glomerulus] && side == right"

PNs: "[Glomerulus] && class == ALPN && side == right"

LNs: "[Glomerulus] && side == right"

LHNs: "[Glomerulus] && class == ALPN && side == right"

MBONs: "[Glomerulus] && class == ALPN && side == right"

LN counts were determined through the PNs that connect to each glomerulus, following the " □[#] upstream" link in the "Related Cells" column for each individual PN and identifying all cells that had "AL local neuron, ALLN" listed under the "Community Labels" column. Many of the same LNs connected to different PNs within the same glomerulus, so these were identified by hand to ensure no LNs were double-counted in the total. LHN counts were determined by looking at downstream partners of PNs labeled with "LH" within the "Top Output Types (Synapses / Partners)" section. Similarly, MBON counts were determined by looking at downstream partners of PNs labeled with "KC" (Kenyon cells) within the "Top Output Types (Synapses / Partners)" section.

Pathways –

The following search terms were used to establish connections between PNs and target cells:

Vertices: Duke's Undergraduate Research Journal Volume 4, Issue 1 | Spring 2025

Input search: "[Glomerulus] && class == ALPN && side == right".

Output searches: "NT == DA", "NT == SER", "Insulin-Producing", and "Clock"

Individual neurons were selected, and the "pathways" tab was navigated using the "connectivity" drop-down menu. The simplest pathway was visualized by clicking "view pathways chart" and selecting the option with the fewest number of hops. For context, it was important to identify the pathway with the minimum number of synapses between points A and B while simultaneously prioritizing synapse strength. Unique cell IDs were revealed by clicking on each "connected cell, and these IDs were then recorded for 3D visualization on the Drosophila brain.

Imaging –

A chosen pathway was visualized in 3D by separating the relevant "cell IDs" with commas and inputting them into the FlyWire search box. "Color By" was changed to "Color By Type," and "layer list panel" and "layer side panel" were selected to determine the colors of particular cell types. If the color labels of two or more cells were too similar to one another (e.g. aqua and blue), new color labels were generated. The "render" option under the "layer list panel" was selected, and the wheel next to "color seed" was clicked. This process was repeated until all cells were colored distinctly. A screenshot of the 3D viewer was taken to preserve our work and visually present neuron morphology and pathways.

Olfactory Receptor Neurons (ORNs) –

The analysis of olfactory receptor neurons (ORNs) across the five examined glomeruli revealed several interesting patterns. DA1 stood out with the highest number of ORNs, totaling 66 (Table 1). Acetylcholine (ACh) was the predominant neurotransmitter used by ORNs across most glomeruli. However, some exceptions were noted: a small subset of DA1 and DA2 ORNs utilized serotonin, while the majority of DC4 ORNs with identified neurotransmitters employed GABA. Interestingly, for VA1v and VA1d glomeruli, the neurotransmitter type remained unidentified for most ORNs (Table 1). A consistent feature observed across all five glomeruli was the bilateral projection of ORNs to both antennal lobes, highlighting the symmetrical nature of these olfactory circuits.

Antennal Lobe Local Neurons (ALLNs) –

In the antennal lobe, the DA1 and DA2 glomeruli connected to a relatively low number of local neurons (LNs), whereas the DC4 glomerulus had the highest number of connecting LNs. Specifically, the DA1 and DA2 glomeruli connected to 38 and 18 LNs, respectively, while the DC4 glomerulus connected to 63 LNs (Table 1). In addition, pheromone-detecting glomeruli were localized to the lateral antennal lobe, whereas repulsive odor-detecting glomeruli were localized more medially.

Figure 1: Localization of pheromone and repulsive food odor-detecting glomeruli in the antennal lobe. Pheromone-detecting glomeruli (DA1, VA1v, VA1d) are located in the lateral AL, whereas repulsive food odor-detecting glomeruli (DA2, DC4) are located in the medial AL.

Projection Neurons (PNs) –

The findings for projection neurons (PNs) in olfactory circuits revealed several key characteristics. We observed convergence from olfactory receptor neurons (ORNs) onto PNs in each glomerulus, as evidenced by the lower number of PNs compared to ORNs. Among the glomeruli studied, DA1 had the highest number of PNs at 11. Most PNs in each glomerulus utilized acetylcholine (ACh) as their neurotransmitter, except for DC4 PNs, which predominantly used GABA.

In the antennal lobe, PNs can be categorized as either ventral (vPNs) or lateral (lPNs) based on their cell body location and projection patterns. The vPNs have cell bodies situated ventral to the antennal lobe and project via the medial antennocerebral tract (mACT) pathway exclusively to the LH (Marin et al., 2002). In contrast, lPNs have cell bodies located lateral to the antennal lobe and project via the inner antennocerebral tract (iACT) pathway to both the MB and LH (Figure 2).

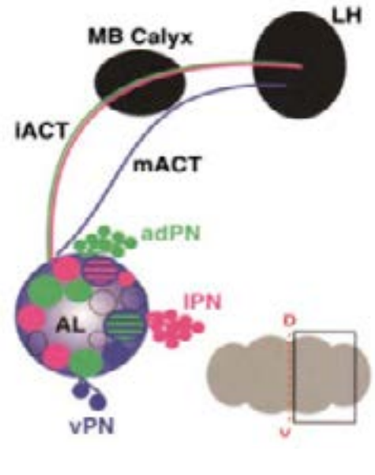

Figure 2: Diagram of the projection pathways of PNs derived from three neuroblast types. Anterodorsal PNs (adPNs) and lateral PNs (lPNs) project via the medial antennocerebral tract (mACT) pathway to both the MB and LH. Ventral PNs (vPNs) project via the inner antennocerebral tract (iACT) pathway to the LH only. Figure adapted from Marin et al., 2002.

The DA1 glomerulus has both lateral PNs (lPNs) and lateral ventral PNs (lvPNs) with cell bodies positioned lateral to the antennal lobe, projecting to both the MB and LH via the iACT pathway. DA1 vPNs, however, project solely to the LH via the mACT pathway (Figure 3). Similar projection patterns were observed in DC4, VA1v, and VA1d glomeruli, with lPNs projecting to both MB and LH via iACT, and vPNs projecting only to LH via mACT (Table 1).

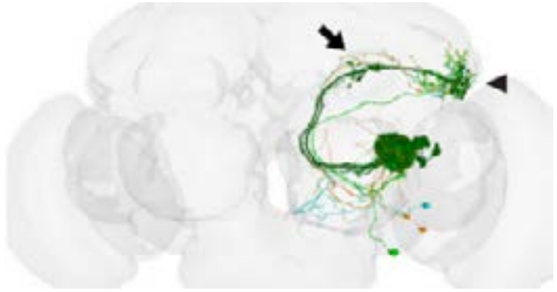

Figure 3: 3D visualization of projections from DA1 glomerular PNs to lateral horn (LH) and mushroom body (MB) neuropils. DA1 lateral PNs (lPNs) are dark green, and ventral PNs (vPNs) are light green. Multi-glomerular lateral ventral PNs (lvPNs) are orange and aqua. The lPNs and lvPNs project to MB and LH via the iACT pathway. The vPNs project to the LH only via the mACT pathway. Lateral horn (LH) is marked by the black arrowhead, and mushroom body (MB) is marked by the black arrow.

Notably, the DA2 glomerulus stood out because it has only lPNs with laterally located cell bodies that project to both MB and LH (Figure 4). Projections from DA2 PNs form two branches, innervating the dorsal and ventral edges of the LH without apparent overlap with other glomerular PNs that innervate central LH regions.

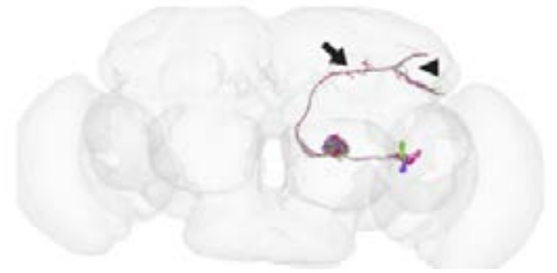

Figure 4. 3D visualization of projections from DA2 glomerular PNs to lateral horn (LH) and mushroom body (MB) neuropils. Each of the 6 ventral PNs (vPNs) has a distinct color and projects via the iACT pathway to the MB (black arrow) and LH (black arrowhead).

The projection patterns of PNs to MB and LH relate closely to the function of olfactory circuits. Simultaneous inputs from dopaminergic (DA) and olfactory neurons to MB Kenyon cells mediate associative learning between odors and rewards or punishments (Marin et al., 2002). The LH, on the other hand, integrates olfactory inputs to mediate

stereotyped behavioral responses to specific odors (Jefferis et al., 2007). Interestingly, PN innervation of the LH maintains the medial to lateral segregation in the antennal lobe, with attractive pheromone-detecting PNs projecting to more dorsolateral LH and repulsive odor-detecting PNs projecting to more ventromedial LH (Figure 5). PN projections to the MB were less spatially segregated and more sparse compared to the LH. We also found that pheromone-detecting PNs innervate more MB neurons, which may support greater behavioral learning and plasticity for courtship behaviors (Table 1).

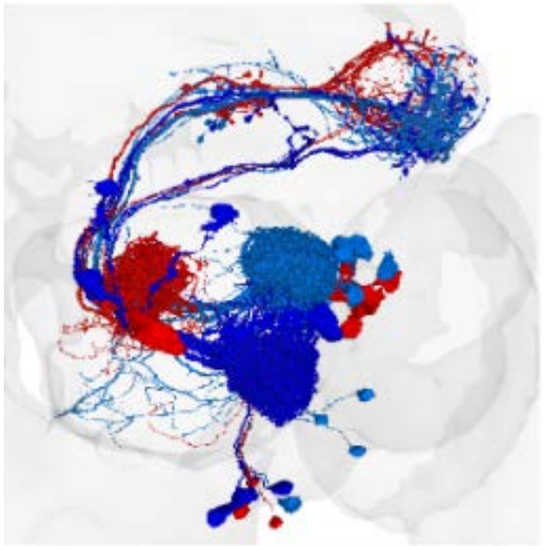

Figure 5: 3D visualization of attractive pheromone-detecting versus repulsive odor-detecting projection neurons for each olfactory circuit. On the right hemibrain, all pheromone-detecting PNs (DA1, VA1v, VA1d) are blue, and all odor-detecting PNs (DA2, DC4) are red. Pheromone-detecting PNs project to the ventrolateral region of the LH, whereas repulsive odor-detecting PNs project to the dorsomedial region of the LH.

Dopaminergic Neurons –

Our examination of dopaminergic cells gave insight into the intricate connections between glomerular projection neurons (PNs) and various brain regions. All five glomerular PNs project to numerous mushroom body (MB) Calyx cells, which converge onto a dorsal paired medium (DPM) neuron that subsequently projects to PAM08 dopaminergic neurons (Keene et. al., 2006). Additionally, DA1, DC4, and VA1d glomerular PNs project to an anterior paired lateral (APL) neuron, an MB interneuron that also project to the PAM08 dopaminergic neuron in the protocerebral anterior medial (PAM) region (Prisco et. al., 2021), which primarily mediates positive reinforcement (Owald and Waddell, 2015). The VA1v PNs exhibit a unique projection pattern, connecting to a superior medial protocerebral (SPM) neuron, which in turn projects to an MB output neuron (MBON) (Li et. al., 2020). This MBON then extends to the PAM12 dopaminergic neuron (Table 2).

The connections between PNs and dopaminergic cells via the lateral horn (LH) are equally complex. DA1, DC4, VA1v, and VA1d PNs project to DSKMP3 dopaminergic neurons through LH neurons. DA1 and DC4 also reach DSKMP3 neurons via superior lateral protocerebrum (SLP) neurons. DA2 PNs have a more intricate pathway, projecting to DSKMP3 dopaminergic neurons through multiple layers of numerous LH neurons. DC4, VA1v, and VA1d PNs also connect to PAM01 dopaminergic neurons via LHCENT3 neurons, which are centrifugal neurons providing feedback from higher-order neurons to the LH and MB (Schlegel et al., 2021). DA1 PNs uniquely project to PAM01 dopaminergic neurons through both MB and LH neurons. Lastly, DA2 PNs project to many LH and SLP neurons, which in turn are connected to PAM01 dopaminergic neurons via a GABAergic lateral horn centrifugal (LHCENT) neuron (Table 3).

Serotonin Neurons –

For each glomerular circuit, PNs projecting to MB and LH neurons connect to distinct populations of serotonergic neurons. We found that all glomeruli except for DC4 have projections to PFNm neurons through MB and/or LH neurons. Specifically, DA1 PNs project to PFNm serotonergic neurons via MB Kenyon cells and LH.CRE neurons that synapse onto MBON neurons (Table 2). In addition, DA2 and VA1v PNs project to PFNm serotonergic neurons via MB neurons to lateral accessory lobe-crepine-posterior nodulus (LCNOp) neurons. Similarly, VA1d PNs project to PFNm serotonergic neurons via both MB and LH neurons, which both project to LCNOp neurons. In contrast, DC4 PN pathways to PFNm

Glomerulus	# of ORNs	# of PNs	# of LNs
DA1 (Or67d)	66 - ACH (43) - SER (5) - N/A (18)	11 - ACH (10) - GABA (1)	38 - GABA - SER - N/A
DA2 (Or56a)	22 - ACH (13) - SER (1) - N/A (8)	6 - ACH (6)	18 - GABA - SER - ACH - GLUT
DC4 (Ir64a)	11 - GABA (3) - ACH (1) - N/A (7)	4 - GABA (3) - ACH (1)	63 - GABA - ACH - SER - N/A
VA1d (Or88a)	46 - ACH (4) - GABA (1) - N/A (41)	5 - ACH (4) - GABA (1)	31 - GABA - ACH - GLUT - SER
VA1v (Or47b)	42 - ACH (5) - GABA (2) - N/A (35)	7 - ACH (5) - GABA (2)	45 - GABA - SER - ACH - N/A

Table 1: Quantification of neuronal types and receptors associated with each glomerulus in the female *D. melanogaster* connectome. The table details the number of olfactory receptor neurons (ORNs), projection neurons (PNs), and local interneurons (LNs) connected to each glomerulus, along with the neurotransmitter type released by each type of neuron and the odor receptor expressed by the ORNs. Neurons with cell bodies on the right side of the brain connectome were quantified and traced. Each glomerulus exhibits distinct odor receptors linked to various functions: Or67d (detects cVA from males, suppresses courtship in males, and increases courtship receptivity in females), Or56a (triggers repulsive behavior), Ir64a (detects acids, mediates avoidance, and is expressed in the coeloconic sensilla ORNs), Or88a (attraction), Or47b (mediates copulation).

or LB1b serotonergic neurons appear convoluted with many nodes or with weak synaptic connections, suggesting that the DC4 circuit does not have strong connections to PFNm serotonergic neurons (Table 2).

We also found that all five glomerular PNs project to LB1b neurons via LH and GNG neurons. Specifically, DA1, VA1v, and VA1d PNs project to LB1b serotonergic neurons via two nodes of LH and gnathal ganglion (GNG) neurons (Table 3). Similarly, DA2 and DC4 PNs project to LB1b serotonergic neurons via three nodes of LH, LH.SLP, and GNG neurons. Yet, the pheromone-detecting PNs appear to have fewer nodes between the PNs and LB1b neurons compared to the odor-detecting PNs (Table 3).

Insulin Neurons –

The projection patterns of olfactory projection neurons (PNs) to insulin-producing cells show distinct pathways through both the mushroom body (MB) and lateral horn (LH). Through the MB pathway, DA1 and DA2 PNs project to insulin-producing cells via APL neurons, which are connected to the ventral median (VM) OA cluster (OA-VPM) neurons, and subsequently to bilateral T-shaped OA-VUM neurons. Notably, DC4, VA1v, and VA1d PNs do not appear to have direct projections to insulin-producing cells through this pathway (Table 2).

Through the LH pathway, different PNs exhibit varied connectivity patterns. DA1 PNs connect to insulin-producing cells via LH neurons to SLP

Glomerulus	Dopamine (DA)	Serotonin (SER)	Insulin	Clock
DA1 (Or67d)		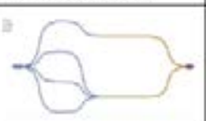	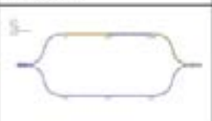	
DA2 (Or56a)	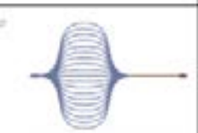			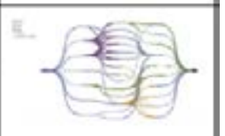
DC4 (Ir64a)		N/A	N/A	N/A
VA1d (Or88a)			N/A	N/A
VA1v (Or47b)			N/A	N/A

Table 2: Pathways from PNs to Target Cells via Mushroom Body. The table shows the connectivity pathways from each of the five glomeruli (DA1, DA2, DC4, VA1d, VA1v) to each type of target cell (DA, SER, insulin, and clock neurons) via intermediate neurons that include MB neurons. The type of neurotransmitter used in the synapse between two neurons corresponds to the color of the pathway between two nodes, and is indicated by the key in the upper left corner of each diagram. The number of synapses connecting two neurons is written as a number on each pathway between two nodes. In each diagram, the projection neuron and target cell correspond to the far left and far right nodes, respectively.

neurons, while DA2 PNs extend this pathway further, projecting via LH neurons to SLP neurons and then to DNpe neurons in the superior medial protocerebrum (SMP). DC4 and VA1d PNs take a different route, projecting to insulin-producing cells through LHAV neurons in the LH to DSKMP3 dopaminergic neurons. VA1v PNs follow a similar pattern, connecting insulin-producing cells via LH neurons to DSKMP3 dopaminergic neurons (Table 3).

Clock Neurons –

For each olfactory circuit, we found that projection neurons (PNs) had more direct pathways to clock neurons through the LH compared to the MB. For pathways connecting to clock neurons through the MB, we found that DA1 PNs project to s-CPDN3C clock neurons via MB calyx neurons to VL1 PNs, connecting to VP1 PNs in the left AL, ultimately projecting to the s-CPDN3C circadian clock neurons in superior medial protocerebrum (SMP). DA2 PNs project to I-LNv clock neurons via MB calyx neurons, diverging to DN1a (dorsal neuron group 1 anterior) neurons in the posterior lateral protocerebrum, followed by connections to medulla tangential neurons that ultimately synapse on the PDF-expressing large ventrolateral clock neurons in the tangential and accessory medulla regions. However, DC4, VA1d, and VA1v did not have clear projections to clock neurons via MB neurons (Table 2).

For pathways connecting to clock neurons through the LH, we found that DA1 PNs project to I-LNv clock neurons via neurons in the LH and anterior ventrolateral protocerebrum (AVLP), then to neurons spanning the AVLP and gnathal ganglia, followed

Glomerulus	Dopamine (DA)	Serotonin (SER)	Insulin	Clock
DA1 (Or67d)				
DA2 (Or56a)	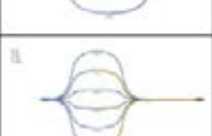			
DC4 (Ir64a)				
VA1d (Or88a)				
VA1v (Or47b)			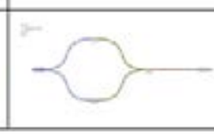	

Table 3. Pathways from PNs to Target Cells via Lateral Horn. The table shows the connectivity pathways from each of the five glomeruli (DA1, DA2, DC4, VA1d, VA1v) to each type of target cell (DA, SER, insulin, and clock neurons) via intermediate neurons that include LH neurons. The type of neurotransmitter used in the synapse between two neurons corresponds to the color of the pathway between two nodes, and is indicated by the key in the upper left corner of each diagram. The number of synapses connecting two neurons is written as a number on each pathway between two nodes. In each diagram, the projection neuron and target cell correspond to the far left and far right nodes, respectively.

by neurons in the posterior lateral protocerebrum (PLP) and medulla (ME), ultimately projecting to an I-LNv clock neuron that bilaterally projects in the ME neuropil. Similarly, DA2 PNs project to I-LNv clock neurons via the LH through AVLP neurons to neurons spanning the PLP and ME, ultimately projecting to the PDF-expressing I-LNv clock neurons in the medulla. In contrast, DC4 and VA1d PNs project to circadian clock neurons in the SMP. Specifically, DC4 adPNs project to s-CPDN3c clock neurons via LH neurons that project to SMP neurons and then to circadian clock neurons in the SMP. Similarly, VA1d adPNs project to s-CPDN3c clock neurons via LH and SLP neurons that connect to SMP neurons that then synapse in the SMP on the circadian clock neurons. Finally, VA1v vPNs project onto 5th-LNv clock neurons via LH neurons that connect to DN1a MB neurons that then connect to the visual projection circadian clock neuron in the SMP (Table 3).

Discussion

Antennal Lobe - Spatial and Functional Segregation

Our findings show distinct spatial and functional segregation between pheromone-detecting and food odor-detecting glomeruli in the antennal lobe (AL). Pheromone-detecting glomeruli (DA1, VA1v, VA1d) are localized laterally, while repulsive odor-detecting glomeruli (DA2, DC4) are positioned more medially.

DA1 exhibits the highest numbers of ORNs (66) and PNs (11), but relatively few LNs (38) among their respective categories. This suggests that there is minimal lateral inhibition and high specificity

for its ligand, cVA. This configuration supports selective attraction behaviors triggered only at low cVA concentrations. Conversely, DC4 displayed the opposite pattern, having the fewest ORNs (11) and PNs (4) but the most LNs (63). This may indicate broad sensory integration and generalized responses to acidic compounds, which rely on the increased LN connectivity. DA2, with the fewest LNs, reflected minimal sensory integration across the AL, emphasizing fast, specific geosmin detection and avoidance hardwired into the fly for survival. In other words, selective detection of geosmin may avoid interference from other olfactory circuits and may be essential for survival.

Overall, DA1 and DA2 circuits exhibit strong selectivity with minimal cross-glomerular input, enabling precise behavioral responses to critical stimuli. In contrast, DC4's LN-rich network suggests broader sensory integration for detecting and processing diverse environmental odors.

PN Projections to LH and MB - Functional Segregation and Pathway Specialization

Our findings highlight that DA2 exhibits unique projection patterns compared to other olfactory circuits. Unlike DA1, VA1v, VA1d, and DC4, which project through both the inner antennocerebral tract (iACT) and medial antennocerebral tract (mACT), DA2 PNs bypass the mACT pathway entirely. This exclusive use of the iACT suggests that DA2 is functionally segregated from other olfactory circuits, reflecting its specialized role in detecting geosmin even at low concentrations.

DA2 PNs target both dorsal and ventral LH regions while avoiding central LH zones. This bifurcated projection may enable the integration of parallel avoidance pathways, enhancing sensitivity to geosmin. In contrast, PNs from other glomeruli project to inner LH regions, emphasizing distinct spatial coding of pheromonal and food-related odors in the LH.

DA2 also exhibits spatial segregation in the MB, which may reinforce its functional segregation. While DA1, VA1v, VA1d, and DC4 exhibit overlapping MB projections, the DA2 circuit's sparse innervation was limited to specific MB zones, reinforcing its role in hardwired avoidance rather than associative learning. In contrast, the broader MB innervation, especially by DA1, likely supports memory and courtship learning. These differences reflect the DA2 circuit's prioritization of rapid, innate avoidance with minimal sensory interference, while other glomeruli balance innate and learned behavioral responses through broad, overlapping projections to both LH and MB.

Lateral Horn (LH) - Behavioral Response Integration

The LH plays a central role in mediating innate and immediate behavioral responses to olfactory stimuli by integrating PN inputs into specific behavioral outputs (Jefferis et al., 2007). PN projections retained the antennal lobe's medial-lateral spatial organization, with pheromone-detecting PNs targeting lateral LH regions and food odor-detecting PNs targeting medial regions.

Pheromone-detecting PNs from DA1, VA1v, and VA1d project to the ventrolateral LH, consistent with their role in mediating attraction. In contrast, food odor-detecting PNs from DA2 and DC4 project more dorsomedially, aligning with their roles in mediating avoidance. Notably, DC4 exhibits broad, diffuse LH innervation which supports general responses to acidic compounds, enabling vast sensory input integration. Conversely, DA2 has highly localized LH innervation, reflecting its high selectivity for geosmin and its hardwired avoidance response.

Thus, our findings suggest that spatially distinct LH innervation patterns encode behavioral valence. Pheromone-specific circuits drive attraction through localized lateral LH innervation, while repulsive food-odor circuits rely on medial LH targets, showing spatially segregated wiring for survival-critical responses.

Mushroom Body (MB) - Associative Learning and Plasticity

The MB mediates associative learning by integrating PN inputs with modulatory signals from dopaminergic (DA) neurons that encode reward or punishment (Marin et al., 2002). Compared to the LH, PN innervation of the MB appears much sparser, likely reflecting the MB's role in flexible, learned behavioral responses rather than innate, reflexive behaviors.

PNs from all five glomeruli sparsely target overlapping regions of the MB. This overlap may enable MB Kenyon Cells (MBNs) to integrate inputs from multiple glomeruli, promoting odor discrimination and memory formation. MB output neurons (MBONs) likely combine MBN activity in unique ways depending on the circuit, supporting distinct learned behavioral responses for different olfactory cues.

Interestingly, pheromone-detecting PNs from DA1, VA1v, and VA1d show broader and denser MB innervation than food-detecting PNs. This suggests enhanced associative learning for courtship-related stimuli. In contrast, the more restricted MB input from food-detecting PNs, especially DA2, reflects limited associative learning for aversive stimuli greater reliance on hardwired avoidance mechanisms rather than learning. Future research should investigate how these innervation patterns shape memory formation, learning plasticity, and circuit modulation.

DA Cell Pathways - Reinforcement and Sexual Behavior Modulation

Drosulfakinin (DSK) dopaminergic signaling has been implicated in promoting female sexual behavior (Wang et al., 2022). In line with this, DA1, VA1v, and VA1d PNs project to DSKMP3 dopaminergic neurons via a single relay from LH neurons, potentially facilitating immediate, pheromone-driven sexual receptivity. In contrast, the DA2 circuit's indirect, multisynaptic pathway to DSKMP3 neurons suggests weaker or more diffuse modulation of avoidance responses to geosmin. Thus, pheromone-detecting circuits may leverage DSK signaling to promote stereotyped, innate attraction behaviors.

All five circuits project to PAM dopaminergic neurons through MB calyx cells converging onto MB output neurons. Because PAM neurons mediate positive reinforcement (Owald and Waddell, 2015), this shared connectivity suggests that even avoidance mediating glomeruli (DA2, DC4) can engage reward pathways, possibly reinforcing adaptive responses such as avoiding toxins or learning about aversive stimuli. However, DA1, VA1v, and VA1d PNs also accessed PAM neurons via additional intermediaries like APL and SPM neurons, suggesting that pheromone-detecting circuits receive stronger positive reinforcement. This could enhance learning and memory formation linked to sexual attraction, allowing flies to integrate pheromone cues with internal states and past experiences.

SER Cell Pathways - Neuromodulatory Integration and Behavioral Context

PFNm serotonergic neurons, associated with the fan-shaped body and protocerebral bridge, influence navigational behaviors, context-dependent action selection, and wakefulness (Hulse et al., 2021; Tomita et al., 2021). All glomeruli except DC4 project to PFNm neurons through MB and/or LH neurons, indicating that pheromone (DA1, VA1v, VA1d) and geosmin-detecting (DA2) circuits may recruit serotonin for modulating behaviors under varying contexts. This could include fine-tuning attraction or avoidance based on internal states or environmental cues. DC4's lack of strong PFNm connectivity suggests that broad acid detection may rely less on neuromodulatory adjustments, maintaining more hardwired avoidance strategies.

Additionally, LB1b serotonergic neurons are linked to bitter taste detection (Sung et al., 2017). All examined circuits project to LB1b neurons via LH and gnathal ganglion (GNG) neurons, although pheromone-detecting pathways had more direct connections than DA2 and DC4. This arrangement hints that pheromone circuits may integrate taste and olfactory cues more efficiently, while food-odor circuits process bitter signals through additional intermediaries. The functional implications of this less direct connection remain an open question, potentially influencing how gustatory and olfactory signals are integrated for avoidance or other behaviors.

Insulin Cell Pathways - Metabolic State and Olfactory Drive

Insulin-producing cells (IPCs) in the pars intercerebralis (PI) regulate metabolism, feeding,

and circadian rhythms (Bisen et al., 2024). Insulin signaling is also required for cVA-mediated attraction (Lebreton et al., 2015), suggesting that DA1 projections to IPCd could form a positive feedback loop. When flies are well-fed and insulin levels are high, the DA1 circuit's excitatory input may strengthen cVA detection and facilitate reproductive behaviors.VA1v, VA1d, and DC4 have dopaminergic inputs via DSKMP3 neurons to IPCs, potentially linking attraction or avoidance circuits to metabolic cues. For instance, the pheromone-driven attraction might be modulated by insulin levels that reflect energy availability, while DC4's broader avoidance could be modulated by metabolic states to optimize foraging and dietary choices. The interplay between insulin signaling and olfaction thus may enhance adaptive decision-making by coupling internal energy balance with olfactory-driven behaviors.

Clock Cell Pathways - Circadian Modulation of Olfactory Responses

Clock neurons in Drosophila's circadian network regulate daily rhythms, influencing behavior timing. I-LNv neurons, producing pigment-dispersing factor (PDF), synchronize other clock neurons and slow circadian pace (Li et al., 2014). Both DA1 and DA2 PNs project to I-LNv neurons via LH, and DA2 PNs also project via the MB to I-LNv neurons. This suggests that both attraction (DA1) and avoidance (DA2) circuits may modulate circadian timing, potentially adjusting activity patterns in response to pheromone availability or toxin presence.

All other glomeruli also formed linear LH pathways to clock neurons, indicating that the circadian system likely integrates multiple olfactory inputs to optimize daily behavior. The relative paucity of simple MB-to-clock pathways may limit the role of learning in circadian modulation. Instead, innate olfactory cues–such as pheromones and toxins–may directly influence internal clocks, ensuring that mating and feeding strategies align with optimal times of the day. Understanding how these circuits tweak circadian rhythms can clarify how environmental and social cues shape daily activity cycles.

Significance and Limitations

Our finding that pheromone and odor-detecting olfactory circuits are spatially segregated in the antennal lobe and LH aligns with previous studies (Jefferis et al., 2007). Because prior studies do not directly compare the five attractive pheromone and repulsive odor circuits, our studies extend these prior findings by showing that the pattern of spatial segregation in the AL and LH applies to all five glomeruli. Our findings also extend on prior studies by highlighting how olfactory inputs to DA, SER, insulin, and clock neuron pathways differ between attractive and repulsive circuits and may relate to the functions associated with these neuromodulatory cells.

However, several limitations must be acknowledged. The connectome data originates from a single female *D. melanogaster* hemibrain, potentially limiting insights into variability, plasticity, and sexual dimorphism in circuit architecture. A key example of sexual dimorphism is the DA1 circuit for cVA detection, which displays sexual dimorphism in the LH and promotes courtship behavior in female *D. melanogaster* and suppresses courtship behavior in male *D. melanogaster* (Kurtovic et al., 2007). Moreover, our analysis focused on structural connectivity rather than functional activity or synaptic strength, leaving open questions about how these networks operate in dynamic, naturalistic conditions. Together, the answers to these questions are termed the "effectome." Future research using functional imaging, genetic manipulations, and behavioral assays will be necessary to validate and refine hypotheses based on our comparative structural approach. Additionally, future research will need to map the pathways that link the brain to the ventral nerve cord (VNC) to understand the entire central nervous system (CNS).

Conclusion

The FlyWire connectome project analyzed five olfactory glomeruli (DA1, DA2, DC4, VA1d, and VA1v) in the Drosophila brain, revealing distinct neuronal compositions and connectivity patterns. We identified a higher number of glomerular PNs and a lower number of LNs for olfactory circuits with high specificity to a compound, such as the DA1 glomerulus for cVA or the DA2 glomerulus for geosmin. We also identified a spatial segregation of attractive pheromone and repulsive odor representations in both the AL and LH, with pheromones represented laterally and odors represented medially. For higher-order pathways to various neuromodulators, we found that pheromone-detecting circuits had more direct projections to dopaminergic DSK neurons promoting female sexual behavior, and a greater number of pathways to dopaminergic PAM neurons for associative learning and positive reinforcement. We found that all olfactory circuits project to PFNm serotonergic neurons for navigational behaviors and LB1b neurons for bitter taste detection, although the DC4 circuit for acid avoidance had less input to serotonin neurons and may receive less serotonergic modulation of acid avoidance. In addition, all olfactory circuits project through the LH to insulin-producing cells, whose activity has been shown to promote cVA attraction and may modulate the activity of other olfactory circuits, suggesting that pheromone-driven attraction or odor repulsion may be modulated by metabolic state. Finally, we found that all five olfactory circuits had inputs to clock neurons primarily through the LH, suggesting that behaviors driven by attractive or repulsive olfactory inputs and circadian rhythms may be mediated by neural pathways with less plasticity compared to pathways through the MB. Consequently, olfactory circuits connected with clock neurons may mediate stereotyped behaviors dependent on circadian time. Overall, our FlyWire connectome study reveals a spatial segregation of olfactory circuits mediating attraction to pheromones and repulsion to odors in the AL and LH, and distinct patterns of connectivity to LH neurons for innate behaviors, MB neurons for associative learning, and neuromodulatory neurons that may provide positive feedback to modulate olfactory-driven attraction and repulsion.

References

1. Ai, M., Min, S., Grosjean, Y., Leblanc, C., Bell, R., Benton, R., & Suh, G. S. (2010). Acid sensing by the Drosophila olfactory system. *Nature, 468*(7324), 691-695.
2. Bisen, R. S., Iqbal, F. M., Cascino-Milani, F., Bockemühl, T., & Ache, J. M. (2024). Nutritional state-dependent modulation of Insulin-Producing Cells in Drosophila. *BioRxiv*, 2024-04.
3. Das Chakraborty, S., & Sachse, S. (2021). Olfactory processing in the lateral horn of Drosophila. *Cell and Tissue Research*, 383, 113-123.
4. Dweck, H. K., Ebrahim, S. A., Thoma, M., Mohamed, A. A., Keesey, I. W., Trona, F., ... & Hansson, B. S. (2015). Pheromones mediating copulation and attraction in Drosophila. *Proceedings of the National Academy of Sciences*, 112(21), E2829-E2835.
5. Hulse, B. K., Haberkern, H., Franconville, R., Turner-Evans, D. B., Takemura, S. Y., Wolff, T., ... & Jayaraman, V. (2021). A connectome of the Drosophila central complex reveals network motifs suitable for flexible navigation and context-dependent action selection. *Elife*, 10.
6. Keene, A. C., Krashes, M. J., Leung, B., Bernard, J. A., & Waddell, S. (2006). Drosophila dorsal paired medial neurons provide a general mechanism for memory consolidation. *Current biology, 16*(15), 1524-1530.
7. Kurtovic, A., Widmer, A., & Dickson, B. J. (2007). A single class of olfactory neurons mediates behavioural responses to a Drosophila sex pheromone. *Nature, 446*(7135), 542-546.
8. Lebreton, S., Trona, F., Borrero-Echeverry, F., Bilz, F., Grabe, V., Becher, P. G., ... & Witzgall, P. (2015). Feeding regulates sex pheromone attraction and courtship in Drosophila females. *Scientific Reports, 5*(1), 13132.
9. Li, F., Lindsey, J. W., Marin, E. C., Otto, N., Dreher, M., Dempsey, G., ... & Rubin, G. M. (2020). The connectome of the adult Drosophila mushroom body provides insights into function. *Elife*, 9, e62576.
10. Li, Y., Guo, F., Shen, J., & Rosbash, M. (2014). PDF and cAMP enhance PER stability in Drosophila clock neurons. *Proceedings of the National Academy of Sciences, 111*(13),

E1284-E1290.

11. Marin, E. C., Jefferis, G. S., Komiyama, T., Zhu, H., & Luo, L. (2002). Representation of the glomerular olfactory map in the Drosophila brain. *Cell, 109*(2), 243-255.

12. Owald, D., & Waddell, S. (2015). Olfactory learning skews mushroom body output pathways to steer behavioral choice in Drosophila. *Current opinion in neurobiology,* 35, 178-184.

13. Prisco, L., Deimel, S. H., Yeliseyeva, H., Fiala, A., & Tavosanis, G. (2021). The anterior paired lateral neuron normalizes odour-evoked activity in the Drosophila mushroom body calyx. *Elife*, 10, e74172.

14. Schlegel, P., Bates, A. S., Stürner, T., Jagannathan, S. R., Drummond, N., Hsu, J., ... & Jefferis, G. S. (2021). Information flow, cell types and stereotypy in a full olfactory connectome. *Elife*, 10, e66018.

15. Stensmyr, M. C., Dweck, H. K., Farhan, A., Ibba, I., Strutz, A., Mukunda, L., ... & Hansson, B. S. (2012). A conserved dedicated olfactory circuit for detecting harmful microbes in Drosophila. *Cell, 151*(6), 1345-1357.

16. Sung, H. Y., Jeong, Y. T., Lim, J. Y., Kim, H., Oh, S. M., Hwang, S. W., ... & Moon, S. J. (2017). Heterogeneity in the Drosophila gustatory receptor complexes that detect aversive compounds. *Nature communications, 8*(1), 1484.

17. Tomita, J., Ban, G., Kato, Y. S., & Kume, K. (2021). Protocerebral bridge neurons that regulate sleep in *Drosophila melanogaster*. *Frontiers in Neuroscience,* 15, 647117.

18. Wang, T., Jing, B., Deng, B., Shi, K., Li, J., Ma, B., ... & Zhou, C. (2022). Drosulfakinin signaling modulates female sexual receptivity in Drosophila. *Elife*, 11, e76025.

Vertices: Duke's Undergraduate Research Journal Volume 4, Issue 1 | Spring 2025

Meet Our Editing Team

EDITORIAL BOARD

Sasha Bacot,
Co-Editor-In-Chief

Sasha (Trinity ‘25) is from South Carolina and is a double major in Biology and Computer Science. She loves being a Vertices peer reviewer because it allows her to delve deeper into what she’s most passionate about: scientific research! Outside of her work with Vertices, Sasha loves to figure skate, listen to music, and try out all the cool restaurants in Durham (especially for boba)!

Kaeden Hill,
Co-Editor-In-Chief

Kaeden (Trinity ‘25) is a Vertices Senior Editor from Atlanta, Georgia, double majoring in biology with a concentration in molecular and cell biology, and evolutionary anthropology with a minor in chemistry. After graduating, he plans to pursue a Ph.D. and a career in research. He is specifically interested in DNA tumor viruses and how their “cellular hijacking” can drive cells towards cancer, and he is a member of the Luftig Lab, studying Epstein-Barr virus and the cancers that it causes. Outside of academics, he loves to hike, travel, ski, scuba dive, collect minerals, and make jewelry.

Eliza Goldstein,
Senior Editor

Eliza (Trinity ’26) is from New York and is majoring in Psychology with a minor in Global Health. She is interested in clinical and social psychology, specifically the intersections and variance of psychopathology among differing backgrounds and experiences. At Duke, she is the Lab Manager for the Culture Lab and a Research Assistant for the Zucker Lab. Outside of research, she enjoys biking, reading, and spending time with her friends.

Vishruth Hanumaihgari,
Senior Editor

Vishruth (Trinity ’27) is from Allentown, Pennsylvania and plans to major in neuroscience. He loves doing research in the lab, and he joined Vertices because he can read other people’s work and help them publish the best possible version of their projects. Outside of Vertices, Vishruth also loves to play basketball and try new foods!

Eric Lee,
Senior Editor

Eric is a junior from Jacksonville, Florida studying premedicine and computer science at Duke. He is particularly interested in the intersections of computational techniques and biomedical psychiatric research. On campus he is passionate about working with research education and mental health organizations. In his free time, he enjoys ping-pong, board/card games, cooking, and music.

PEER REVIEW TEAM

Isaac Ayo’ Oyegbade

Isaac (Fuqua ‘25) is from western Nigeria and majors in Strategy & Corporate Finance for his MBA degree. Prior, he obtained a Biochemistry B.Sc. in 2015 and became a Chartered Accountant in 2022. He has worked for 9 years in Banking, Consulting & Finance across the EMEA & the U.S. Outside of Vertices, he is on Duke’s Racial Equity Advisory Council and is the Vice-President of External Affairs & Alumni Engagement for the Duke MBA Consulting Club and the Business in Africa Club. He imagines himself a pro-pickleball player and an amateur skateboarder.

Emerson Cortazar

Emerson (Pratt ‘28) is from Charlotte, North Carolina and is majoring in Electrical and Computer Engineering. In his free time, he enjoys baking, reading books, and watching movies.

Mandy Fuller

Mandy (Trinity ‘28) is from Miami Beach, Florida and plans to major in Neuroscience and Sociology with a minor in Chemistry on the pre-med track. Within Sociology, she has a concentration in Crime, Law, and Justice and will begin as a teaching assistant for Incarceration Nation in the Fall. Outside of Vertices, she is the Creative Director for TedxDuke and an active volunteer with Duke HAND (Helping Alzheimer’s and Other Neurodegenerative Diseases). In her free time, she enjoys traveling, going to the gym, spending time with friends, and listening to music.

Gage Gruett

Gage (Trinity ’28) is from Austin, Texas and is majoring in Neuroscience with a minor in Art History and Chemistry. Outside of Vertices, he studies eating disorders in the Duke Center for Eating Disorders (DCED) Lab, optogenetics in the Mooney lab, and spearheads events for the National Alliance on Mental Illness (NAMI) as their Executive Publicity Officer. In his free time, he enjoys thrifting at local stores, ranking cafes and movies, and volunteering to help describes and curate art exhibits for incarcerated artists through Durham’s local Impartial non-profit!

Jinny Guo

Jinny (Trinity ’28) is from Pennsylvania and is majoring in Biology and Computer Science with a certificate in Innovation and Entrepreneurship. Outside of Vertices, she studies tissue regeneration after severe radiation injury in the Lee Lab, dances with Synergy Dance Company, and plans large on-campus events as part of DUU’s Special Event Committee. Besides research, she enjoys swimming, running, dancing, and watching shows and movies in her free time.

Hannah Hortman

Hannah (Trinity ‘26) is from Raleigh, North Carolina and majoring in Neuroscience with minors in Computer Biology and Chinese. She studies therapeutic targets for Parkinson’s Disease in the Calakos Lab. Beyond her work as a Vertices peer editor, Hannah enjoys dancing, figure skating, painting, and trying new restaurants!

Arielle Kim

Arielle Kim (Trinity ‘26) is a Duke University undergraduate majoring in Biology with minors in Computer Science and Computational Biology and Bioinformatics! She is particularly drawn to the intersection of microbiology and ecology, and she is currently exploring symbiotic systems involving fungi and their photobionts as a member of the Lutzoni Lab.

Sai Gayathri Kurup

I am a biology major with a chemistry minor on the premed track. On campus, I am involved in vision health research, clinical volunteering, and science journalism

Daniel Levin

Daniel (Trinity ‘27) is from Pittsburgh, PA, studying chemistry and biology. His research at Duke focuses on understanding the role of noncoding RNA during immune responses. After graduating, he aspires to pursue a Ph.D. and research the chemical origins of life. Outside of the lab, Daniel enjoys ice skating and gardening.

Zishen Li

Zishen (Trinity ’27) is from Xi’an, Shaanxi, China, planning on majoring in biology and minoring in visual arts on the pre-med track. Zishen is interested in science communication as well as how art and science can be combined. Outside of Vertices, she is a part of the TIRTL Lab studying the immune responses to transplants. She also enjoys volunteering with Help Desk, acting with Duke Chinese Theater, playing ball sports, and exploring new things!

Krystal Liu

Krystal Liu is a first-year student at Duke who plans to double major in Economics and History. She is very interested in writing academic papers and loves reviewing them. She also enjoys traveling, sports, and hanging out with her friends.

Ben Mei-Dan

Ben (Trinity ‘28) is from Boulder, Colorado. Likely majoring in Biology, he has a deep interest in physiology, biomechanics, and the broad field of wilderness medicine. In his free time, he enjoys challenging himself in the mountains, playing guitar, listening to great music, and spending time with friends.

Max Niu

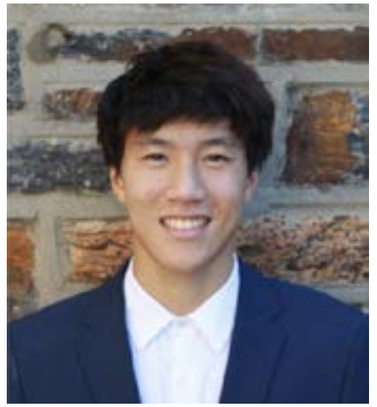

Max (Trinity ’28) is from Marlboro, New Jersey and is majoring in computer science with a concentration in machine learning and marine science & conservation. He is specifically interested in the application of machine learning and other forms of technology in marine science. He is a part of the MaRRS Lab, conducting his own research project on leveraging machine learning to analyze data from whale tagging. Outside of academics, he loves playing pickleball and tennis, swimming, hiking, traveling, snowboarding, scuba diving, and weight lifting.

Anuskha Peer

Anushka (Trinity ‘28) is majoring in Chemistry is from the Bay Area, California. She’s specifically interested in microbiology and drug discovery and loves learning about new research fields through peer editing. Outside of Vertices, she enjoys volunteering in Hospice, playing the flute in the Duke Wind Symphony, and getting cookies from Insomnia!

Harry Pratt

Harry (Trinity ’27) is from New York and is majoring in Biology with a minor in Chemistry on the pre-med track. Outside of Vertices, he studies neurodegeneration in the Sanders Lab and volunteers to address social determinants of health in a clinical setting with Help Desk. In his free time, he enjoys playing music, and is a drummer in a band on campus called The Trench.

Daliya Rizvi

Daliya (Trinity ‘27) is studying biochemistry and applied ethics on the premed track. She is interested in the intersection of novel cancer treatments and the bioethical issues posed by long-term end-of-life care. Outside of Vertices, she is passionate about music, research, reading, and running track.

Canaan Salles-Spar

Canaan (Pratt ‘27) is a Civil Engineering and Marine Science double major from New York. He is interested in understanding the interactions between built systems and the environment. This summer, Canaan is spending the time at the Duke Marine Lab conducting research on oyster reef restoration and hanging out by the beach.

Ainsley Scheiner

Ainsley (Trinity ’26) is from New York, NY and majoring in Biology with a concentration in Cell & Molecular Biology. Beyond her interest in scientific writing, Ainsley researches starvation resistance and metabolism in C. elegans in the Baugh Lab and loves to try Wilson workout classes and visit the Arts Annex with her friends.

Will Sun

Will (Trinity ‘27) is an undergraduate student who intends to major in biology with a concentration in ecology, marine science and conservation from San Jose, CA. Outside of working in the Miao Lab on integrative immunology, he also enjoys playing basketball, watching sunsets, and eating ramen.

Asher Wallen

I am a freshman in the Trinity College of Arts and Sciences, and I am a prospective biology major with a certificate in health policy. I am passionate about translational research, especially related to the life sciences, through the lens of science communication.

Naomi Wordofa

Naomi (Trinity ‘28) is from Monterey, California and hopes to major in Biology and Global Health. Outside of school, she enjoys long-distance running, playing the violin and doing photography.

Meet Our Design Team

Rachel Wu

Rachel (Pratt ‘28) is a biomedical engineering and cs major from Omaha Nebraska. She is interested in computational biology and how machine learning can be used on biological data, and is currently working in the Hickey Lab. Outside of academics, she plays viola in the Duke Sumphony Orchestra and enjoys exploring new restaurants with friends

Alice (Hanzhi) Zhang

Alice (Trinity ’28) hails from Tianjin, China, and is majoring in Biology with a keen interest in receptor mechanisms and nanofiber immunotherapy delivery. Outside research, Alice is an astronomy enthusiast, is working toward her private pilot license, and enjoys applying aromatherapy!

Ura Zhang

A young but passionate biology researcher, public welfare initiator, outdoor enthusiasts, and scenery photographer.

AJ Kochuba,
Artistic Director

AJ (Trinity ‘25) is from Cary, North Carolina, studying neuroscience, psychology, and visual arts on the pre-med track. AJ is particularly interested in humanities-based approaches to medical practice and research and hopes to enrich the symbiotic relationship between the fields of science and arts. Outside of Vertices, AJ can be found hosting arts- and identity-focused events and competing on the pickleball courts.

Gaby Dunn

Gaby is a junior from South Florida with too many interests that she is trying to find a major for. She is fascinated by the intersections of education, art, & STEM. When procrastinating, she enjoys rock climbing, critiquing movies, and spending time outdoors.

Chelsea Gan

Chelsea (Trinity ‘27) is from Miami, Florida and is majoring in Chemistry with a minor in Gender, Sexuality, and Feminist Studies. Outside of Vertices, she can be found researching malaria host-parasite interactions with the Derbyshire lab or wheel throwing pottery at the Arts Annex.

Amanda Li

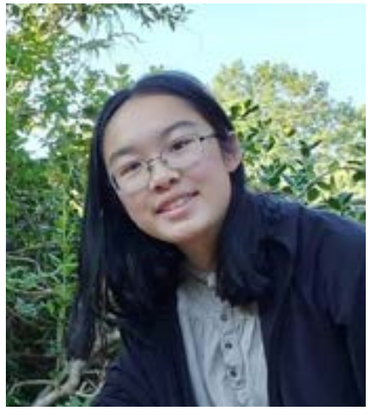

Amanda (Pratt ‘27) is from Charlotte, North Carolina and is majoring in biomedical engineering. She loves learning about anything and everything, doodling in her spare time, and exploring new things.

Ava Kocher

Ava Kocher (Trinity ‘27) is from Massachusetts and majoring in Biology with a concentration in Marine Biology. She is interested in animal sensory systems and the intersection of art and science. Outside of school, she loves backpacking, live music, and swimming with sea creatures.

Monet Shum

Monet (Trinity ’27) is from Aldie, Virginia studying linguistics, computer science, and classical languages. Outside of Vertices, she also works with Duke’s Wang Lab and the JustScience Center and enjoys beading and walking in the Duke Gardens.

Acknowledgements

VERTICES EXECUTIVE BOARD

Co-Editors in Chief
Sasha Bacot
Kaeden Hill

Senior Editors
Eliza Goldstein
Vishruth Hanumaihgari
Eric Lee

Artistic Director
AJ Kochuba

Director of Outreach
Will Sun

Community Events Director
Daliya Rizvi

PEER REVIEW TEAM

Anushka Aggarwal
Matthew Ahlers
Beren Berber
Meghna Bukkapatnam
Poorvaja Chandramouli
Arjun Saha Choudhury
Chloe Chun
Emerson Cortazar
Lara Dincer
Mandy Fuller
Gage Gruett
Jinny Guo
Cooper Herrett
Hannah Hortman
Vatsal Jain
Lara Kendall
Arielle Kim
Sai Gayathri Kurup
Daniel Levin
Andy Li
Runda Li
Zishen Li
Bernard Liang
Krystal Liu
Keyan Miao
Max Niu
Isaac Oyegbade
Anushka Peer
Ananya Pinnamaneni
Harry Pratt
Daliya Rizvi
Canaan Salles-Spar
Avneesh Saravanapavan
Ainsley Scheiner
Anisha Sharma
Alok Sinha
William Sun
Asher Wallen
Naomi Wordofa
Rachel Wu
Sophia Zhang
Alice Hanzhi Zhang
Emma Zhang
Ura Zhang

DESIGN

Spring 2025 Issue & Layout Design
Monet Shum

Cover & Article Graphics
Gaby Dunn
Ava Kocher
Chelsea Gan
Monet Shum

Website Design
Zishen Li

FACULTY/EXPERT REVIEWERS

Richard J Wong | Duke Nicholas School of the Environment | PhD Candidate
Lauren Jenkins | Duke Nicholas School of the Environment | PhD Candidate
Brian Silliman | Duke Nicholas School of the Environment | Professor
Whitney Robinson | Duke University School of Medicine | Associate Professor of Obstetrics and Gynecology
Jackie Bao | Duke Institute for Brain Sciences | Student
Ashley Jia | Duke University Department of Biology | PhD Candidate